Springer Proceedings in Physics 163

Boyka Aneva
Mihaela Kouteva-Guentcheva *Editors*

Nonlinear Mathematical Physics and Natural Hazards

Selected Papers from the International School and Workshop held in Sofia, Bulgaria, 28 November–02 December, 2013

Springer

Springer Proceedings in Physics

Volume 163

More information about this series at http://www.springer.com/series/361

Boyka Aneva · Mihaela Kouteva-Guentcheva
Editors

Nonlinear Mathematical Physics and Natural Hazards

Selected Papers from the International School and Workshop held in Sofia, Bulgaria, 28 November–02 December, 2013

Springer

Editors
Boyka Aneva
Theoretical and Mathematical Physics Department
Institute for Nuclear Research and Nuclear Energy
Bulgarian Academy of Sciences
Sofia
Bulgaria

Mihaela Kouteva-Guentcheva
Department of Computer-Aided Engineering, Faculty of Structural Engineering
University of Architecture, Civil Engineering and Geodesy
Sofia
Bulgaria

ISSN 0930-8989 ISSN 1867-4941 (electronic)
Springer Proceedings in Physics
ISBN 978-3-319-14327-9 ISBN 978-3-319-14328-6 (eBook)
DOI 10.1007/978-3-319-14328-6

Library of Congress Control Number: 2014959277

Springer Cham Heidelberg New York Dordrecht London

Printed on acid-free paper

Springer International Publishing AG Switzerland is part of Springer Science+Business Media (www.springer.com)

Foreword

Advancing hazard-resistant design demands an understanding of what happens when a disaster occurs. Documenting and sharing the key lessons learned from extreme events around the world contribute significantly to advancing research and practice in hazards engineering. Sustainable development of different scale administrative-territorial units (ATU) requires an adequate comprehensive risk assessment due to relevant natural hazards, considering the links between the risk sources and elements. Therefore, risk assessments, analysis, and forecasts for the overall impact in the realization of a national threat as natural hazards with certain characteristics on given territory have become a very actual scientific problem with the related practical, social, and economic aspects. The materials in this book concern the mathematical physics background tools for modeling and analysis of catastrophic events and natural hazards; available information sources—national and international specialized databases (data acquiring and data processing); engineering use of these data.

This book reflects our recent regional collaboration with leading European experts in: (i) better understanding and modeling the nonlinear natural hazard phenomena that might cause ecological and socioeconomical disasters and (ii) mitigating the negative risk consequences associated with the earthquake disasters.

The book is addressed to physicists, geophysicists, earthquake engineers, as well as to every other young and senior researcher interested in the problems of nonlinear mathematical physics and natural disasters and relevant multi- and interdisciplinary collaborations.

Sofia
Bulgaria

Boyka Aneva
Mihaela Kouteva-Guentcheva

Preface

This book is a collection of selected papers from the International School and Workshop on *Nonlinear Mathematical Physics and Natural Hazards* which was held in Sofia, in the period November 28–December 02, 2013. The scientific forum was organized with the UNESCO financial support as an activity within the Southeast European Network for Mathematical and Theoretical Physics, SEENET MTP, thus extending fundamental research to applied science. It was devoted to current advanced achievements in the field of nonlinear mathematical physics and modeling of critical phenomena that could cause catastrophic events to occur. This multidisciplinary meeting brought together scientists developing mathematical and computational methods for the study and analysis of nonlinear phenomena and working actively to apply these tools and create conditions to mitigate and reduce the negative consequence of natural and socioeconomic disaster risk. Ten plenary talks and ten shorter session talks focused on different theoretical and applied aspects of the natural hazards were given. All the sessions were followed by interesting fruitful multidisciplinary discussions. The young researchers presented high-quality research results in ten posters at the special poster session, organized for the participating young scientists and students.

An important part of the meeting was the open discussion at the **Round Table Discussion on Perspectives of Collaboration on Disaster Risk Assessment and Management in Southeast Europe and Joint EU Projects** moderated by the representative of the UNESCO Regional Bureau for Science and Culture in Europe, Venice—Mr. M. Scalet. This special session was focused on the UNESCO contribution to current and future multidisciplinary collaboration and promotion of proposals for international research and applied science projects.

The International School and Workshop on *Nonlinear Mathematical Physics and Natural Hazards* has achieved the twofold objective aimed by the organization of this scientific meeting:

(a) Presentation of current advanced research achievements on modeling and analysis of critical natural phenomena and their applications for reducing the natural hazards risk, for mitigation of the negative consequences of natural and socioeconomic disasters for the individuals and the society as a whole.
(b) Extending and strengthening the inter- and multidisciplinary collaboration at regional, the Balkans, and European level to contribute to our joint efforts on mitigation of the negative consequence of natural disasters.

An immediate step to further extending the communications and collaboration between the scientists in the Balkan region was the mobility program realized in the form of four scientific visits in the region (at: the University of Nis, IZIIS, Skopje and the Seismological Observatory, Skopje, Technical University of Istanbul and the Bogazici University, Istanbul) that came out as a follow-up activity of this meeting.

The International School and Workshop on *Nonlinear Mathematical Physics and Natural Hazards* combined the traditional school type lectures with shorter talks given by advanced researchers and informal discussions at the end of each session and of every working day. The presented latest developments on specialized topics and state-of-the-art reviews on the research in the fields of nonlinear mathematical physics in relation to natural hazards and risk mitigation met the active interest of the young auditorium. Both the high scientific and methodological quality lectures and the friendly meeting atmosphere were highly appreciated by all the participants and the sincere will and hope for future meetings and mobility of young people in the region were declared. The meeting had successful impact on the motivation of young people who decided to choose the mathematical and physical sciences application to natural hazards as their professional field.

The major topics covered by the meeting were:

– Self-organizing Systems;
– Markov Processes and Stochastic Dynamics; Chaotic Dynamics;
– Exactly Solvable and Integrable Systems;
– Soliton Physics;
– Seismic Hazard and Seismic Risk;
– Seismic Monitoring and Networking; Earthquake Engineering Monitoring;
– Early Warning Systems.

Modern quantum field theory and statistical mechanics distinguish between two types of systems: Type I is massive and its behavior follows the exponential law and Type II is critical or massless and its behavior is subject to power law. Many systems in nature and society have dynamics, whose behavior exhibits power law, such as earthquakes, snow avalanches, landslides, superconducting vortices, forest fires, rainfall, stock market indices, the extinction of species in biology, etc. These events appear in quite diverse areas from atomic to social scale. A power law probability distribution does not decay as a Poisson one and there is a finite chance for a big catastrophic event to occur.

Advanced hazard-resistant sustainable development demands an understanding of what happens when a disaster occurs. Documenting and sharing the key lessons learned from extreme events around the world contribute significantly to advancing research and practice in hazards engineering. Adequate comprehensive risk assessment, analysis, and forecasts relevant to different scale territories exposed to various natural hazards have become a very actual complex scientific problem with the explicit practical, social, and economic aspects. For this reason, the materials in this book concern the mathematical physics background tools for modeling and analysis of catastrophic events and natural hazards; available information sources—national and international specialized databases (data acquiring and data processing); engineering use of these data. Disaster Risk Mitigation concerns initiatives and measures, which might enable a society to cope with risks and hazards, minimizing potential for loss of lives and properties as a result of different hazards. Introducing education and the culture of prevention at all levels is a must, called by the occurrence of major disasters, continuously caused by different hazards. The book is a step forward to capacity building in Southeast Europe through development of skills, exchange of knowledge and training on mathematical methods for modeling nonlinear phenomena, disaster risk preparedness, and natural hazards mitigation.

The materials in this book are divided into two major parts following the scientific program of the meeting:

Part I—Nonlinear Mathematical Physics Towards Critical Phenomena;
Part II—Seismic Hazard and Risk.

Among the topics covered in the first part are predictions and correlations in self-organized criticality, space-time structure of extreme current and activity events in exclusion processes, quantum spin chains and integrability of many-body systems, applications of discriminantly separable polynomials, MKdV-type of equations, and chaotic behavior in Yang–Mills theories. The second part is devoted to probabilistic seismic hazard assessment, seismic risk mapping, seismic monitoring, networking and data processing in Europe, mainly in Southeast Europe.

This volume is addressed to physicists, geophysicists, earthquake engineers, and to every other young and senior researcher interested in the problems of nonlinear mathematical physics and natural disasters and relevant multi- and interdisciplinary collaborations.

The editors express their sincere gratitude to all the authors of this volume for their contributions. The precious UNESCO Regional Bureau for Science and Culture in Europe, Venice, support and sponsorship are highly appreciated by all the participants in this initiative. The support of the local organizations and authorities (Institute for Nuclear Research and Nuclear Energy and Bulgarian Academy of Sciences) is kindly acknowledged.

Sofia
Bulgaria

Boyka Aneva
Mihaela Kouteva-Guentcheva

Committees

Organizing Committee

Boyka Aneva (Bulgaria)
Giuliano F. Panza (ICTP, Trieste, Italy)
Peter Varga (Hungary)
Mihaela Kouteva-Guentcheva (Bulgaria)
Mario Scalet (UNESCO Venice office)

Scientific Committee

Boyka Aneva (Bulgaria)
Radu Constantinescu (Romania)
Gheorghe Marmureanu (Romania)
Giuliano Panza (Italy)
Peter Varga (Hungary)

Invited Lecturers

G. Chouliaras
D. Dojcinovski
G. Marmureanu
G.F. Panza
A. Peresan
G. Pruessner
M. Radulian
G. Schuetz
A. Zabrodin

The Scientific Sessions and the Round table

The Poster Sessions

The Social Events

Program of the Meeting

(The presentations can be found at the website of the meeting http://www.inrne.bas.bg/international-school-sofia/)

Conference venue: Kedar Hotel, Dom na Uchenia
1113 Sofia, Geo Milev, 50 Shipchenski Prohod Blvd.
+359 2 8702140, +359 2 8710009
Arrival day: 28.11.2013; Departure day: 02.12.2013

Thursday, 28.11.2013	Arrival day
18:00	Registration of Participants
Friday, 29.11.2013	
9:00 am	**Opening of the meeting** *UNESCO Representative,* *Representatives of the Bulgarian Academy of Sciences and INRNE* *Representative of the Organizing Committee*
Session Seismic Hazard and Seismic Risk *Chairman: G. Chouliaras*	
9:30–10:15	***G.F. Panza, A. Peresan, A. Magrin, F. Vaccari (ICTP),*** The Hazard in Using Earthquakes Probabilities for Seismic Hazard Assessment
10:15–11:00	***G. Marmureanu, C.O. Cioflan, Al. Marmureanu, C. Ionescu (National Institute for Earth Physics (NIEP))***, Nonlinear Seismology the Actual Seismology in this Century
11:00–11:30	**Coffee break**
11:30–12:15	***D. Dojcinovski (IZIIS, Skopje)***, Seismic Monitoring of Structures—a Tool for Urban Seismic Hazard Reduction
12:15–12:45	***K. Hadjiyski, S. Simeonov*** (NIGGG-BAS) Seismic monitoring and Instrumentation for Earthquake Engineering Application in Bulgaria
13:00	**Lunch**

(continued)

(continued)

Session Chaotic Dynamics *Chairman: R. Constantinescu*	
15:00–15:30	***A. Nicolaidis (Aristotle University of Thessaloniki),*** The Chaotic versus Regular Behavior in Yang–Mills Theories
15:30–16:00	***K. Kukic (University of Belgrade), V. Dragovic (Mathematical Institute, SANU),*** The Application of the Discriminantly Separable Polynomials in Dynamical Systems
16:00–16:30	**Coffee break**
Development Session *Moderator: M. Scalet*	
16:30–18:30	***Round Table Discussion*** Perspectives of collaboration on Disaster Risk Assessment and Management in Southeast Europe and joint EU projects. Moderated by UNESCO
19:00	**Welcome cocktail**
19:30	**Dinner**
Saturday, 30.11.2013	
Session Soliton Physics and Integrability *Chairman: A. Nicolaidis*	
9:15–10:00	***A. Zabrodin (ITEP, Moscow)***, Spectra of integrable quantum magnets via classical many-body systems
10:00–10:30	***R. Constantinescu (University of Craiova)***, Symmetries and Invariant Solutions for Evolutionary Equations
10:30–11:00	***V. Gerdjikov (INRNE-BAS),*** Riemann–Hilbert Problems, Families of Commuting Operators and Soliton Equations
11:00–11:30	**Coffee break**
11:30–12:00	***D. Mladenov (University of Sofia)***, Bianchi cosmological models as integrable geodesic flows
12:00–12:30	***T. Popov (INRNE-BAS)***, Parastatistics and Homotopy Algebras
12:30–13:00	***N. Nikolov (INRNE*-BAS)**, An operadic bridge between renormalization theory and vertex algebras
13:00	**Lunch**
	Session Stochastic Dynamics and Self-organizing Systems *Chairman: A. Zabrodin*
15:30–16:15	***G. Schuetz (FZ Julich),*** The Space-time Structure of Extreme Current Events in the ASEP
16:15–17:00	***G. Pruessner (Imperial College, London)***, Self-Organized Criticality: It's Past and a Recent Field Theory
17:00–17:30	**Coffee break**
17:30–19:00	**Poster Session**
19:30	**Conference Dinner**
Sunday, 01.12.2013	
	Session Nonlinear Seismology and Early Warning Systems *Chairman: A. Peresan*
9:30–10:15	***M. Radulian (NIEP)***, Nonlinear dynamics in Vrancea source: numerical simulation

(continued)

(continued)

10:15–11:00	***C. Ionescu, Al. Marmureanu, G. Marmureanu (NIEP),*** Romanian-Bulgarian early warning system (EWS) developed for strong Vrancea earthquakes
11:00–11:30	**Coffee break**
	Session Seismic Monitoring and Networking *Chairman: D. Dojcinovski*
11:30–12:00	***M. Popa (NIEP)***, Romanian Network for Seismic and Crustal Movement Monitoring
12:00–12:30	***D. Cernih (Seismological Observatory, Skopje)***, Seismic Monitoring and Data Processing in Seismological Observatory in Skopje—Republic of Macedonia—basis for a complex geophysical monitoring
13:00	**Lunch**
	Session Prognostic Seismic Hazard Assessment *Chairman: G. Marmureanu*
16:15–17:00	***G. Chouliaras (Institute of Geodynamics, Athens)***, Statistical Seismology and Earthquake Prediction in Greece
17:00–17:30	**Coffee break**
17:30–18:15	***A. Peresan (ICTP), A. Nekrasova, V. Kossobokov (MITP-RAN), G.F. Panza (ICTP)***, Predicting Earthquakes and Related Ground Shaking: Testing and Validation Issues
18:30	**Closing**
19:30	**Dinner**
Monday, 02.12.2013	**Departure**

List of Poster Presentations

C. Babalic (University of Craiova)—Multipoles Soliton Solutions for Tzitzeika Type Equations

Gergana Georgieva (University of Sofia)—Upper mantle structure beneath Bulgaria

Bozhin Karaivanov (University of Sofia)—About Alcaraz method for determination of critical exponents in sandpiles

E.F. Manea, D. Toma, C.O. Cioflan, Ghe. Marmureanu, M. Radulian, S. Balan (NIEP, Bucharest)—Steps in seismic risk mapping for Romania capital city

I.E. Nastase (NIEP, Bucharest)—The NIEP network of permanent GPS stations

Emilian Panaintescu, Mihai Stoicescu, Isabela Stefarta (University of Craiova)—Nonlinear electronic circuits modeling neural flows

V.S. Gerdjikov (INRNE-BAS), D.M. Mladenov, A.A. Stefanov, S.K. Varbev (University of Sofia)—One parameter family of MKdV equations related to so(8) algebra

V.S. Gerdjikov (INRNE-BAS), D.M. Mladenov, A.A. Stefanov, S.K. Varbev (University of Sofia)—New type of equations related to sl(n) algebra

D. Arnaudov, R.C. Rashkov and T. Vetsov (University of Sofia)—On the algebraic curves for circular and folded strings in AdS5 × S5

R.C. Rashkov, H. Dimov and S. Mladenov (University of Sofia)—String approach to strong coupling phenomena: ABJM case

List of the Participants

Anca Opris National Institute for Earth Physics, Bucharest, Romania
Boyka Aneva Institute for Nuclear Research and Nuclear Energy, INRNE, Bulgarian Academy of Sciences, Sofia, Bulgaria
Corina Babalic University of Craiova, Craiova, Romania
Tudor Balacescu University of Craiova, Craiova, Romania
Dragana Cernih Seismological Observatory of the Faculty of Natural Sciences and Mathematics, Ss. Cyril and Methodius University, Skopje, Macedonia
Gerasimos Chouliaras Institute of Geodynamics, National Observatory of Athens, Athens, Greece
Carmen Cioflan National Institute for Earth Physics, Bucharest, Romania
Radu Constantinescu University of Craiova, Craiova, Romania
Marina Cuta University of Craiova, Craiova, Romania
Danilo Delibasic Faculty of Natural Sciences and Mathematics, University of Nis, Nis, Serbia
Dragi Dojcinovski Institute of Earthquake Engineering and Engineering Seismology, IZIIS, University Ss. Cyril and Methodius, Skopje, Macedonia
Katerina Drogreska Seismological Observatory of the Faculty of Natural Sciences and Mathematics, Ss. Cyril and Methodius University, Skopje, Macedonia
Kiril Hadjyiski National Institute of Geophysics, Geodesy and Geography, NIGGG, Bulgarian Academy of Sciences, Sofia, Bulgaria
Mihail Garevski Institute of Earthquake Engineering and Engineering Seismology, IZIIS, University Ss. Cyril and Methodius, Skopje, Macedonia
Gergana Georgieva Faculty of Physics, Sofia University "St. Kliment Ohridski", Sofia, Bulgaria
Vladimir Gerdjikov Institute for Nuclear Research and Nuclear Energy, INRNE, Bulgarian Academy of Sciences, Sofia, Bulgaria
Irena Gjorgjeska Institute of Earthquake Engineering and Engineering Seismology, IZIIS, University Ss. Cyril and Methodius, Skopje, Macedonia
Eduard Nastase National Institute for Earth Physics, Bucharest, Romania
Nikola Filipovic Faculty of Natural Sciences and Mathematics, University of Nis, Nis, Serbia

Bozhin Karaivanov Theoretical Physics Department, Faculty of Physics, Sofia University "St. Kliment Ohridski", Sofia, Bulgaria
Petar Kokarchev Theoretical Physics Department, Faculty of Physics, Sofia University "St. Kliment Ohridski", Sofia, Bulgaria
Mihaela Kouteva Faculty of Structural Engineering, University of Architecture, Civil Engineering and Geodesy, Sofia, Bulgaria
Katarina Kukic University of Belgrade, Belgrade, Serbia
Manea Elena Florinela National Institute for Earth Physics, Bucharest, Romania
Gheorghe Marmureanu National Institute for Earth Physics, Bucharest, Romania
Dimitar Mladenov Theoretical Physics Department, Faculty of Physics, Sofia University "St. Kliment Ohridski", Sofia, Bulgaria
Stephan Mladenov Theoretical Physics Department, Faculty of Physics, Sofia University "St. Kliment Ohridski", Sofia, Bulgaria
Julia Mutaphchieva Theoretical Physics Department, Faculty of Physics, Sofia University "St. Kliment Ohridski", Sofia, Bulgaria
Jasmina Najdovska Seismological Observatory of the Faculty of Natural Sciences and Mathematics, Ss. Cyril and Methodius University, Skopje, Macedonia
Dimitar Nedanovski Institute for Nuclear Research and Nuclear Energy, INRNE, Bulgarian Academy of Sciences, Sofia, Bulgaria
Argyris Nicolaidis Aristotle University of Thessaloniki, Thessaloniki, Greece
Nikolay Nikolov Institute for Nuclear Research and Nuclear Energy, INRNE, Bulgarian Academy of Sciences, Sofia, Bulgaria
Emilian Panaitescu University of Craiova, Craiova, Romania
Antonella Perezan University of Trieste and ICTP, Trieste, Italy
Todor Popov Institute for Nuclear Research and Nuclear Energy, INRNE, Bulgarian Academy of Sciences, Sofia, Bulgaria
Marian Predatu University of Craiova, Craiova, Romania
Gunnar Preussner Imperial College London, UK
Mircea Radulian National Institute for Earth Physics, Bucharest, Romania
Mario Scalet UNESCO Venice Office
Gunter Schuetz Forschungszentrum, Juelich, Germany
Radmila Shalikj Institute of Earthquake Engineering and Engineering Seismology, IZIIS, University Ss. Cyril and Methodius, Skopje, Macedonia
Svetoslav Simeonov National Institute of Geophysics, Geodesy and Geography, NEGGG, Bulgarian Academy of Sciences, Sofia, Bulgaria
Luiza Stefirta University of Craiova, Craiova, Romania
Aleksandar Stephanov Theoretical Physics Department, Faculty of Physics, Sofia University "St. Kliment Ohridski", Sofia, Bulgaria
Mihai Stoicescu University of Craiova, Craiova, Romania
Zhivko Stoyanov Theoretical Physics Department, Faculty of Physics, Sofia University "St. Kliment Ohridski", Sofia, Bulgaria
Alina Streche University of Craiova, Craiova, Romania
Stanislav Varbev Theoretical Physics Department, Faculty of Physics, Sofia University "St. Kliment Ohridski", Sofia, Bulgaria

Tsvetan Vetsov Theoretical Physics Department, Faculty of Physics, Sofia University "St. Kliment Ohridski", Sofia, Bulgaria
Alina Vladut University of Craiova, Craiova, Romania
Soichiro Yasukawa UNESCO Paris
Anton Zabrodin Institute for Theoretical and Experimental Physics, ITEP, Moscow, Russia

Contents

Contributors

V. Čejkovska Seismological Observatory of the Faculty of Natural Sciences and Mathematics, Ss. Cyril and Methodius University, Skopje, Macedonia

D. Černih Seismological Observatory of the Faculty of Natural Sciences and Mathematics, Ss. Cyril and Methodius University, Skopje, Macedonia

C.O. Cioflan Department of Engineering Seismology, National Institute for Earth Physics, Magurele, Bucharest, Romania

Vladimir Dragović The Department of Mathematical Sciences, University of Texas at Dallas, Richardson, TX, USA; Mathematical Institute SANU, Belgrade, Serbia

V.S. Gerdjikov Institute of Nuclear Research and Nuclear Energy, Bulgarian Academy of Sciences, Sofia, Bulgaria

Daniela Ghica National Institute for Earth Physics, Magurele, llfov, Romania

V.G. Kossobokov Institute of Earthquake Prediction Theory and Mathematical Geophysics, Russian Academy of Sciences, Moscow, Russian Federation; The Abdus Salam International Centre for Theoretical Physics, SAND Group, Trieste, Italy; Institut de Physique du Globe de Paris, Paris, France; International Seismic Safety Organization (ISSO), Arsita, Italy

Katarina Kukić Faculty for Traffic and Transport Engineering, University of Belgrade, Belgrade, Serbia

E.F. Manea National Institute for Earth Physics, Department of Engineering Seismology, Magurele, Bucharest, Romania; Faculty of Physics, Department of Atmospheric Physics, University of Bucharest, Bucharest, Romania

Gh. Marmureanu Department of Engineering Seismology, National Institute for Earth Physics, Magurele, Bucharest, Romania

D.M. Mladenov Theoretical Physics Department, Faculty of Physics, Sofia University "St. Kliment Ohridski", Sofia, Bulgaria

Eduard Nastase National Institute for Earth Physics, Magurele, llfov, Romania

Cristian Neagoe National Institute for Earth Physics, Magurele, llfov, Romania

A. Nekrasova Institute of Earthquake Prediction Theory and Mathematical Geophysics, Russian Academy of Sciences, Moscow, Russian Federation; The Abdus Salam International Centre for Theoretical Physics, SAND Group, Trieste, Italy

A. Nicolaidis Theoretical Physics Department, Aristotle University of Thessaloniki, Thessaloniki, Greece

G.F. Panza The Abdus Salam International Centre for Theoretical Physics, SAND Group, Trieste, Italy; Department of Mathematics and Geosciences, University of Trieste, Trieste, Italy; International Seismic Safety Organization (ISSO), Arsita, Italy; Institute of Geophysics, China Earthquake Administration, Beijing, People's Republic of China

A. Peresan The Abdus Salam International Centre for Theoretical Physics, SAND Group, Trieste, Italy; Department of Mathematics and Geosciences, University of Trieste, Trieste, Italy; International Seismic Safety Organization (ISSO), Arsita, Italy

Mihaela Popa National Institute for Earth Physics, Magurele, llfov, Romania

Gunnar Pruessner Department of Mathematics, Imperial College London, London, UK

Mircea Radulian National Institute for Earth Physics, Magurele, llfov, Romania

Gunter M. Schütz Institute for Complex Systems II, Forschungszentrum Jülich, Jülich, Germany; Interdisziplinäres Zentrum für Komplexe Systeme, Universität Bonn, Bonn, Germany

A.A. Stefanov Theoretical Physics Department, Faculty of Physics, Sofia University "St. Kliment Ohridski", Sofia, Bulgaria

D. Toma-Danila National Institute for Earth Physics, Department of Engineering Seismology, Magurele, Bucharest, Romania; Faculty of Geography, University of Bucharest, Bucharest, Romania

S.K. Varbev Theoretical Physics Department, Faculty of Physics, Sofia University "St. Kliment Ohridski", Sofia, Bulgaria

A. Zabrodin Institute of Biochemical Physics, Moscow, Russia; ITEP, Moscow, Russia; International Laboratory of Representation Theory and Mathematical Physics, National Research University Higher School of Economics, Moscow, Russia

Part I
Nonlinear Mathematical Physics Towards Critical Phenomena

Chapter 1
Predictions and Correlations in Self-Organised Criticality

Gunnar Pruessner

Abstract Whether Self-Organised Criticality (SOC) can be used as a tool for prediction of events and event sizes has been subject to quite some debate in the past. While conflicting opinions about predictability have been put forward, there has always been widespread agreement that strong correlations exist in SOC. The following brief review summarises some insights from the study of correlations in SOC models.

1.1 Introduction

Self-Organised Criticality (SOC) was introduced by Bak et al. [1] as an explanation for the frequent occurrence of long time correlations in nature, which were argued to go hand in hand with long ranged spatial correlations. These power law correlations cannot be neglected by "compartmentalising" a system, as each small section is correlated to and thus interacts with every other small section. As the resulting spatio-temporal structures are fractal, Bak, Tang and Wiesenfeld also provided an explanation for the frequent occurrence of fractals in nature and thus gave the research into spatio-temporal fractals in nature a purpose [2].

Although SOC started its life at the interface between condensed matter physics and dynamical systems, it was much more readily embraced by the statistical mechanics community. This is illustrated in the early overview article by Bak and Chen [3]. Although SOC has gone through many revisions, the key concept remains intact: Self-Organised Criticality (supposedly) takes place whenever a spatially extended, non-linearly interacting, slowly driven, intermittent system evolves spontaneously towards the critical point of a continuous phase transition, which is characterised by non-trivial scaling and spatio-temporal power-law correlations.

Unfortunately, over the years SOC became less sharply defined, to the extent that it became unclear whether it describes a phenomenon or provides an explanation

G. Pruessner (✉)
Imperial College London, Department of Mathematics, 180 Queen's Gate, SW7 2AZ London, UK
e-mail: g.pruessner@imperial.ac.uk

B. Aneva and M. Kouteva-Guentcheva (eds.),
Nonlinear Mathematical Physics and Natural Hazards,
Springer Proceedings in Physics 163, DOI 10.1007/978-3-319-14328-6_1

for it. Some of it is owed to a broadening of the scope of some of its proponents, as testified by Bak and Paczuski's [4] review that relates contingency in nature to SOC. There can be no doubt that SOC was conceived in very general terms and applied early on to a whole range of important questions and research fields, such as $1/f$ noise [1, 5], evolution [6, 7], turbulence [8], and earthquakes [9, 10].

In the following, I will try to leave all controversy behind and focus on the question of predictability in SOC. This section will be finished by a brief definition of some of the key models in SOC. I will then review some of the literature on SOC and predictability, in particular in the context of earthquakes. This will be followed by some analytical considerations and by a numerical study presented in Sect. 1.2.1.

1.1.1 The Bak-Tang-Wiesenfeld Model

The Bak-Tang-Wiesenfeld (BTW) Model is the model that started SOC as a field. Its original definition was published in [1], but underwent a small revision shortly afterwards [11]. In that latter form, it is known as the *Abelian* sandpile model. On a d-dimensional lattices sites $\mathbf{n}$ carry $z_{\mathbf{n}}(i) \geq 0$ particles. To *drive* the sandpile, a site $\mathbf{n}$ is chosen at random (and uniformly) and $z_{\mathbf{n}}(i+1) = z_{\mathbf{n}}(i) + 1$ is increased by one. The time i here refers to the *macroscopic* time scale, which is discrete and essentially counts the number of driving steps taken. If a site $\mathbf{n}$ exceeds a certain, globally fixed threshold, $z_{\mathbf{n}}(i) > z^c = q - 1$, it "topples", whereby each of its q nearest neighbours $\mathbf{n}'$ receives one particle, $z_{\mathbf{n}'}(i) \to z_{\mathbf{n}'}(i) + 1$ while its height is reduced by q, $z_{\mathbf{n}}(i) \to z_{\mathbf{n}}(i) - q$. A toppling may give rise to a nearest neighbour exceeding the threshold in turn, which may result in further topplings.

The topplings take place on the microscopic time scale, which is here not stated explicitly as opposed to the macroscopic one, i, which remains unchanged during an avalanche, which is the totality of all topplings following a particle addition by the external drive. As is common among all SOC Models, driving takes place only after an avalanche has finished, i.e. relaxation is very fast compared to the driving, known as a separation of time scale. Because this dynamics preserves the number of particles in the system, a dissipation mechanism must balance the influx by the external driving. Such dissipation is implemented by open boundaries: If a site along on open boundary topples, some of the particles are lost to the missing nearest neighbours.

The fingerprint of criticality is the presence of long ranged spatio-temporal correlations, i.e. correlations that are power law functions in time and space. Because correlation functions are difficult to capture and analyse, derived observables are normally used, in particular the spatio-temporal properties of the avalanches, such as their size s_i (total number of topplings), their area (number of distinct sites toppling) and their duration T_i (number of microscopic time steps, assuming that sites exceeding the threshold are updated simultaneously).

Although the BTW Model is the paradigmatic model of SOC, to this day it remains unclear whether it displays non-trivial scaling [12–14]. On the other hand, the BTW

model is one of the few models in SOC that have been investigated analytically with great success [15–19], even when these studies did not address the question of scaling of entire avalanches directly. The so-called wave-decomposition [20, 21] led to certain conjectures about the governing exponents, but those rely on the assumption of scaling, which is ultimately not supported by numerics.

In the following section I will briefly review two more models before analysing results for the Manna Model with respect to predictability in some detail.

1.1.2 The Olami-Feder-Christensen and the Manna Models

The SOC model best known for its seismological applications is the Olami-Feder-Christensen (OFC) Model [10]. Derived from the Burridge-Knopoff Model [22], it has a continuous local state variable and allows for a degree of dissipation as expected for the relaxation mechanism governing the earth crust. More specifically, on a d-dimensional[1] (hypercubic) lattice each site $\mathbf{n}$ is subject to a certain force $z_{\mathbf{n}}$, which is uniformly ramped up across the system. Once the force at a site reaches the threshold, $z_{\mathbf{n}}(i) = z^c = 1$, the driving stops and a fraction $\alpha q \leq 1$ of the force is re-distributed evenly among its q nearest neighbours, which may in turn exceed the threshold, thereby giving rise to an avalanche. Sites along the boundaries may transfer force across the system's boundary, where it is dissipated. The driving is restored until the force somewhere reaches the threshold. By the model's definition, this is the largest force left after the latest avalanche has ceased.

The OFC model has been extensively studied numerically e.g. [26–31], in particular in two dimensions, but also beyond. Similar to the BTW model, a somewhat mixed picture emerges: In the conservative limit $\alpha = 1/q$, scaling behaviour is widely accepted [26, 31–33], but in the presence of bulk dissipation, $\alpha < 1/q$, the situation is much less clear e.g. [27, 34–38]. Due to its deterministic nature, the OFC Model is prone to periodic behaviour, exploring only a very small fraction of phase space, even when the continuous state variable allows in principle for very rich, even chaotic behaviour. Middleton and Tang [39] pointed at the importance of boundaries in particular for small α, which allows the periodic behaviour to be broken.

The crucial differences between the OFC Model and the BTW Model are continuous state variable, in-built bulk dissipation and the lack of Abelianess[2] in the former. Both, the BTW and the OFC Model, have a deterministic bulk dynamics; if the BTW is driven deterministically, say at the same site, periodic patterns emerge also [40–42]. However, because of the continuous state variable $z_{\mathbf{n}}$ the OFC Model may escape periodicity. One may wonder whether both models nevertheless are trapped in some small phase space volume and are thus unable to fully develop scaling [39, 43, 44].

---

[1] In one dimension, the OFC Model may not display (non-trivial) scaling at all [23, 24], although the closely related Train Model [25] seems to.

[2] Technically, this is a somewhat complicated feature, but in principle Abelianess means that the order of updates of sites about to topple is irrelevant.

There are, in fact, very few SOC models which display all features expected from SOC: Non-trivial spatio-temporal scaling (in particular in correlation functions) without the need to tune an apparent control-parameter to the critical value. One such key model is the Manna Model [45], more specifically, its Abelian variant which is due to Dhar [46]. This is the model used in Sect. 1.2.1 to discuss and illustrate correlations in SOC.

In the Abelian Manna Model, sites $\mathbf{n}$ again carry an non-negative, integer number of particles $z_{\mathbf{n}} \in \mathbb{N}$, but when they exceed the threshold of $z^c = 1$, they re-distribute two of the particles among *randomly and uniformly* chosen nearest neighbours. Again, particles may be lost when sites along the open boundaries topple. Similar to the BTW Model, driving takes place by incrementing the number of particles at a randomly chosen site and ceases while an avalanche is running. However, the randomness in the bulk dynamics allows for a deterministic driving on the same site, resulting in scaling identical to that found in the Oslo Model [47, 48]. The Manna Model displays clear, robust scaling behaviour even in one dimension [45, 48–58].

An intricate link exists between the scaling of the Manna Model, the Oslo Model and the quenched Edwards-Wilkinson equation [48, 59, 60]. As a result, correlations on the *macroscopic* time scale are very well understood in the Manna Model [61]. This will be further discussed in Sect. 1.2.1.

In the following, I will not discuss the thorny issue as to whether or not SOC applies to seismic events, but rather focus on the implications, i.e. if SOC applies, what does that mean for predictability?

1.2 Predictability in SOC

Historically, SOC was put forward by its proponents as a challenge to predictability [62], because activity in SOC systems lacks regularity and it may appear as if it can strike anywhere in the system at any point. While it is clear that SOC systems do not display a periodic onset of activity, it is also clear that correlations exist. In fact, correlations in SOC are algebraic and should therefore provide a very good basis for predictions [63]. In fact, correlations can be used for predictions in the OFC Model [64].

In an email contribution to a discussion on predictability of seismic events, Bak [65] qualified his standpoint further:

> […] earthquakes in SOC models are clustered in time and space […]
>
> We can 'predict' that it is relatively safe to stay in a region with little recent historical activity, as everyone knows. There is no characteristic timescale where the probability starts increasing, as would be the case if we were dealing with a periodic phenomenon. The phenomenon is fractal in space and time, ranging from minutes and hours to millions of years in time, and from meters to thousands of kilometers in space. This behaviour could hardly be more different from Christopher Scholz's description that "SOC refers to a global state…containing many earthquake generating faults with uncorrelated states" and that in the SOC state "earthquakes of any size can occur randomly anywhere at any time".

Before addressing the question whether predictions can be made in SOC systems, one should carefully define what "prediction" refers to. A Poisson process, where each time interval has the same probability to be struck by an event may be seen as the least predictable system. However, if the rate of the events are themselves random variables, then estimating these rates provides a certain level of predictability: It is one thing to say "an event can strike with the same probability at any time" (which says nothing about probabilities) and another to say "on average n events occur over a time interval t" (which is a clear probabilistic statement). Both can derived without the notion of correlations beyond the estimation of a rate in the latter.

In SOC, however, subsequent avalanche sizes are generally correlated. As discussed in detail in [66, Sect. 8.5.4.1], some models can be mapped to a description of their dynamics in the language of interfaces. Avalanche sizes s_i and s_j, with indices $i, j \in \mathbb{N}$ indicating the macroscopic time, i.e. the sequential numbering of events triggered by (roughly) equal initial driving steps, become uncorrelated over a macroscopic time proportional to the fluctuations of the interface. These fluctuations (sometimes referred to as the "wandering" of the interface) scale like L^{χ} with the linear extension L of the system, where χ is the roughness exponent. The ratio $|i-j|/L^{\chi}$ therefore provides a measure for the strength of correlations.

The roughness is known to be related to the (fractal) avalanche dimension D via $D = \chi + d$ [59, 60], which characterises the avalanche frequencies

$$\mathscr{P}(s; L) = s^{-\tau}\mathscr{G}(s/L^{D}), \tag{1.1}$$

i.e. the probability density function of obtaining an avalanche of size s in a system with linear extension L. To ease notation, metric factors [66] have been omitted here and in the following. The exponent τ is the avalanche size exponent, which is often related to the avalanche dimension via the average avalanche size, which scales like $L^{D(2-\tau)}$.

The interface description strictly applies only for boundary-drive. In principle, a second, *microscopic* time scale L^{z} is set by the dynamical exponent z for a system with linear extension L. If the average microscopic time for an avalanche is $\langle T\rangle \propto L^{z(2-\alpha)} = L^{D(1-\tau)+z}$, then correlations on this relaxational time scale decay like $|i-j|\langle T\rangle / L^{z} \propto |i-j|/L^{D(\tau-1)}$, since $D(1-\tau) = z(1-\alpha)$ [66]. Here, α is known as the avalanche duration exponent.

In general, one may expect avalanche sizes to be anti-correlated: A large avalanche is rarely followed by another large avalanche. In fact, there may be very little "energy" left in the system after a system-wide avalanche. In some systems, anti-correlations can be derived analytically [67]. A small avalanche, however, does not pose a constraint. The relation between large and small avalanches are therefore asymmetric: Large ones prevent large ones, but small ones have little or no effect on subsequent avalanches.

The two point correlation function of avalanches sizes s_i, s_j is therefore expected to follow [66, Sect. 8.5.4.1],

$$C(i-j) = \langle s_i s_j \rangle - \langle s_i \rangle \langle s_j \rangle = L^{2D(2-\tau)} \mathscr{C}\left(\frac{|i-j|}{L^{D(\tau-1)}}, \frac{|i-j|}{L^{\chi}} \right), \tag{1.2}$$

and negative for $i - j \neq 0$. The finite size scaling exponent $2D(2-\tau)$ in the equation above is chosen to accommodate $\langle s_i s_j \rangle - \langle s_i \rangle \langle s_j \rangle$ being a multiple of $\langle s \rangle^2 \propto L^{2D(2-\tau)}$ rather than $\langle s^2 \rangle \propto L^{D(3-\tau)}$, as it is reasonable to assume that $\langle s_i s_j \rangle$ converges smoothly to $\langle s_i \rangle \langle s_j \rangle$, whereas $\langle s_i s_j \rangle$ is expected to be singular at $i = j$, if one assumes anti-correlations. In other words, one may anticipate that $C(0) \propto L^{D(3-\tau)} > 0$ and $C(i-j) \propto L^{2D(2-\tau)} < 0$ for $i \neq j$, discontinuously in some suitable limit.

1.2.1 Correlations in the Manna Model

It is relatively straight-forward to measure the correlation function $C(i-j)$ of (1.2). As suggested above, the focus is on $i - j \neq 0$. The following measurements have been taken for the Manna Model in one dimension. Each system was equilibrated for at least 250,000 avalanches (using relatively small system sizes from $L = 64$ to $L = 256$) and statistics was taken from about 4×10^6 measurement. The Mersenne Twister [68] was used as the random number generator throughout.

In the Manna Model $D = 2.253(14)$, $D(2-\tau) = 2$, $z = 1.445(10)$ and $z(1-\alpha) = D(1-\tau)$ [57], so that $D(\tau-1) = D-2 = 0.253(14)$ and $\chi = D-1 = 1.253$ in (1.2) are clearly different. Figure 1.1 shows a collapse of $C(i-j)$ for $i - j > 0$ according to (1.2), but ignoring the dependence on $|i-j|/L^{\chi}$, i.e. $C(i-j)/L^{2D(2-\tau)} \propto \tilde{\mathscr{C}}(|i-j|/L^{D(\tau-1)})$. If $C(i-j)/L^{2D(2-\tau)}$ was plotted against $|i-j|/L^{\chi}$ no collapse would occur. On the other hand, the *shorter* time scale $L^{D(\tau-1)}$ dominates, which may be related to the fact that the interface picture may not apply for the Manna Model which is driven (at randomly chosen sites) in the bulk.

To test this hypothesis, Fig. 1.2 shows a collapse of $C(i-j)$ for the one-dimensional, boundary-driven Manna Model. Due to the driving at the boundary,

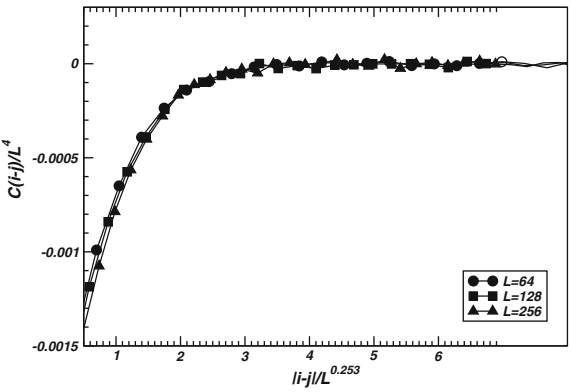

Fig. 1.1 Data collapse of the avalanche size autocorrelation function in the one-dimensional, bulk-driven Manna Model, to confirm (1.2). The collapse could be improved further either by mild adjustments of the exponents or by increasing system size (and possibly also statistics). For technical details see text

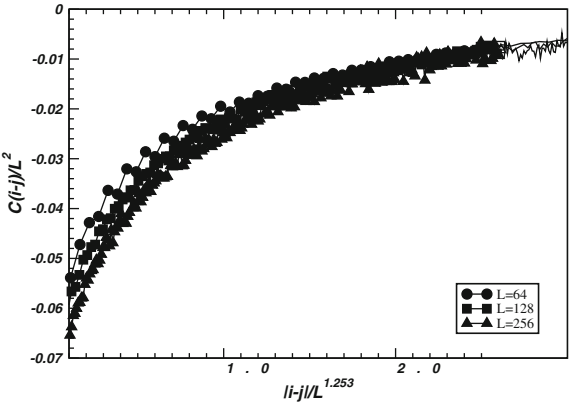

Fig. 1.2 Data collapse of the avalanche size autocorrelation function in the one-dimensional, boundary-driven Manna Model, to confirm (1.2). The collapse could be improved further either by mild adjustments of the exponents or by increasing the system size (and possibly also statistics). For technical details see text

many avalanches terminate early so that a very much increased statistics is required in order to reduce statistical noise to reasonable levels (4×10^6 avalanches for equilibration and about 10^9 avalanches for statistics). This time, the collapse is based on the time scale L^{χ}, but because $D(2-\tau) = 1$ for boundary driving, $\chi = D - d$ coincides with $D(\tau - 1) = D - 1$ as $d = 1$.

1.3 Conclusion

Having confirmed (1.2) in the Manna Model, it is worthwhile speculating about the scaling form of the joint probability function $P(s_i, s_j; |i-j|)$ for the avalanche sizes s_i and s_j obtained $|i-j|$ driving steps apart. For very large $|i-j|$ the joint probability factorises

$$\lim_{|i-j|\to\infty} P(s_i, s_j; L, |i-j|) = P(s_i, L)P(s_j, L) = (s_i s_j)^{-\tau}\mathscr{G}(s_i/L^D)\mathscr{G}(s_j/L^D) \tag{1.3}$$

with avalanche exponent τ, scaling function $\mathscr{G}(x)$ and avalanche dimension D, (1.1). What is the effect of moderate $|i-j|$? Firstly, the time scale to compare to may be either $L^{\chi} = L^{D-d}$ (as is the case in the boundary-driven Manna Model) or $L^z/L^{z(2-\alpha)}$ (as is the case in the bulk-driven Manna Model).

Regardless of the time scale, correlations in SOC models generally produce anti-correlations, whereby large avalanches are likely to be suppressed in the immediate aftermath of large ones. In SOC, the situation is much more fortunate than in real seismic event, as the system can be globally surveyed in SOC, so that it is always known whether a (large) avalanche has terminated or not—the avalanche is finished when everything than can topple has toppled. Whatever has been dislodged during an SOC avalanche is likely to contribute to that very same avalanche. What appears to be two consecutive big events in "real" seismology, may be one big event in a

corresponding SOC Model, which feeds into the ongoing debate about fore- and aftershocks [10, 69–74].

Accepting, however, that large avalanches prevent consecutive (or, in fact, preceding) large avalanches, i.e. that large avalanches repel each other, on a (macroscopic) time scale below, say L^{D-1}, the upper cutoff for consecutive avalanches may be modified to

$$P(s_i, s_j; L, |i-j|) = P(s_i, L)P(s_j, L) = (s_i s_j)^{-\tau}\mathcal{G}(s_i/s_c(s_j, L; i-j))\mathcal{G}(s_j/s_c(s_i, L; i-j)) \tag{1.4}$$

with an s_i-dependent cutoff for s_j, such as

$$s_c(s_i, L; i-j) = \min(L^D, \alpha s_i |i-j|/L^{D-1}) \tag{1.5}$$

with some suitable pre-factor α. It is worth noting that (1.4) does not factorise, because s_c depends on s_i or s_j. However, this remains speculation and requires considerable numerical effort to be tested. It illustrates, however, that there is some, limited predictive power in SOC: Given correlations, only certain joint probability function are possible. Their characteristic time scale determines essentially the (approximately Poissonian) rate with which large avalanches occur. Big systems have a lower rate of their biggest events.

An interesting lesson can be learnt for the interface picture: Numerics suggest that the time scale set by the roughness of the interface applies only for boundary-drive, which is when the interface mapping strictly applies. For bulk-drive, surely the situation is different. However, for boundary-drive in one dimension, there is no difference between the scaling of the roughness $L^\chi = L^{D-1}$ and the time scale set by $L^z/\langle T\rangle = L^{D(\tau-1)} = L^{D-1} = L^\chi$. One may therefore wonder, whether there is only one time scale throughout, namely $L^z/\langle T\rangle$, which is equal to L^χ whenever the interface mapping applies. One may be tempted to test this hypothesis in $d > 1$, where $\chi = D - d$ is no longer identical to $D - 1$, but one may wonder how well the interface picture works in $d > 1$ at all. Because measuring correlations $C(i - j)$ in dimensions greater than unity is computationally very expensive, this is left to future investigations.

Acknowledgments GP gratefully acknowledges the kind support by EPSRC Mathematics Platform grant EP/I019111/1.

References

1. P. Bak, C. Tang, K. Wiesenfeld, Phys. Rev. Lett. **59**(4), 381 (1987)
2. L.P. Kadanoff, Phys. Today **39**(2), 6 (1986). doi:10.1063/1.2814878
3. P. Bak, K. Chen, Physica D **38**(1–3), 5 (1989). Proceedings of a conference held in honour of Benoit B. Mandelbrot's 65th birthday, Les Mas d'Artigny (Vence), France, 1–4 Oct 1989
4. P. Bak, M. Paczuski, Proc. Natl. Acad. Sci. USA **92**(15), 6689 (1995)
5. P. Bak, C. Tang, K. Wiesenfeld, Phys. Rev. A **38**(1), 364 (1988)
6. P. Bak, K. Sneppen, Phys. Rev. Lett. **71**(24), 4083 (1993)

7. K. Sneppen, P. Bak, H. Flyvbjerg, M.H. Jensen, Proc. Natl. Acad. Sci. USA **92**(11), 5209 (1995)
8. P. Bak, K. Chen, C. Tang, Phys. Lett. A **147**(5–6), 297 (1990)
9. P. Bak, C. Tang, K. Wiesenfeld, in *Cooperative Dynamics in Complex Physical Systems*, Proceedings of the Second Yukawa International Symposium, Kyoto, Japan, 24–27 Aug 1988, Springer Series in Synergetics, vol. 43, ed. by H. Takayama (Springer, Berlin, Germany, 1989), Springer Series in Synergetics, vol. 43, pp. 274–279
10. Z. Olami, H.J.S. Feder, K. Christensen, Phys. Rev. Lett. **68**(8), 1244 (1992)
11. D. Dhar, Phys. Rev. Lett. **64**(14), 1613 (1990)
12. A. Chessa, H.E. Stanley, A. Vespignani, S. Zapperi, Phys. Rev. E **59**(1), R12 (1999)
13. S. Lübeck, Phys. Rev. E **61**(1), 204 (2000)
14. P.L. Dorn, D.S. Hughes, K. Christensen, On the avalanche size distribution in the btw model (2001). Preprint from http://www.cmth.ph.ic.ac.uk/kim/papers/preprints/preprint_btw.pdf. Accessed 19 Oct 2010
15. S.N. Majumdar, D. Dhar, Physica A **185**(1–4), 129 (1992)
16. E.V. Ivashkevich, J. Phys. A: Math. Gen. **27**(11), 3643 (1994)
17. S. Mahieu, P. Ruelle, Phys. Rev. E **64**(6), 066130 (2001)
18. P. Ruelle, Phys. Lett. B **539**(1), 172 (2002)
19. M. Jeng, Phys. Rev. E **71**(1), 016140 (2005)
20. D. Dhar, S.S. Manna, Phys. Rev. E **49**(4), 2684 (1994)
21. E.V. Ivashkevich, D.V. Ktitarev, V.B. Priezzhev, Physica A **209**(3–4), 347 (1994)
22. R. Burridge, L. Knopoff, Bull. Seismol. Soc. Am. **57**(3), 341 (1967)
23. S. Zhang, Z. Huang, E. Ding, J. Phys. A: Math. Gen. **29**(15), 4445 (1996)
24. F. Wissel, B. Drossel, New J. Phys. **7**(1), 5 (2005)
25. M. de Sousa Vieira, Phys. Rev. A **46**(10), 6288 (1992)
26. K. Christensen, Z. Olami, Phys. Rev. A **46**(4), 1829 (1992)
27. P. Grassberger, Phys. Rev. E **49**(3), 2436 (1994)
28. C.J. Pérez, Á. Corral, A. Díaz-Guilera, K. Christensen, A. Arenas, Int. J. Mod. Phys. B **10**(10), 1111 (1996)
29. H. Ceva, Phys. Lett. A **245**(5), 413 (1998)
30. S. Lise, M. Paczuski, Phys. Rev. E **63**(3), 036111 (2001)
31. K. Christensen, N.R. Moloney, *Complexity and Criticality* (Imperial College Press, London, UK, 2005)
32. I.M. Jánosi, J. Kértesz, Physica A **200**(1–4), 179 (1993)
33. T.P. Peixoto, C.P.C. Prado, Physica A **342**(1–2), 171 (2004)
34. J.E.S. Socolar, G. Grinstein, C. Jayaprakash, Phys. Rev. E **47**(4), 2366 (1993)
35. S. Bottani, B. Delamotte, Physica D **103**(1–4), 430 (1997)
36. S. Lise, M. Paczuski, Phys. Rev. E **64**(4), 046111 (2001)
37. B. Drossel, Phys. Rev. Lett. **89**(23), 238701 (2002)
38. F. Wissel, B. Drossel, Phys. Rev. E **74**(6), 066109 (2006)
39. A.A. Middleton, C. Tang, Phys. Rev. Lett. **74**(5), 742 (1995)
40. M. Creutz, Physica A **340**(4), 521 (2004). Proceedings of the Symposium Complexity and Criticality: in Memory of Per Bak (1947–2002), Copenhagen, Denmark, 21–23 Aug 2003
41. K. Wiesenfeld, J. Theiler, B. McNamara, Phys. Rev. Lett. **65**(8), 949 (1990)
42. S. Lübeck, N. Rajewsky, D.E. Wolf, Eur. Phys. J. B **13**(4), 715 (2000)
43. F. Torvund, J. Fryland, Phys. Scripta **52**, 624 (1995)
44. N. Mousseau, Phys. Rev. Lett. **77**(5), 968 (1996)
45. S.S. Manna, J. Phys. A: Math. Gen. **24**(7), L363 (1991)
46. D. Dhar, Physica A **263**(1–4), 4 (1999). Proceedings of the 20th IUPAP International Conference on Statistical Physics, Paris, France, 20–24 Jul 1998
47. K. Christensen, Á. Corral, V. Frette, J. Feder, T. Jssang, Phys. Rev. Lett. **77**(1), 107 (1996)
48. H. Nakanishi, K. Sneppen, Phys. Rev. E **55**(4), 4012 (1997)
49. L. Pietronero, A. Vespignani, S. Zapperi, Phys. Rev. Lett. **72**(11), 1690 (1994)
50. A. Ben-Hur, O. Biham, Phys. Rev. E **53**(2), R1317 (1996)

51. A. Chessa, A. Vespignani, S. Zapperi, Comp. Phys. Comm. **121–122**, 299 (1999). Proceedings of the Europhysics Conference on Computational Physics CCP 1998, Granada, Spain, 2–5 Sept 1998
52. O. Biham, E. Milshtein, O. Malcai, Phys. Rev. E **63**(6), 061309 (2001)
53. R. Pastor-Satorras, A. Vespignani, Eur. Phys. J. B **19**(4), 583 (2001)
54. R. Dickman, J.M.M. Campelo, Phys. Rev. E **67**(6), 066111 (2003)
55. S. Lübeck, P.C. Heger, Phys. Rev. E **68**(5), 056102 (2003)
56. S. Lübeck, Int. J. Mod. Phys. B **18**(31/32), 3977 (2004)
57. H.N. Huynh, G. Pruessner, L.Y. Chew, J. Stat. Mech. **2011**(09), P09024 (2011)
58. H.N. Huynh, G. Pruessner, Phys. Rev. E **85**, 061133 (2012)
59. M. Paczuski, S. Boettcher, Phys. Rev. Lett. **77**(1), 111 (1996)
60. G. Pruessner, Phys. Rev. E **67**(3), 030301(R) (2003)
61. L. Pickering, G. Pruessner, K. Christensen, Avalanche size moments in soc models are linear in the driving (2012). To be published
62. P. Bak, C. Tang, J. Geophys. Res. **94**(B11), 15635 (1989)
63. D. Sornette, M.J. Werner, in *Encyclopedia of Complexity and Systems Science*, vol. 9, ed. by R.A. Meyers (Springer, New York, 2009), pp. 7872–7891
64. S.L. Pepke, J.M. Carlson, Phys. Rev. E **50**(1), 236 (1994)
65. P. Bak. Earthquake precursors and crustal 'transients' (1999). http://www.nature.com/nature/debates/earthquake/equake_10.html. Accessed 13 Jun 2014
66. G. Pruessner, *Self-Organised Criticality* (Cambridge University Press, Cambridge, 2012)
67. P. Welinder, G. Pruessner, K. Christensen, New J. Phys. **9**(5), 149 (2007)
68. M. Matsumoto, T. Nishimura, ACM Trans. Model. Comp. Sim. **8**(1), 3 (1998)
69. K. Christensen, Z. Olami, J. Geophys. Res. **97**(B6), 8729 (1992)
70. Z. Olami, K. Christensen, Phys. Rev. A **46**(4), R1720 (1992)
71. S. Hergarten, H.J. Neugebauer, Phys. Rev. Lett. **88**(23), 238501 (2002)
72. P. Bak, K. Christensen, L. Danon, T. Scanlon, Phys. Rev. Lett. **88**(17), 178501 (2002)
73. P. Bak, K. Christensen, L. Danon, T. Scanlon, Proc. Natl. Acad. Sci. USA **99**(Suppl. 1), 2509 (2002). (Colloquium)
74. Y.Y. Kagan, Phys. Earth Planet. Interiors **135**(2–3), 173 (2003)

Chapter 2
The Space-Time Structure of Extreme Current and Activity Events in the ASEP

Gunter M. Schütz

Abstract A fundamental question in the study of extreme events is whether during a rare and strong fluctuation a system exhibits phenomena that are qualitatively different from its typical behaviour. We answer this question quantitatively for the asymmetric simple exclusion processes (ASEP) on a ring, conditioned to an atypically large particle current or an atypical large hopping activity. We show that this classical problem is related to the integrable quantum Heisenberg ferromagnet. For strongly atypical fluctuations we show that the equal-time density correlations decay algebraically, as opposed to the typical stationary correlations which are short-ranged. We compute the exact dynamical structure factor which shows that that the dynamical exponent in the extreme regime is $z = 1$ rather than the KPZ exponent $z = 3/2$ for typical behaviour. An open problem is the transition point from typical to extreme.

2.1 Introduction

In a many-body system with noisy dynamics intrinsic fluctuations may occur that drive characteristic properties of the system far away from their typical values. An example of this problem, that has attracted great attention in the last decade, are fluctuations of the entropy production and related thermodynamic quantities such as heat and work [1, 2]. Of interest in this context are not only the tails of the probability distribution or the the statistics of extreme events, but particularly the space-time structure of the system undergoing such a rare and intrinsic fluctuation.

Generally, in equilibrium systems, time-reversal symmetry implies that the fluctuation out of an extreme event is the mirror image of the fluctuation that led into it. Unfortunately, little more can be said generally. In systems that are driven permanently out of equilibrium, even less is known. The distribution of the entropy

G.M. Schütz (✉)
Institute for Complex Systems II, Forschungszentrum Jülich, 52425 Jülich, Germany
e-mail: g.schuetz@fz-juelich.de

G.M. Schütz
Interdisziplinäres Zentrum für Komplexe Systeme, Universität Bonn, Brühler Straße 7, 53119 Bonn, Germany

B. Aneva and M. Kouteva-Guentcheva (eds.),
Nonlinear Mathematical Physics and Natural Hazards,
Springer Proceedings in Physics 163, DOI 10.1007/978-3-319-14328-6_2

production satisfies the Gallavotti-Cohen symmetry (or similar relations [1, 2]). However, the absence of time-reversal symmetry does not allow for generally valid predictions of temporal behaviour.

A notable exception from this unfortunate state of affairs are driven diffusive systems, i.e., lattice gas models for stochastic interacting particle systems [5–8]. For example, it could be demonstrated for a specific lattice gas model, the zero-range process with open boundary conditions [9, 10], that a failure of the celebrated Gallavotti-Cohen symmetry [3, 4] of the distribution function for entropy production can arise from a real-space condensation phenomenon [11, 12]. A macroscopic fluctuation theory, based on the seminal papers [13, 14] allows for the computation of macroscopic density profiles during a long event of strongly atypical particle current or hopping activity. Interestingly, for a particular model system, the asymmetric simple exclusion process (ASEP, see below) a dynamical phase transition occurs from a macroscopically flat density profile to a travelling shock/antishock wave (atypically low current in the driven case [15]) or a phase separation arises (low activity in the undriven system [16]). Microscopic information about atypically low currents has recently been obtained for the ASEP [17, 18] by making use of the mapping of the generator of the ASEP to the Heisenberg quantum ferromagnet.

Following [19, 20] we use this approach to consider here the microscopic space-time structure of the ASEP for *large* atypical current, and, going beyond our earlier work, also for atypical activity. We derive detailed information about equal-time correlations, relaxation times and the dynamical structure function, which indicate a qualitative change of the typical dynamics in the universality class of the Kardar-Parisi-Zhang equation with dynamical exponent $z = 3/2$ [21] to a ballistic universality class with $z = 1$ [22] during extreme events of strong current or activity.

2.2 Grandcanonical Conditioning for the ASEP

We proceed to define the model and to exhibit its relationship to the ferromagnetic Heisenberg quantum spin chain. Then we define the conditioned dynamics and illustrate the setting for independent particles.

2.2.1 The Asymmetric Simple Exclusion Process

The asymmetric simple exclusion process (ASEP) [6–8] with periodic boundary conditions is a lattice gas model for a driven diffusive system where each site k on a ring of L sites can be occupied by at most one particle. Particles hop randomly to empty nearest neighbour sites after an exponentially distributed random time with mean $1/(p + q)$. A jump to the right (in clockwise direction) is attempted with probability $p/(p + q)$ and to the left (anticlockwise) with probability $q/(p + q)$. If the target site is already occupied, the jump attempt is rejected. Physically, this

models an on-site excluded-volume interaction. We shall set $p = we^{\phi}$ and $q = we^{-\phi}$. Here w plays the role of an attempt frequency of jumps and ϕ is proportional to a driving force that acts on the particles. Without loss of generality we shall assume $\phi > 0$ throughout this article. We denote a microscopic configuration of the ASEP η and the local occupation number by $\eta(k) \in \{0, 1\}$. The total number of particles $N = \sum_k \eta(k)$ is conserved. Originally the model was introduced in a biophysics context to describe the kinetics of biopolymerization on RNA [23, 24] and independently in the probabilistic literature to study the emergence of large scale hydrodynamic behaviour [25].

2.2.1.1 Master Equation

This Markovian jump dynamics can be described in terms of a master equation for the time evolution for the probability $P(\eta, t)$ to find the configuration η at time $t \geq 0$. It is convenient to introduce a column vector $|P(t)\rangle$ which has these 2^L probabilities as components. To this end we assign to a configuration η a canonical basis vector $|\eta\rangle = |\eta(1)\rangle \otimes |\eta(1)\rangle \otimes \cdots \otimes |\eta(L)\rangle \in (\mathbb{C}^2)^{\otimes L}$ where $|0) = (1, 0)^T$ and $|1) = (0, 1)^T$ are the canonical basis vectors of $\mathbb{C}^2$ and the superscript T denotes transposition [7]. By introducing also a dual basis of row vectors $\langle\eta|$ and inner product $\langle\eta|\eta'\rangle = \delta_{\eta,\eta'}$ we can write $P(\eta, t) = \langle\eta|P(t)\rangle$ with $|P(t)\rangle := \sum_\eta P(\eta, t)|\eta\rangle$. The master equation then takes the form

$$\frac{d}{dt}|P(t)\rangle = -H|P(t)\rangle \tag{2.1}$$

where the off-diagonal matrix elements $H_{\eta',\eta}$ of the generator H are the negative transition rates for transitions from η to η' and the diagonal elements are the inverse sojourn times of a configuration η, i.e., $H_{\eta,\eta} = \sum'_\eta H_{\eta',\eta}$. Notice that this construction implies that the summation vector $\langle s| := \sum_\eta \langle\eta|$ is a left eigenvector of H with eigenvalue 0. This property expresses conservation of probability $d/dt \sum_\eta P(\eta, t) = d/dt\langle s|P(t)\rangle = -\langle s|H|P(t)\rangle = 0$.

The corresponding right eigenvector with eigenvalue 0 is a stationary distribution $|P^*\rangle$ of the process. For periodic boundary conditions and fixed number of particles N this is the uniform distribution that gives equal probability to all microscopic configurations with N particles, independently of the driving force ϕ which is a direct consequence of pairwise balance [26]. From these uniform canonical distributions one can construct also a grand canonical distribution which is uncorrelated, i.e., on each lattice on finds a particle with probability ρ, independent of the occupation of other sites. In the thermodynamic limit these two stationary distributions become equivalent for $\rho = N/L$. The stationary current takes the form $j^* = 2w \sinh(\phi)\rho(1 - \rho)$. The apparent (and unphysical) divergence of the current with the driving force stems from the fact that for convenience we have chosen the time scale of the process to be given by p and q. As will be seen below a physically more natural choice is a normalization by the inverse mean time $p + q = 2w \cosh(\phi)$ of jump attempts of a single particle.

The time-dependent solution of (2.1) has the simple form $|P(t)\rangle = \exp(-Ht)|P_0\rangle$ for an initial distribution $|P_0\rangle := |P(0)\rangle$. In particular, we have for the transition probability $P(\eta_2, t|\eta_1, 0)$ into a configuration η_2, starting from η_1,

$$P(\eta_2, t|\eta_1, 0) = \langle \eta_2 | \mathrm{e}^{-Ht} | \eta_1 \rangle. \tag{2.2}$$

For the expectation of a function $f(\eta)$ we obtain

$$\langle f(t) \rangle := \sum_{\eta} F(\eta) P(\eta, t) = \langle \eta | \hat{f} \mathrm{e}^{-Ht} | P_0 \rangle \tag{2.3}$$

where $\hat{f} = \sum_\eta f(\eta)|\eta\rangle\langle\eta|$ is a diagonal matrix with the values $f(\eta)$ on its diagonal. The real part of eigenvalues of the generator are the inverse relaxation times of the system.

2.2.1.2 Link to Quantum Systems

The point behind choosing the tensor basis is the fact that the generator H of the ASEP takes the form

$$H = -w \sum_{k=1}^{L} \left[\mathrm{e}^{\phi} (\sigma_k^+ \sigma_{k+1}^- - \hat{n}_k(\mathbb{1} - \hat{n}_{k+1})) + \mathrm{e}^{-\phi} (\sigma_k^- \sigma_{k+1}^+ - (\mathbb{1} - \hat{n}_k)\hat{n}_{k+1}) \right] \tag{2.4}$$

with the matrices

$$\sigma^+ = \begin{pmatrix} 0 & 1 \\ 0 & 0 \end{pmatrix}, \quad \sigma^- = \begin{pmatrix} 0 & 0 \\ 1 & 0 \end{pmatrix}, \quad \hat{n} = \begin{pmatrix} 0 & 0 \\ 0 & 1 \end{pmatrix}, \tag{2.5}$$

the two-dimensional unit matrix $\mathbb{1}$ and the notation $\hat{x}_k := \mathbb{1} \otimes \cdots \otimes \hat{x} \otimes \ldots \mathbb{1}$ indicating that the two-dimensional matrix $\hat{x}$ acts non-trivially on the factor k in tensor space, corresponding to site k in the ring. One recognizes in (2.4) the quantum Hamiltonian of the spin-1/2 Heisenberg ferromagnet with an imaginary Dzyaloshinsky-Moriya interaction term [27, 28]. This is an integrable model that can be solved with the Bethe ansatz. The form of the master equation (2.1) and of the generator (2.4) has given this tensor basis approach the name quantum Hamiltonian formalism. It allows the application of mathematical techniques borrowed from quantum mechanics to treat this problem of classical stochastic dynamics.

For future purposes we split H into three parts

$$H = H^+ + H^- + H^0 \tag{2.6}$$

where $H^+ = -we^{\phi} \sum_k \sigma_k^+ \sigma_{k+1}^-$ generates jumps to the right, $H^- = -we^{-\phi} \sum_k \sigma_k^- \sigma_{k+1}^+$ generates jumps to the left and H^0 is the diagonal part for the conservation of probability.

2.2.1.3 Non-interacting Particles

For reference purposes we also consider non-interacting particles. In this case each lattice site can be occupied by an arbitrary integer number $\eta(k) \in \mathbb{N}$ of particles. The generator H takes form [29, 30]

$$H = -w \sum_{k=1}^{L} \left[e^{\phi} (\hat{a}_k^- \hat{a}_{k+1}^+ - \hat{n}_k) + e^{-\phi} (\hat{a}_k^+ \hat{a}_{k+1}^- - \hat{n}_{k+1}) \right] \tag{2.7}$$

where the infinite-dimensional local hopping matrices have matrix elements $(\hat{a}^+)_{ij} = \delta_{i,j+1}$, $(\hat{a}^-)_{ij} = i\delta_{i+1,j}$ (with $i, j \in \mathbb{N}$) and with the diagonal number operator $(\hat{n})_{ij} = i\delta_{i,j}$. Notice that here a^+ (a^-) creates (annihilates) a particle. In the single-site basis one has $\hat{a}^+|k) = |k+1)$ $\forall k \in \mathbb{N}$ and $\hat{a}^-|0) = 0$, $\hat{a}^-|k) = k|k-1)$ $\forall k \geq 1$. The number operator is given by $\hat{n} = \hat{a}^+\hat{a}^-$. These operators commute at different sites and satisfy the harmonic oscillator algebra $[\hat{a}_k^-, \hat{a}_l^-] = [\hat{a}_k^+, \hat{a}_l^+] = 0$, $[\hat{a}_k^-, \hat{a}_l^+] = \delta_{k,l}$ for the same site. In quantum language (2.7) is the Hamiltonian for non-interacting bosons hopping on a lattice under the influence of an driving field with imaginary amplitude, analogous to the Dzyaloshinsky-Moriya interaction. Also the generator (2.7) can be split naturally into three parts analogous to (2.6).

The ground state with eigenvalue 0, corresponding to the stationary distribution of the system, is the projection on N particles of the grand canonical factorized distribution where on each lattice site the number of particles is Poisson distributed with parameter ρ. Here ρ is the average particle density. The factorization property of the grand canonical distribution implies the absence of density correlations between different sites. The dynamics of fluctuations can be studied by considering the dynamical structure function $S(r,t) = \langle \eta(k+r,t)\eta(k,0) \rangle - \rho^2$ where the expectation is taken in the stationary distribution. Since the particles are non-interacting, the dynamical structure function satisfies a lattice diffusion equation with a constant drift term. On large space and time scales its solution is the Gaussian which is invariant under dynamical scaling $r \to ar$, $t \to a^z t$ where $z = 2$ is the dynamical exponent of the diffusive universality class.

2.2.2 Grandcanonically Conditioned Dynamics

The master equation describes the evolution of the probability distribution of the configurations η, but does not provide any information about the number of jumps that have occurred to reach a given final configuration at some time T. To describe

also these properties of the process we introduce $J^{\pm}(T)$ as the number of jumps to the right (left) up to time T and also the integrated current $J(T) := J^{+}(T) - J^{-}(T)$ and the integrated activity $A(T) := J^{+}(T) + J^{-}(T)$. These are random numbers with initial value 0 at time 0 that depend on the particular realization of the stochastic dynamics.

2.2.2.1 Joint Generating Function

Following [1, 31] the joint generating function $Y(\lambda, \mu, T) = \langle \exp(\lambda J(T) + \mu A(T)) \rangle$ for the distribution of A and J is given by

$$Y(\lambda, \mu, T) = \langle s | \mathrm{e}^{-\tilde{H}(\lambda,\mu)T} | P_0 \rangle. \tag{2.8}$$

Here

$$\tilde{H}(\lambda, \mu) = \mathrm{e}^{\lambda+\mu} H^{+} + \mathrm{e}^{-\lambda+\mu} H^{-} + H^{0} \tag{2.9}$$

which in the case of the ASEP is also an integrable quantum Heisenberg ferromagnet with imaginary Dzyaloshinsky-Moriya interaction. For non-interacting particles one has a similar expression with the generator (2.7).

Notice that the generating function is by definition the average over all final microscopic configurations η and all realizations of the process with final values $J(T) = J$ and $A(T) = A$. This generating function is formally analogous to a grandcanonical partition function where the intensive variables λ and μ are conjugate to the extensive variables J and A (proportional to time T and length L).

Analogously we can study grandcanonically conditioned expectations of functions $f(\eta)$ of a configuration η. These are the quantities

$$\langle f(T) \rangle_{P_0}^{\lambda,\mu} := \langle s | \hat{f} \mathrm{e}^{-\tilde{H}(\lambda,\mu)T} | P_0 \rangle / Y(\lambda, \mu, T) \tag{2.10}$$

In particular, for $f(\eta) = \mathbf{1}_{\eta}$ which is represented by the projector $\hat{f} = |\eta\rangle\langle\eta|$ we find for the grand-canonically conditioned probability distribution $P^{\lambda,\mu}(\eta, T) := \langle \eta | \mathrm{e}^{-\tilde{H}(\lambda,\mu)T} | P_0 \rangle / Y(\lambda, \mu, T)$. Therefore the fundamental quantity of interest is the weighted probability distribution

$$|P^{\lambda,\mu}(T)\rangle := \mathrm{e}^{-\tilde{H}(\lambda,\mu)T} | P_0 \rangle. \tag{2.11}$$

In the limit $T \to \infty$ we have asymptotically

$$\mathrm{e}^{-\tilde{H}(\lambda,\mu)T} \sim \frac{|g\rangle\langle g|}{\langle g | g \rangle} \mathrm{e}^{-g(\lambda,\mu)T} \tag{2.12}$$

where $g(\lambda, \mu)$ is the lowest eigenvalue of $\tilde{H}(\lambda, \mu)$ and $|g\rangle$ ($\langle g|$) is the corresponding right (left) eigenvector whose components we denote by $g^R_{\lambda,\mu}(\eta)$ ($g^L_{\lambda,\mu}(\eta)$). Since $\tilde{H}(\lambda, \mu)$ is in general not symmetric the notion of the lowest eigenvalue refers to the lowest real part.

2.2.2.2 Optimal Paths

With this approach one can study also how the particle configuration behaves at intermediate times t within the conditioning time interval $[0, T]$. This yields the answer to the question how the *typical* time evolution of an *untypical* fluctuation is realized, or, in other words, what is the optimal path that a random variable takes under conditioned dynamics. The conditional expectation of a one-time observables $f(\eta)$ at time t is given by

$$\langle f(t)\rangle^{\lambda,\mu,T}_{P_0} := \langle s|\mathrm{e}^{-\tilde{H}(\lambda,\mu)(T-t)}\hat{f}\mathrm{e}^{-\tilde{H}(\lambda,\mu)t}|P_0\rangle/Y(\lambda,\mu,T) \tag{2.13}$$

For long conditioning period $T \to \infty$ we define edge intervals $[0, u]$ and $[T - v, T]$ and consider $t \in [u, T - v]$. In the limit $u, v \to \infty$ we use (2.12) to find that $\langle f(t)\rangle^{\lambda,\mu,T}_{P_0} \to \langle g|\hat{f}|g\rangle/\langle g|g\rangle =: \sum_\eta f(\eta)P^*_{\lambda,\mu}(\eta)$ is independent of t inside the observation window and also independent of the initial distribution. The interpretation is that between an initial transient period and a final transient period the conditioned system is in a stationary state with stationary conditional distribution

$$P^*_{\lambda,\mu}(\eta) = g^R_{\lambda,\mu}(\eta)g^L_{\lambda,\mu}(\eta)/Z(\lambda,\mu). \tag{2.14}$$

Here $Z(\lambda, \mu) = \langle g|g\rangle = \sum_\eta g^R_{\lambda,\mu}(\eta)g^L_{\lambda,\mu}(\eta)$ is the normalization factor.

For two observables $f_a(\eta)$, $f_b(\eta)$ at different times $t_1, t_2 \in [u, T - v]$ with $t_1 \le t_2$ one finds in the limit $u, v \to \infty$

$$\langle f_b(t_2)f_a(t_1)\rangle^{\lambda,\mu,T}_{P_0} \to \langle g|\hat{f}_b\mathrm{e}^{-[\tilde{H}(\lambda,\mu)-g(\lambda,\mu)]\tau}\hat{f}_a|g\rangle/Z(\lambda,\mu) \tag{2.15}$$

with $\tau = t_2 - t_1$. As expected from a stationary process, the two-time correlation function depends only on the time difference τ.

2.2.2.3 Effective Dynamics

Defining the diagonal matrix $\Delta(\lambda, \mu)$ with the components $g^L_{\lambda,\mu}(\eta)$ of the *left* eigenvector on the diagonal and defining the transformed Hamiltonian

$$G = \Delta\tilde{H}\Delta^{-1} - g \tag{2.16}$$

we can rewrite (2.15) as

$$\langle f_b(t_2) f_a(t_1)\rangle_{P_0}^{\lambda,\mu,T} \to \langle s|\hat{f}_b \mathrm{e}^{-G(\lambda,\mu)\tau}\hat{f}_a|P^*_{\lambda,\mu}\rangle. \tag{2.17}$$

In other words, the conditioned two-time correlation function turns into the stationary correlation function of an effective process given by G. This effective process is a dynamics under which the atypical, conditioned dynamics of the original process become unconditioned, typical dynamics [32]. It realizes an optimal path (in the sense described above) as typical path. The stationary distribution of this effective process is given by (2.14).

2.2.3 Conditioned Dynamics in the Noninteracting Case

It is instructive to apply the grandcanonical conditioning to the case of non-interacting particles. Since in this case H^+, H^- and H^0, defined in (2.7) through (2.9), all mutually commute, all eigenvectors are independent of μ and λ. Because of the harmonic oscillator algebra all terms can be diagonalized simultaneously by Fourier transformation (see e.g. [7] for details). In terms of the Fourier modes p one obtains $\tilde{H} = \sum_p \varepsilon(p)\hat{b}_p^+\hat{b}_p^-$ where the momenta p are of the form $p = 2\pi m/L$ with $m \in \{0, 1, 2, \ldots, L-1\}$ and the summation over all p amounts to a summation over all m. For the single-particle energy one has

$$\varepsilon(p) = w\left[2\cosh\phi - \mathrm{e}^{\mu}(\mathrm{e}^{\lambda+\phi}\mathrm{e}^{ip} + \mathrm{e}^{-\lambda-\phi}\mathrm{e}^{-ip})\right] \tag{2.18}$$

The N-particle eigenstates are of the form $\hat{b}^+_{p_1}\ldots\hat{b}^+_{p_N}|0\rangle$ where $|0\rangle$ is the vacuum state with no particles. The corresponding eigenvalues are the sum of the single particle energies with momenta p_i. Hence the lowest eigenvalue in the N-particle sector is obtained for choosing all momenta to be 0 which yields

$$g(\lambda,\mu) = Nw\left[2\cosh\phi - \mathrm{e}^{\mu+\lambda+\phi} - \mathrm{e}^{\mu-\lambda-\phi}\right]. \tag{2.19}$$

This result allows us to describe the effective conditioned dynamics. Since the ground state does not depend on μ and λ we have that the transformation matrix Δ is the unit operator. Hence

$$G = \tilde{H} - g = -w\mathrm{e}^{\mu}\sum_{k=1}^{L}\left[\mathrm{e}^{\lambda+\phi}(\hat{a}_k^-\hat{a}_{k+1}^+ - \hat{n}_k) + \mathrm{e}^{-\lambda-\phi}(\hat{a}_k^+\hat{a}_{k+1}^- - \hat{n}_{k+1})\right] \tag{2.20}$$

which is similar to the original process (2.7), but with renormalized hopping rates

$$\tilde{p} = \mathrm{e}^{\lambda+\mu}p, \quad \tilde{q} = \mathrm{e}^{-\lambda+\mu}q. \tag{2.21}$$

Therefore conditioning on higher than typical activity ($\mu > 0$) corresponds to a higher frequency $\tilde{w} = we^{\mu}$ for jumps. Conditioning on higher than typical current ($\lambda > 0$) corresponds to a stronger driving force $\tilde{\phi} = \phi + \lambda$. All other fluctuations in the dynamics remain unchanged. Therefore, non-interacting particles conditioned on high activity and/or current behave essentially like under typical conditions, except that jumps occur with higher frequency and the hopping bias is stronger. Phrased differently, one can generate the effective dynamics, where the untypical extreme behaviour of the original dynamics becomes typical, just by changing the jump frequency and the driving field. Conditioning on extreme behaviour does not lead to any change in universal properties of the dynamics. Long-range correlations in the stationary distribution remain absent and one has diffusive relaxation with dynamical exponent $z = 2$.

It is natural to define the intrinsic time scale of the process by normalizing by the inverse sum of the hopping rates, i.e., the mean sojourn time of a particle. Then the normalized effective dynamics becomes independent of μ, i.e., conditioning on untypical activity does not change the normalized dynamics. In the limit of high current ($\lambda \to \infty$) the hopping becomes totally asymmetric.

2.3 Results for the ASEP

Even though the Hamiltonian (2.6) is exactly solvable via Bethe ansatz it is very hard to extract for general λ and μ explicit results for the weighted distribution (2.11) for finite time T or the stationary correlations (2.17) in the infinite-time limit. Nevertheless, some special cases can be studied in some detail.

2.3.1 Bethe Ansatz Equations

In order to obtain the Bethe ansatz equations for the spectrum of $\tilde{H}$ we introduce new notation. Instead of labelling basis vectors by occupation number we choose the particle positions which we shall denote by $k_i \mod L$ for the ith particle and by $\mathbf{k} = \{k_1, \ldots, k_N\}$ the ordered set of all coordinates. The particle label $i \in \{1, 2, \ldots, N\}$ is associated with the particles whose order remains preserved in the time evolution. We also introduce $\mathbf{z} = \{z_1, \ldots, z_N\}$ where the z_i can be thought of as exponentials of (possibly complex) pseudomomenta and the quantities

$$a_{ij} = \tilde{p} + \tilde{q} z_i z_j - (p + q) z_i . \tag{2.22}$$

Notice the appearance of the modified rates (2.21) in this definition.

The Bethe ansatz for the right eigenvectors $|\mathbf{z}\rangle$ (see e.g. [19, 28, 31] for the present context) is given by

$$|\mathbf{z}\rangle = \sum_{1\le k_1<k_2<k_3\le L} \sum_{\sigma\in S_N} A_\sigma\, z_{\sigma(1)}^{k_1} z_{\sigma(2)}^{k_2} \ldots z_{\sigma(N)}^{k_N} |\mathbf{k}\rangle = \sum_{1\le k_1<k_2<k_3\le L} Y(\mathbf{k})|\mathbf{k}\rangle \tag{2.23}$$

where the second sum is over all permutations σ of the N particle labels and the coefficients A_σ are given by

$$\frac{A_{\ldots\sigma(ij)\ldots}}{A_{\ldots ij\ldots}} = -\frac{a_{ji}}{a_{ij}} = -\frac{p\mathrm{e}^{\lambda+\mu} + q\mathrm{e}^{-\lambda+\mu} z_i z_j - (p+q)z_j}{p\mathrm{e}^{\lambda+\mu} + q\mathrm{e}^{-\lambda+\mu} z_i z_j - (p+q)z_i}. \tag{2.24}$$

Periodic boundary conditions leads to a quantization condition: The Bethe roots z_j satisfy the Bethe ansatz equations

$$z_k^L = (-1)^{N-1} \prod_{i=1}^{N} \frac{p\mathrm{e}^{\lambda+\mu} + q\mathrm{e}^{-\lambda+\mu} z_i z_k - (p+q)z_k}{p\mathrm{e}^{\lambda+\mu} + q\mathrm{e}^{-\lambda+\mu} z_i z_k - (p+q)z_i} \tag{2.25}$$

for arbitrary N. The eigenvalue $\varepsilon(\mathbf{z})$ of a Bethe eigenvector is a sum of single-particle excitation energies

$$\varepsilon(\mathbf{z}) = \sum_{i=1}^{N} \varepsilon(z_i) \tag{2.26}$$

where $\varepsilon(z_i) = -z_i a_{ii}(z^{-1})$ (cf. (2.18) with the identification $z = \mathrm{e}^{ip}$). The rescaled single-particle energies read

$$\tilde{\varepsilon}(z) = \frac{2\mathrm{e}^{-\mu}\cosh(\phi) - \mathrm{e}^{\phi+\lambda} z - \mathrm{e}^{-\phi-\lambda} z^{-1}}{\mathrm{e}^{\phi+\lambda} + \mathrm{e}^{-\phi-\lambda}}. \tag{2.27}$$

For typical behaviour $\lambda = \mu = 0$ the Bethe ansatz equations (2.25) have been analyzed in [27, 28]. It turns out that the real part of the energy gap, which yields the inverse of the longest relaxation time, scales with system size as L^{-z} with the dynamical exponent $z = 3/2$ of the Kardar-Parisi-Zhang (KPZ) universality class [21]. Therefore the exclusion interaction changes the dynamical universality class from diffusive (in the non-interacting case) to KPZ. The stationary distribution, however, is uncorrelated, as is the case for non-interacting particles.

2.3.2 *Stationary State for High Activity or High Current*

In the limit of high activity $\mu \to \infty$ or high current $|\lambda| \to \infty$ the Bethe equations (2.25) simplify considerably. The right hand side reduces to the factor $(-1)^{N-1}$ which

means that the Bethe roots are of the form $z_k = \mathrm{e}^{2\pi i m_k/L}$ where m_k is either integer (N odd) or half integer (N even). As pointed out in [19] the model becomes a free fermion system. The N-particle wave function $Y(\mathbf{k})$ becomes a Slater determinant

$$Y(\mathbf{k}) = \det \begin{vmatrix} z_1^{k_1} & z_1^{k_2} & \cdots & z_1^{k_N} \\ z_2^{k_1} & z_2^{k_2} & \cdots & z_2^{k_N} \\ \cdots & \cdots & \cdots & \cdots \\ z_N^{k_1} & z_N^{k_2} & \cdots & z_N^{k_N} \end{vmatrix}. \tag{2.28}$$

Following [19] the ground state corresponds to the choice of Bethe roots $m_k = k - (N-1)/2$ with $k = 0, 1, 2, \ldots, N-1$. The stationary distribution can then be expressed in the form of a double product

$$P_L(\mathbf{k}) = \frac{2^{N(N-1)}}{L^N} \prod_{1 \le i < j \le N} \sin^2\left(\pi \frac{k_i - k_j}{L}\right) \tag{2.29}$$

From this one obtains the well-known expression [33] for the static two-point density correlation for the particle occupation numbers

$$S(r) := \langle \eta(k)\eta(k+r)\rangle - \rho^2 = -\frac{\sin^2 r\pi\rho}{r^2\pi^2}. \tag{2.30}$$

Remarkably, the correlations decay algebraically, unlike for typical dynamics where the stationary distribution is uncorrelated, or in the non-interacting case where also the conditioned stationary distribution is uncorrelated.

For the stationary current per site we find after rescaling of the time scale

$$j^* = \frac{\tanh(\tilde{\phi}) \sin(\pi\rho)}{L \sin(\pi/L)} \tag{2.31}$$

with $\tilde{\phi} = \phi + \lambda$. In this quantity another interesting feature appears: The finite-size corrections are of order $1/L^2$ rather than of order $1/L$ which is expected from typical behaviour in systems with short-range interactions. In the thermodynamic limit $L \to \infty$ we get

$$j^* = \frac{1}{\pi} \tanh(\tilde{\phi}) \sin(\pi\rho) \tag{2.32}$$

2.3.3 Dynamical Properties

The relaxational behaviour is encoded in the spectrum of $\tilde{H}$, which can be computed using the free fermion structure of the process conditioned on large activity $\mu \to \infty$.

In order to do so we rescale time by the effective single-particle sojourn time and adapt the approach of [19] to the present case where

$$\tilde{H} = -\frac{1}{2\cosh\tilde{\phi}} \sum_{k=1}^{L} \left[\mathrm{e}^{\tilde{\phi}} \sigma_k^+ \sigma_{k+1}^- + \mathrm{e}^{-\tilde{\phi}} \sigma_k^- \sigma_{k+1}^+ \right] \tag{2.33}$$

In the limit $\lambda \to \infty$ we recover the case of large current studied in [19, 20].

2.3.3.1 Longest Relaxation Time

From the ground state choice of the Bethe roots one obtains the lowest excited state by exchanging the root with $m = 0$ with $m = -1$. The real part of the spectral gap, i.e., the inverse of the longest relaxation time τ_L in a finite system of size L is independent of $\tilde{\phi}$ and given by

$$1/\tau_L = 2\sin(\pi\rho)\sin\left(\frac{\pi}{L}\right) \propto 1/L \tag{2.34}$$

where $\rho = N/L$ is the particle density.

For large L the gap is inversely proportional to the system size, unlike in the unconstrained ASEP where the real part of the spectrum gap scales as $O(1/L^{3/2})$ [27, 28] with the dynamical exponent $z = 3/2$ of the KPZ universality class. We conclude that the conditioned dynamics is in a different dynamical universality class, characterized by a dynamical exponent $z = 1$ and first studied by Spohn [22] in the context of the related model with long-range interactions. Indeed, generalizing the work of [19] it is readily seen that the generator G of the effective process in the symmetric case $\tilde{\phi} = 0$ is identical with the quantum Hamiltonian of Spohn. As pointed out in that work this symmetric case can be interpreted classically as a system of non-intersecting random walks or quantum mechanically as a lattice model of Dyson's Brownian motion of the eigenvalues of a random matrix [34]. Non-intersecting random walks appear also in the study of diffusive pair annihilation processes and many different techniques (see e.g. [35–38] and references therein) allow for a detailed analysis of this problem.

2.3.3.2 Dynamical Structure Function

This ballistic universality class can be studied in terms of the dynamic structure factor which is defined as the Fourier transform of the time-dependent stationary correlation function $S_{L,N}(r,t) = \langle \eta(k+r,t)\eta(k,0)\rangle - \rho^2$. In order to compute this quantity we follow the approach of [20]. We introduce the Fourier transform

$$\hat{S}_{L,N}(p,t) = \sum_{r=0}^{L-1} \mathrm{e}^{-2\pi i p n/L} S_L(r,t) \tag{2.35}$$

which has the particle-hole symmetry, i.e., $\hat{S}_{L,L-N}(p,t) = \hat{S}_{L,N}(-p,t)$. Therefore we can restrict the computation to the case $0 \le \rho \le 1/2$. After some computation one finds from the free-fermion property

$$\begin{aligned}\hat{S}_{L,N}(p,t) = \frac{1}{L}\sum_{k=0}^{N-1}\left[\mathrm{e}^{(\varepsilon_k-\varepsilon_{k+p})t} - \mathrm{e}^{-(\varepsilon_k-\varepsilon_{k-p})t}\right] \\ + \frac{1}{L}\sum_{k=0}^{N-1}\sum_{l=N}^{L-1} \mathrm{e}^{-(\varepsilon_k-\varepsilon_l)t}\delta_{p,k-l}\end{aligned} \tag{2.36}$$

where in contrast to [20]

$$\varepsilon_k = -\frac{1}{2\cosh\tilde{\phi}}\left(\mathrm{e}^{\tilde{\phi}}\mathrm{e}^{-i\alpha_k} + \mathrm{e}^{-\tilde{\phi}}\mathrm{e}^{i\alpha_k}\right) \tag{2.37}$$

with

$$\alpha_k = \frac{2\pi}{L}\left(k - \frac{N-1}{2}\right). \tag{2.38}$$

This yields

$$\begin{aligned}\varepsilon_k - \varepsilon_{k-p} &= -\frac{\mathrm{e}^{\tilde{\phi}}\left(1-\mathrm{e}^{\frac{2\pi i p}{L}}\right)\mathrm{e}^{-i\alpha_k} + \mathrm{e}^{-\tilde{\phi}}\left(1-\mathrm{e}^{\frac{-2\pi i p}{L}}\right)\mathrm{e}^{i\alpha_k}}{\cosh\tilde{\phi}} \\ &= \left(1-\cos\left(\frac{2\pi p}{L}\right)\right)\cos\alpha_k + \sin\left(\frac{2\pi p}{L}\right)\sin\alpha_k \\ &\quad + i\tanh\tilde{\phi}\left[\sin\left(\frac{2\pi p}{L}\right)\cos\alpha_k - \left(1-\cos\left(\frac{2\pi p}{L}\right)\right)\sin\alpha_k\right]\end{aligned} \tag{2.39}$$

Taking the thermodynamic limit $L \to \infty$ with density $\rho = N/L$ fixed turns the sums into integrals as in [20] and thus yields an exact expression valid for all $p \in [-\pi, \pi]$ and $t \ge 0$. In order to explore the large-scale behaviour of the dynamic structure factor we study the behaviour for small momentum p and large times t. To this end we define the scaling variable $u = p^z t$ and the limit $t \to \infty$ with u fixed. Inspection of (2.39) shows that non-trivial scaling behaviour is obtained for $z = 1$, as expected from the scaling of the energy gap (2.34). In this scaling we have $t(1-\mathrm{e}^{ip}) = -iut$ and therefore

$$\hat{S}(u) = \frac{|u|}{2\pi t}\mathrm{e}^{-iu\tanh\tilde{\phi}\cos\rho\pi - |u|\sin\rho\pi} \tag{2.40}$$

which is valid for all $\rho \in [0, 1]$. We read off the collective velocity

$$v_c = \tanh \tilde{\phi} \cos \rho\pi \tag{2.41}$$

of the lattice gas. Hence for conditioning on high activity we recover the universal scaling function of the ASEP conditioned on high current even for finite current. Conditioned on an atypical current amounts only to a shift in the driving field $\phi \to \tilde{\phi}$. By comparing with (2.32) one sees that one has $v_c = \partial j^*/\partial\rho$ as in lattice gases with static short-range correlations. To our knowledge this is the first verification of this relation for a lattice gas with long-range correlations. The validity is in agreement with the notion [39] that this relation should remain generally valid for static correlations that decay faster than $1/r$.

2.4 Conclusions and Open Questions

The perhaps most significant results of our studies are the emergence of long-range stationary correlations and the change of the dynamical universality class from KPZ to ballistic as one goes from typical to high activity or current. Hence, in a state of extremely high current or activity the ASEP does not behave essentially like "normal", with just upscaled parameter values as is the case for non-interacting particles. It is important to understand whether this is specific for the ASEP (where it can be traced to the underlying non-intersecting random walks) or whether this is a generic phenomenon for driven diffusive systems.

A more specific open problem concerns the location of the phase transition point. Does the ballistic universality class arise for any finite deviation from the typical activity or current, or is some threshold required? This question can be addressed by a careful analysis of the Bethe ansatz equations (2.25) along the lines of [27, 28], since the finite-size scaling of the spectral gap of the generator will reveal the dynamical exponent. Also the answer to this question could be of interest beyond the ASEP.

Acknowledgments Much of what is presented here results from joint work with V. Popkov and D. Simon to whom the author is indebted for many fruitful discussions. This work was supported by Deutsche Forschungsgemeinschaft.

References

1. R.J. Harris, G.M. Schütz, Fluctuation theorems for stochastic dynamics. J. Stat. Mech. P07020 (2007)
2. U. Seifert, Stochastic thermodynamics, fluctuation theorems, and molecular machines. Rep. Prog. Phys. **75**, 126001 (2012)

3. G. Gallavotti, E.G.D. Cohen, Dynamical ensembles in stationary states. J. Stat. Phys. **80**, 931–970 (1995)
4. J.L. Lebowitz, H. Spohn, A gallavotti-cohen-type symmetry in the large deviation functional for stochastic dynamics. J. Stat. Phys. **95**, 333–365 (1999)
5. B. Schmittmann, R.K.P. Zia, in *Phase Transitions and Critical Phenomena*, ed. by C. Domb, J. Lebowitz (Academic Press, London, 1995)
6. T.M. Liggett, *Stochastic Interacting Systems: Contact Voter and Exclusion Processes* (Springer, Berlin, 1999)
7. G.M. Schütz, in *Phase Transitions and Critical Phenomena*, vol. 19, ed. by C. Domb, J. Lebowitz (Academic Press, London 2001), pp. 1–251
8. A. Schadschneider, D. Chowdhury, K. Nishinari, *Stochastic Transport in Complex Systems* (Elsevier, Amsterdam, 2010)
9. M.R. Evans, T. Hanney, 2005 Nonequilibrium statistical mechanics of the zero-range process and related models. J. Phys. A: Math. Gen. **38**, R195–R240 (2005)
10. E. Levine, D. Mukamel, G.M. Schütz, Zero-range process with open boundaries. J. Stat. Phys. **120**(5–6), 759–778 (2005)
11. R.J. Harris, A. Rakos, G.M. Schütz, Breakdown of Gallavotti-Cohen symmetry for stochastic dynamics. Europhys. Lett **75**(2), 227–233 (2006)
12. R.J. Harris, V. Popkov, G.M. Schütz, Dynamics of instantaneous condensation in the ZRP conditioned on an atypical current. Entropy **15**(11), 5065–5083 (2013)
13. B. Derrida, J.L. Lebowitz, E.R. Speer, Large deviation of the density profile in the steady state of the open symmetric simple exclusion process. J. Stat. Phys. **107**, 599–634 (2002)
14. L. Bertini, A. De Sole, D. Gabrielli, G. Jona Lasinio, C. Landim, Macroscopic fluctuation theory for stationary non-equilibrium states. J. Stat. Phys. **107**, 635–675 (2002)
15. T. Bodineau, B. Derrida, Distribution of current in non-equilibrium diffusive systems and phase transitions. Phys. Rev. E **72**, 066110 (2005)
16. V. Lecomte, J.P. Garrahan, F. Van Wijland, Inactive dynamical phase of a symmetric exclusion process on a ring. J. Phys. A: Math. Theor. **45**, 175001 (2012)
17. V. Belitsky, G.M. Schütz, Microscopic structure of shocks and antishocks in the ASEP conditioned on low current. J. Stat. Phys. **152**, 93–111 (2013)
18. V. Belitsky, G.M. Schütz, Antishocks in the ASEP with open boundaries conditioned on low current. J. Phys. A: Math. Theor. **46**, 295004 (2013)
19. V. Popkov, D. Simon, G.M. Schütz, ASEP on a ring conditioned on enhanced flux. J. Stat. Mech. P10007 (2010)
20. V. Popkov, G.M. Schütz, Transition probabilities and dynamic structure factor in the ASEP conditioned on strong flux. J. Stat. Phys. **142**(3), 627–639 (2011)
21. M. Kardar, G. Parisi, Y.-C. Zhang, Dynamic scaling of growing interfaces Phys. Rev. Lett. **56**, 889 (1986)
22. H. Spohn, Bosonization, vicinal surfaces, and hydrodynamic fluctuation theory. Phys. Rev. E **60**, 6411–6420 (1999)
23. J.H. MacDonald, Gibbs and AC Pipkin. Kinetics of biopolymerization on nucleic acid templates, Biopolymers **6**, 1–25 (1968)
24. G.M. Schütz, The Heisenberg chain as a dynamical model for protein synthesis—some theoretical and experimental results. Int. J. Mod. Phys. B **11**(1–2), 197–202 (1997)
25. F. Spitzer, Interaction of Markov processes. Adv. Math. **5**, 246–290 (1970)
26. G.M. Schütz, R. Ramaswamy, M. Barma, Pairwise balance and invariant measures for generalized exclusion processes. J. Phys. A: Math. Gen. **29**(4), 837–843 (1996)
27. L.H. Gwa, H. Spohn, Six-vertex model, roughened surfaces, and an asymmetric spin Hamiltonian. Phys. Rev. Lett. **68**, 725 (1992)
28. D. Kim, Bethe ansatz solution for crossover scaling functions of the asymmetric XXZ chain and the KPZ-type growth model. Phys. Rev. E **52**, 3512–3524 (1995)
29. M. Doi, Second quantization representation for classical many-particle system J. Phys. A: Math. Gen. **9** 1465–1477 (1976)

30. L. Peliti, Path integral approach to birth-death processes on a lattice. J. Phys. France **46**, 1469–1483 (1985)
31. B. Derrida, C. Appert, Universal large deviation function of the Kardar-Parisi-Zhang equation in one dimension. J. Stat. Phys. **94**, 1–30 (1999)
32. D. Simon, Construction of a coordinate Bethe ansatz for the asymmetric simple exclusion process with open boundaries. J. Stat. Mech. P07017 (2009)
33. E. Lieb, T. Schultz, D. Mattis, Two soluble models of an antiferromagnetic chain. Ann. Phys. **16**, 407–466 (1961)
34. F.J. Dyson, A brownian motion model for the eigenvalues of a random matrix. J. Math. Phys. **3**, 1191–1198 (1962)
35. F. Colomo, A.G. Isergin, V.E. Korepin, V. Tognetti, Temperature Correlation functions in the XX0 Heisenberg chain. Theor. Math. Phys. **94**(1), 11–38 (1993)
36. G.M. Schütz, Diffusion-annihilation in the presence of a driving field. J. Phys. A: Math. Gen. **28**(12), 3405–3415 (1995)
37. A. Ayyer, K. Mallick, Exact results for an asymmetric annihilation process with open boundaries. J. Phys. A: Math. Theor. **43**(4), 045003 (2010)
38. M. Katori, H. Tanemura, Complex Brownian motion representation of the Dyson model, Electron. Commun. Probab. **18**(4), 1–16 (2013)
39. R.M. Grisi, G.M. Schütz, Current symmetries for particle systems with several conservation laws. J. Stat. Phys. **145**(6), 1499–1512 (2011)

Chapter 3
Quantum Spin Chains and Integrable Many-Body Systems of Classical Mechanics

A. Zabrodin

Abstract This note is a review of the recently revealed intriguing connection between integrable quantum spin chains and integrable many-body systems of classical mechanics. The essence of this connection lies in the fact that the spectral problem for quantum Hamiltonians of the former models is closely related to a sort of inverse spectral problem for Lax matrices of the latter ones. For simplicity, we focus on the most transparent and familiar case of spin chains on N sites constructed by means of the $GL(2)$-invariant R-matrix. They are related to the classical Ruijsenaars-Schneider system of N particles, which is known to be an integrable deformation of the Calogero-Moser system. As an explicit example the case $N = 2$ is considered in detail.

3.1 Introduction

In this paper we present some results of [1–4] in a short compressed form and in the simplest possible setting. First of all let us explain what we mean by "quantum spin chains" and "integrable many-body systems of classical mechanics".

The best known example of integrable quantum spin chain is the isotropic (XXX) homogeneous Heisenberg model with spin $\frac{1}{2}$ on an 1D lattice with coupling between nearest neighbours. Throughout the paper, we use the words "spin chain" in a broader sense, not implying existence of any local Hamiltonian of the Heisenberg type. In fact integrable local Hamiltonians in general do not exist for inhomogeneous spin chains

A. Zabrodin (✉)
Institute of Biochemical Physics, 4 Kosygina, 119334 Moscow, Russia
e-mail: zabrodin@itep.ru

A. Zabrodin
ITEP, 25 B. Cheremushkinskaya, 117218 Moscow, Russia

A. Zabrodin
International Laboratory of Representation Theory and Mathematical Physics,
National Research University Higher School of Economics,
20 Myasnitskaya Ulitsa, 101000 Moscow, Russia

B. Aneva and M. Kouteva-Guentcheva (eds.),
Nonlinear Mathematical Physics and Natural Hazards,
Springer Proceedings in Physics 163, DOI 10.1007/978-3-319-14328-6_3

which are closely involved in our story. However, such models still make sense as generalized spin chains with long-range interaction and a family of commuting (non-local) Hamiltonians. We call them inhomogeneous XXX spin chains. Alternatively, one may prefer to keep in mind inhomogeneous integrable lattice models of statistical mechanics rather than spin chains as such. In either case, the final goal of the theory is diagonalization of transfer matrices which are generating functions of commuting conserved quantities. This is usually achieved by one or another version of the Bethe ansatz method.

The integrable model of classical mechanics we are mainly interested in is the N-body system of particles on the line called the Ruijsenaars-Schneider (RS) model [5, 6]. It is often referred to as an integrable relativistic deformation of the famous Calogero-Moser (CM) model with inversely quadratic pair potential [7–9].

As is common for integrable models, the classical dynamics can be represented in the Lax form, i.e., as an isospectral deformation of a $N \times N$ matrix called the Lax matrix. Matrix elements of this matrix are simple functions of coordinates and momenta of the particles while the eigenvalues are integrals of motion. In a nutshell, the essence of the quantum-classical (QC) duality

$$\boxed{\text{Quantum integrable models}} \longleftrightarrow \boxed{\text{Classical many-body systems}}. \tag{3.1}$$

lies in the fact that spectra of quantum Hamiltonians of a model from the left hand side appear to be encoded in the algebraic properties of the Lax matrix for a classical system from the right hand side.

In the case of the inhomogeneous XXX spin chain, a refined version of (3.1) is

$$\boxed{\text{Quantum XXX spin-}\frac{1}{2}\text{ chain on } N \text{ sites}} \longleftrightarrow \boxed{\text{Classical } N\text{-body RS model}}. \tag{3.2}$$

More precisely, the spectral problem for the quantum Hamiltonians of the inhomogeneous XXX spin chain on N sites is reduced to a sort of an *inverse* spectral problem for the $N \times N$ Lax matrix for the classical RS system. Given its spectrum and the coordinates of the particles, the problem is to find possible values of their momenta compatible with these data. In general this problem has many solutions which just yield different eigenvalues of the quantum Hamiltonians. In a special scaling limit, the XXX spin chain turns into the Gaudin spin model [10]. On the right hand side of (3.2), this corresponds to the non-relativistic limit of the RS system:

$$\boxed{\text{Quantum Gaudin model}} \longleftrightarrow \boxed{\text{Classical CM model}}. \tag{3.3}$$

The QC duality is traced back to [11], where joint spectra of some finite-dimensional operators were linked to the classical Toda chain. The existence of an unexpected link between the quantum Gaudin and the classical CM models was first pointed out in [12, 13], see also [14–16]. In a more general set-up, the correspondence

between quantum and classical integrable systems was independently derived [1, 3, 17, 18] as a corollary of an embedding of the commutative algebra of spin chain Hamiltonians into an infinite integrable hierarchy of soliton equations known as the modified Kadomtsev-Petviashvili (mKP) hierarchy. Namely, the most general generating function of commuting integrals of motion of the spin chain (the "master T-operator") was shown to satisfy the bilinear identity and the Hirota bilinear equations for the tau-function of the mKP hierarchy [19, 20].

Although only a limited number of examples are available at the moment, the very phenomenon of the existence of hidden non-standard connections between quantum and classical integrable systems seems to be rather general. Presumably, it can be thought of as a new kind of a correspondence (or duality) principle in the realm of integrable systems. In [4], the QC duality (3.2), (3.3) was checked directly using the Bethe ansatz solution of integrable spin chains. The role of this duality in the context of supersymmetric gauge theories and branes was discussed in [4, 21, 22].

It is worthwhile to stress that the both sides of the correspondence, i.e. quantum and classical integrable systems, participate in the game as two faces of one entity on an equal-rights basis. In the theory of quantum models, there are some fundamental relations, exact for any $\hbar \neq 0$, which assume the form of classical equations of motion for some other system. (One of such examples is the classical integrable dynamics naturally realized in the space of conserved quantities of quantum integrable models, see [1] and earlier works [23–27].) At the same time, given a many-body problem of classical mechanics, one may extract from it, by addressing some non-traditional questions about the system, the spectral properties of a quantum model. This picture becomes valid and meaningful if the systems from both sides are integrable. It might be interesting to combine the hypothetical "correspondence principle" based on the QC duality with the standard correspondence principle of quantum mechanics.

Let us outline the contents of the paper.

In Sect. 3.2, we start with the most familiar example of integrable spin chain: the Heisenberg model with spin $\frac{1}{2}$ and periodic boundary conditions (the XXX magnet) solved by H. Bethe in 1931 [28]. The "spin variables" are vectors from the spaces $\mathbb{C}^2$ at each site. However, this model itself is too degenerate to be directly linked to a classical many-body system. To this end, we need an inhomogeneous version of the model with twisted boundary conditions. Such a generalized XXX model has $N + 2$ free parameters which are N "inhomogeneity parameters" on each site and 2 eigenvalues of the twist matrix which is assumed to be diagonal. The generalized XXX model can be naturally constructed in the framework of the Quantum Inverse Scattering Method (QISM) developed by the former Leningrad school [29–31]. In the inhomogeneous model, the locality of spin interactions does not take place. Instead, there are N non-local commuting Hamiltonians (which are cousins of the Gaudin ones). They can be simultaneously diagonalized using the algebraic Bethe ansatz.

In Sect. 3.3, the necessary formulae related to the classical RS model are presented, including the Lax matrix. The rules of the quantum-classical correspondence between the integrable models are explained in Sect. 3.4. As an example we consider the case $N = 2$, where all calculations can be done directly by hands (Sect. 3.5). Finally,

in Sect. 3.6 we give some remarks on the scaling limit to the Gaudin model which corresponds, on the classical side, to the non-relativistic limit of the RS system. Some generalizations and perspectives are briefly discussed in the concluding Sect. 3.7.

3.2 The Heisenberg Spin Chain and Its Generalizations

The Hamiltonian of the isotropic Heisenberg spin chain (also called the XXX-magnet) with periodic boundary condition is

$$\mathbf{H}^{\mathrm{xxx}} = 2\sum_{j=1}^{N}\left(\mathbf{s}_x^{(j)}\mathbf{s}_x^{(j+1)} + \mathbf{s}_y^{(j)}\mathbf{s}_y^{(j+1)} + \mathbf{s}_z^{(j)}\mathbf{s}_z^{(j+1)} - \mathbf{I}\right), \qquad N+1 \equiv 1,$$

where the spin operators $(\mathbf{s}_x, \mathbf{s}_y, \mathbf{s}_z) = \vec{\mathbf{s}}$ are expressed through the Pauli matrices as

$$\mathbf{s}_x = \frac{1}{2}\begin{pmatrix} 0 & 1 \\ 1 & 0 \end{pmatrix}, \quad \mathbf{s}_y = \frac{1}{2}\begin{pmatrix} 0 & -i \\ i & 0 \end{pmatrix} \quad \mathbf{s}_z = \frac{1}{2}\begin{pmatrix} 1 & 0 \\ 0 & -1 \end{pmatrix}$$

and $\mathbf{I} = \mathbf{1}^{\otimes N}$ is the identity operator (Hereafter $\mathbf{1}$ stands for the identity matrix in $\mathbb{C}^2$). We will also use $\mathbf{s}_+ = \mathbf{s}_x + i\mathbf{s}_y = \begin{pmatrix} 0 & 1 \\ 0 & 0 \end{pmatrix}$, $\mathbf{s}_- = \mathbf{s}_x - i\mathbf{s}_y = \begin{pmatrix} 0 & 0 \\ 1 & 0 \end{pmatrix}$, $\mathbf{s}_1 = \frac{1}{2}\mathbf{1} + \mathbf{s}_z = \begin{pmatrix} 1 & 0 \\ 0 & 0 \end{pmatrix}$ and $\mathbf{s}_2 = \frac{1}{2}\mathbf{1} - \mathbf{s}_z = \begin{pmatrix} 0 & 0 \\ 0 & 1 \end{pmatrix}$. The operator $\vec{\mathbf{s}}^{(j)} = \mathbf{1}^{\otimes(j-1)} \otimes \vec{\mathbf{s}} \otimes \mathbf{1}^{\otimes(N-j)}$ acts non-trivially at the jth site of the chain. Clearly, they commute for any $j' \neq j$. The Hamiltonian acts in the 2^N-dimensional linear space $\mathcal{V} = \otimes_{j=1}^{N} V_j$, $V_j \cong \mathbb{C}^2$. Basis vectors in this space can be constructed as tensor products of local vectors with definite z-projection of spin, i.e., eigenvectors of $\mathbf{s}_z$.

Note that $\mathbf{P}_{ij} = \frac{1}{2}\left(\mathbf{I} + 4\vec{\mathbf{s}}^{(i)}\vec{\mathbf{s}}^{(j)}\right)$ is the permutation operator of the ith and jth spaces, and so the Heisenberg Hamiltonian can be written in the form $\mathbf{H}^{\mathrm{xxx}} = \sum_j \mathbf{P}_{j\ j+1} - N\mathbf{I}$.

The Hamiltonian commutes with the operator

$$\mathbf{M} = \frac{1}{2}\sum_{j=1}^{N}(\mathbf{I} - 2\mathbf{s}_z^{(j)}) = \sum_{j=1}^{N}\mathbf{s}_2^{(j)} \tag{3.4}$$

which counts the total number of spins in the chain with negative z-projection. Namely, the states in which M spins look down (and so the rest $N - M$ spins look up) are eigenstates for the operator $\mathbf{M}$ with the eigenvalue M. The space of states $\mathcal{V}$ is decomposed in the direct sum of eigenspaces for the operator $\mathbf{M}$: $\mathcal{V} = \bigoplus_{M=0}^{N} \mathcal{V}(M)$, $\mathbf{M}\mathcal{V}(M) = M\mathcal{V}(M)$. It is clear that

$$\dim \mathcal{V}(M) = \binom{N}{M} = \frac{N!}{M!(N-M)!}\,.$$

In particular, $\mathcal{V}(0)$ and $\mathcal{V}(N)$ are one-dimensional spaces generated by the states in which all spins look up or down respectively.

The common spectral problem for the operators $\mathbf{H}^{\rm XXX}$ and $\mathbf{M}$, $\mathbf{H}^{\rm XXX}\Psi = E\Psi$, $\mathbf{M}\Psi = M\Psi$, has the famous Bethe ansatz solution [28]. The eigenvalues E for $0 \le M \le [N/2]$ are given by the formula

$$E = \sum_{\alpha=1}^{M} \varepsilon(v_\alpha), \quad \varepsilon(v) = -\frac{4}{1+4v^2}\,, \tag{3.5}$$

where the auxiliary quantities v_α (the Bethe roots) are to be found from the system of algebraic equations

$$\left(\frac{v_\alpha + \frac{i}{2}}{v_\alpha - \frac{i}{2}}\right)^N = \prod_{\beta=1,\beta\neq\alpha}^{M} \frac{v_\alpha - v_\beta + i}{v_\alpha - v_\beta - i} \tag{3.6}$$

(the Bethe equations). Different solutions to this system give energies of different eigenstates.

The exact solution of the Heisenberg spin chain is possible due to the fact that the model is integrable. This means that there is a sufficiently large family of independent commuting operators, one of which is the Heisenberg Hamiltonian. The other operators of this family are higher integrals of motion. A general prescription how to construct models possessing higher integrals of motion is provided by the Quantum Inverse Scattering Method (QISM) [29, 30].

We start by reformulating the XXX spin chain in the framework of the QISM, following [31]. Such a reformulation makes integrability of the model explicit and, what is even more important, it suggests natural integrable generalizations of the XXX chain.

Let $V_0 \cong \mathbb{C}^2$ be another copy of the complex linear space $\mathbb{C}^2$ (the auxiliary space). The quantum Lax operator at the jth site acts non-trivially in $V_0 \otimes V_j$. It is

$$\mathsf{L}_j(x) = x\mathbf{1}\otimes\mathbf{I} + \eta\mathbf{P}_{0j} = \Big(x+\frac{\eta}{2}\Big)\mathbf{1}\otimes\mathbf{I} + 2\eta\,\vec{\mathbf{s}}\otimes\vec{\mathbf{s}}\,, \tag{3.7}$$

or, in the block-matrix form,

$$\mathsf{L}_j(x) = \begin{pmatrix} x\mathbf{I} + \eta\mathbf{s}_1^{(j)} & \eta\,\mathbf{s}_-^{(j)} \\ \eta\,\mathbf{s}_+^{(j)} & x\mathbf{I} + \eta\mathbf{s}_2^{(j)} \end{pmatrix}. \tag{3.8}$$

The variable $x \in \mathbb{C}$ is called the (quantum) spectral parameter. The extra parameter η introduced here for the reason clarified below is not actually essential because it can be eliminated by a rescaling of the spectral parameter (unless one tends it to 0 as in the limit to the Gaudin model [10]). The Heisenberg Hamiltonian does not depend on η which is usually put equal to $i = \sqrt{-1}$ in this context. The L-operator satisfies the "$RLL = LLR$" intertwining relation

$$\mathsf{R}(x - x')\,\mathsf{L}_j(x) \otimes \mathsf{L}_j(x') = \mathsf{L}_j(x') \otimes \mathsf{L}_j(x)\,\mathsf{R}(x - x'),$$

where the quantum R-matrix $\mathsf{R}(x)$ acts in the tensor product of two auxiliary spaces $V_0 \cong V_{0'} \cong \mathbb{C}^2$. In the natural basis in $\mathbb{C}^2 \otimes \mathbb{C}^2$ it is

$$\mathsf{R}(x) = \begin{pmatrix} x+\eta & 0 & 0 & 0 \\ 0 & \eta & x & 0 \\ 0 & x & \eta & 0 \\ 0 & 0 & 0 & x+\eta \end{pmatrix} = \eta\,\mathbf{1} \otimes \mathbf{1} + x\mathbf{P}_{00'}. \tag{3.9}$$

Note that in this particular case the R-matrix is almost the same object as the quantum L-operator: they differ only by a permutation operator of the two spaces, so that the intertwining relation is equivalent to the Yang-Baxter equation for the R-matrix. The quantum transfer matrix is defined as

$$\mathbf{T}(x) = \mathrm{tr}_0\Big[\mathsf{L}_1(x)\mathsf{L}_2(x)\,\ldots\,\mathsf{L}_N(x)\Big] = 2\mathbf{I}\,x^N + \mathbf{J}_{N-1}x^{N-1} + \cdots + \mathbf{J}_1 x + \mathbf{J}_0\,. \tag{3.10}$$

The intertwining relation implies that the transfer matrices with different spectral parameters (and the same η) commute: $[\mathbf{T}(x),\ \mathbf{T}(x')] = 0$ for any x, x'. In its turn, this implies that the operators $\mathbf{J}_k$ in (3.10) all commute with each other. At the same time, the operator $\mathbf{J}_0$ is proportional to the cyclic permutation of the chain:

$$\mathbf{J}_0 = \mathbf{T}(0) = \eta^N \mathbf{P}_{12}\mathbf{P}_{23}\mathbf{P}_{34}\ldots\mathbf{P}_{N-1\ N}\mathbf{P}_{N1}$$

while the Hamiltonian of the spin chain is given by

$$\mathbf{H}^{\mathrm{xxx}} = \eta\frac{d}{dx}\,\log\mathbf{T}(x)\Big|_{x=0} - N\mathbf{I} = \eta\mathbf{J}_0^{-1}\mathbf{J}_1 - N\mathbf{I}.$$

The operators $\mathbf{J}_0^{-1}\mathbf{J}_k$ are then the higher integrals of motion. The operator $J_0^{-1}J_1$ is local due to the special property of the quantum Lax operator $\mathsf{L}_j(0) = \eta\mathbf{P}_{0j}$ and the homogeneity of the chain. The operator $\mathbf{M}$ (see (3.4)) commutes not only with $\mathbf{H}^{\mathrm{xxx}}$ but with the whole one-parametric family $\mathbf{T}(x)$, and the Bethe states are common eigenstates for the $\mathbf{T}(x)$ and $\mathbf{M}$: $\mathbf{T}(x)\Psi = T(x)\Psi$, $\mathbf{M}\Psi = M\Psi$.

The transfer matrix $\mathbf{T}(x)$ can be diagonalized by means of the algebraic Bethe ansatz method. The eigenvalues $T(x)$ are given by the formula

$$T(x) = (x+\eta)^N \prod_{\alpha=1}^{M} \frac{x-u_\alpha-\eta}{x-u_\alpha} + x^N \prod_{\alpha=1}^{M} \frac{x-u_\alpha+\eta}{x-u_\alpha}\,. \tag{3.11}$$

The Bethe roots u_α are to be found from the system of Bethe equations

$$\left(\frac{u_\alpha+\eta}{u_\alpha}\right)^N = \prod_{\beta=1,\beta\neq\alpha}^{M} \frac{u_\alpha-u_\beta+\eta}{u_\alpha-u_\beta-\eta}\,, \tag{3.12}$$

where is implied that $0 \le M \le [N/2]$. The eigenvalues of the Heisenberg Hamiltonian, in terms of the Bethe roots, are given by the formula

$$E = \sum_{\alpha=1}^{M} \frac{\eta^2}{u_\alpha(u_\alpha+\eta)}$$

which is equivalent to (3.5) under the substitution $v_\alpha = \dfrac{iu_\alpha}{\eta} + \dfrac{i}{2}$.

The XXX model can be generalized, preserving integrability, in two ways: (a) by making it inhomogeneous and (b) by imposing twisted boundary conditions. The former is based on the possibility to introduce an inhomogeneity parameter at each site which does not spoil the intertwining relation:

$$\mathsf{R}(x-x')\,\mathsf{L}_j(x-x_j)\otimes\mathsf{L}_j(x'-x_j) = \mathsf{L}_j(x'-x_j)\otimes\mathsf{L}_j(x-x_j)\,\mathsf{R}(x-x').$$

The latter is due to the $GL(2)$-invariance of the R-matrix (3.9): $g\otimes g\,\mathsf{R}(x) = \mathsf{R}(x)\,g\otimes g$ for any $g \in GL(2)$. This property implies that commutativity of the transfer matrices still holds if one inserts a matrix $g \in GL(2)$ in the auxiliary space before taking trace. For simplicity, we assume that g is diagonal:

$$g = \begin{pmatrix} w_1 & 0 \\ 0 & w_2 \end{pmatrix}. \tag{3.13}$$

The generalizations (a) and (b) can be applied simultaneously, which leads to the most general one-parametric family of commuting operator-valued polynomials in x:

$$\mathbf{T}(x) = \mathbf{T}(x; g, \eta, \{x_j\}) = \mathrm{tr}_0\Big[g\,\mathsf{L}_1(x-x_1)\mathsf{L}_2(x-x_2)\,\ldots\,\mathsf{L}_N(x-x_N)\Big]. \tag{3.14}$$

These operators commute for different x's and the same η, g and x_j:

$$[\mathbf{T}(x; g, \eta, \{x_j\}),\ \mathbf{T}(x'; g, \eta, \{x_j\})] = 0.$$

Similarly to (3.10), one can expand

$$\mathbf{T}(x) = \mathbf{I}\,\mathrm{tr}\, g\, x^N + \mathbf{J}_{N-1}x^{N-1} + \cdots + \mathbf{J}_1 x + \mathbf{J}_0, \tag{3.15}$$

the $\mathbf{J}_k$'s being commuting integrals of motion. Note, in particular, that $\mathbf{J}_{N-1} = \eta\sum_i \mathbf{g}^{(i)}$, where $\mathbf{g}^{(i)}$ is the operator acting as the matrix g at the ith site: $\mathbf{g}^{(i)} := \mathbf{1}^{\otimes(i-1)} \otimes g \otimes \mathbf{1}^{\otimes(N-i)}$. In general there is no way to construct local Hamiltonians from the $\mathbf{J}_k$'s. Instead, assuming that all the x_j's are distinct and in general position (meaning that $x_i - x_j \neq \pm\eta$ for all i, j), one can define *non-local* Hamiltonians as residues of $\mathbf{T}(x)/\prod_j (x - x_j)$ (cf. [32]):

$$\frac{\mathbf{T}(x)}{\prod_{j=1}^N (x - x_j)} = \mathrm{tr}\, g \cdot \mathbf{I} + \sum_{j=1}^N \frac{\eta\,\mathbf{H}_j}{x - x_j}\,.$$

In general, the Hamiltonians $\mathbf{H}_j = \mathbf{H}_j(\eta, g, \{x_i\})$ imply a long-range interaction involving all spins in the chain. Their explicit form is

$$\mathbf{H}_i = \overrightarrow{\prod_{j=i+1}^{N}} \left(\mathbf{I} + \frac{\eta\,\mathbf{P}_{ij}}{x_i - x_j}\right) \mathbf{g}^{(i)} \overrightarrow{\prod_{j=1}^{i-1}} \left(\mathbf{I} + \frac{\eta\,\mathbf{P}_{ij}}{x_i - x_j}\right), \tag{3.16}$$

where we use the notation $\overrightarrow{\prod_{j=1}^{m}} A_j = A_1 A_2 \ldots A_m$ for the ordered product. It follows from the definition that $\sum_{j=1}^N \mathbf{H}_j = \sum_{j=1}^N \mathbf{g}^{(j)}$.

The operator $\mathbf{M}$ (3.4) still commutes with $\mathbf{T}(x)$ and all the $\mathbf{H}_j$'s, so, again, all these operators are diagonalized simultaneously: $\mathbf{T}(x)\Psi = T(x)\Psi$, $\mathbf{H}_j\Psi = H_j\Psi$, $\mathbf{M}\Psi = M\Psi$. The algebraic Bethe ansatz gives the following result. The eigenvalues $T(x)$ and H_j are given by the formulae

$$T(x) = w_1 \prod_{k=1}^N (x - x_k + \eta) \prod_{\alpha=1}^M \frac{x - u_\alpha - \eta}{x - u_\alpha} + w_2 \prod_{k=1}^N (x - x_k) \prod_{\alpha=1}^M \frac{x - u_\alpha + \eta}{x - u_\alpha}, \tag{3.17}$$

$$H_j = w_1 \prod_{k=1,\neq j}^N \frac{x_j - x_k + \eta}{x_j - x_k} \prod_{\alpha=1}^M \frac{x_j - u_\alpha - \eta}{x_j - u_\alpha}. \tag{3.18}$$

The Bethe roots u_α are to be found from the system of Bethe equations

$$\frac{w_1}{w_2} \prod_{k=1}^N \frac{u_\alpha - x_k + \eta}{u_\alpha - x_k} = \prod_{\beta=1,\beta\neq\alpha}^M \frac{u_\alpha - u_\beta + \eta}{u_\alpha - u_\beta - \eta}\,, \tag{3.19}$$

where it is implied that $0 \le M \le [N/2]$.

3.3 The Ruijsenaars-Schneider Model

The RS model [5, 6] is an integrable model of classical mechanics. It is an N-body system of interacting particles on the line with the Hamiltonian

$$\mathcal{H}_1^{\mathrm{RS}} = \eta^{-1} \sum_{i=1}^{N} e^{-\eta p_i} \prod_{k=1,\neq i}^{N} \frac{x_i - x_k + \eta}{x_i - x_k}\,. \tag{3.20}$$

For some reason it is often called the relativistic deformation of the Calogero-Moser model, the parameter η being the inverse "velocity of light". The Hamiltonian equations of motion $\begin{pmatrix} \dot{x}_i \\ \dot{p}_i \end{pmatrix} = \begin{pmatrix} \partial_{p_i} \mathcal{H}_1^{\mathrm{RS}} \\ -\partial_{x_i} \mathcal{H}_1^{\mathrm{RS}} \end{pmatrix}$ give the following connection between velocity and momentum

$$\dot{x}_i = -e^{-\eta p_i} \prod_{k=1,\neq i}^{N} \frac{x_i - x_k + \eta}{x_i - x_k} \tag{3.21}$$

and the equations of motion

$$\ddot{x}_i = -\sum_{k\neq i} \frac{2\,\eta^2 \dot{x}_i \dot{x}_k}{(x_i - x_k)((x_i - x_k)^2 - \eta^2)}\,, \qquad i = 1, \ldots, N. \tag{3.22}$$

The RS model is known to be integrable, with the higher integrals of motion in involution being given by $\mathcal{H}_k^{\mathrm{RS}} = \eta^{-1} \mathrm{tr}\,(\mathsf{Y}^{\mathrm{RS}})^k$, where $\mathsf{Y}^{\mathrm{RS}} = \mathsf{Y}^{\mathrm{RS}}(\{x_i\}; \{\dot{x}_i\})$ is the Lax matrix of the model. Its matrix elements are $\mathsf{Y}_{ij}^{\mathrm{RS}} = \dfrac{\eta \dot{x}_i}{x_i - x_j - \eta}$, i.e.,

$$\mathsf{Y}^{\mathrm{RS}}(\{x_i\}; \{\dot{x}_i\}) = \begin{pmatrix} -\dot{x}_1 & \frac{\eta\dot{x}_1}{x_1 - x_2 - \eta} & \frac{\eta\dot{x}_1}{x_1 - x_3 - \eta} & \cdots & \frac{\eta\dot{x}_1}{x_1 - x_N - \eta} \\ \frac{\eta\dot{x}_2}{x_2 - x_1 - \eta} & -\dot{x}_2 & \frac{\eta\dot{x}_2}{x_2 - x_3 - \eta} & \cdots & \frac{\eta\dot{x}_2}{x_2 - x_N - \eta} \\ \vdots & \vdots & \vdots & \ddots & \vdots \\ \frac{\eta\dot{x}_N}{x_N - x_1 - \eta} & \frac{\eta\dot{x}_N}{x_N - x_2 - \eta} & \frac{\eta\dot{x}_N}{x_N - x_3 - \eta} & \cdots & -\dot{x}_N \end{pmatrix}. \tag{3.23}$$

Equations of motion (3.22) are equivalent to the Lax equation $\dot{\mathsf{Y}}^{\mathrm{RS}} = [\mathsf{B}, \mathsf{Y}^{\mathrm{RS}}]$, where

$$\mathsf{B}_{ij} = \left(\sum_{k\neq i} \frac{\dot{x}_k}{x_i - x_k} - \sum_{k} \frac{\dot{x}_k}{x_i - x_k + \eta} \right) \delta_{ij} + \frac{\dot{x}_i}{x_i - x_j} (1 - \delta_{ij}).$$

The Lax equation implies that all eigenvalues of the Lax matrix are integrals of motion.

Let $\mathsf{X} = \mathrm{diag}(x_1, x_2, \ldots, x_N)$ be the diagonal matrix with the diagonal entries being coordinates of the particles. It is easy to check that the matrices X, Y^{RS} satisfy the commutation relation

$$[\mathsf{X}, \mathsf{Y}^{\mathrm{RS}}] = \eta \mathsf{Y}^{\mathrm{RS}} + \eta \dot{\mathsf{X}} \mathsf{E}, \tag{3.24}$$

where E is the $N \times N$ matrix of rank 1 with all entries equal to 1. Note also that the Lax matrix Y^{RS} can be represented in the form

$$\mathsf{Y}^{\mathrm{RS}} = \dot{\mathsf{X}}\, \mathsf{C}, \tag{3.25}$$

where C is the Cauchy matrix $\mathsf{C}_{ij} = \dfrac{\eta}{x_i - x_j - \eta}$.

3.4 The Quantum-Classical Duality

Consider the Lax matrix (3.23) of the N-particle RS model, where the x_i's are identified with the inhomogeneity parameters x_i at the sites of the spin chain and the inverse "velocity of light", η, is identified with the parameter η introduced in the quantum L-operator (3.8). Let us also substitute $\dot{x}_i = -H_i$:

$$\mathsf{Y}^{\mathrm{RS}}(\{x_i\}; \{-H_i\}) = \begin{pmatrix} H_1 & \frac{\eta H_1}{x_2 - x_1 + \eta} & \frac{\eta H_1}{x_3 - x_1 + \eta} & \ldots & \frac{\eta H_1}{x_N - x_1 + \eta} \\ \frac{\eta H_2}{x_1 - x_2 + \eta} & H_2 & \frac{\eta H_2}{x_3 - x_2 + \eta} & \ldots & \frac{\eta H_2}{x_N - x_2 + \eta} \\ \vdots & \vdots & \vdots & \ddots & \vdots \\ \frac{\eta H_N}{x_1 - x_N + \eta} & \frac{\eta H_N}{x_2 - x_N + \eta} & \frac{\eta H_N}{x_3 - x_N + \eta} & \ldots & H_N \end{pmatrix}. \tag{3.26}$$

The decomposition (3.25) for the matrix (3.26) acquires the form

$$\mathsf{Y}^{\mathrm{RS}}(\{x_i\}; \{-H_i\}) = -\mathsf{H}\mathsf{C}, \tag{3.27}$$

where $\mathsf{H} = \mathrm{diag}(H_1, H_2, \ldots, H_N)$.

The claim is that if the H_i's are eigenvalues of the Hamiltonians of the spin chain in the invariant subspace $\mathcal{V}(M)$, then the first $N - M$ eigenvalues of this matrix coincide with eigenvalues of the twist matrix w_1 while the rest M eigenvalues coincide with w_2:

$$\mathrm{Spec}\,(\mathsf{Y}^{\mathrm{RS}}) = \Big(\underbrace{w_1,\ldots,w_1}_{N-M},\ \underbrace{w_2,\ldots,w_2}_{M}\Big). \tag{3.28}$$

This means that the values of the higher RS Hamiltonians are

$$\eta\mathcal{H}_k^{\mathrm{RS}} = (N-M)w_1^k + Mw_2^k. \tag{3.29}$$

In general, the matrix Y^{RS} with multiple eigenvalues is not diagonalizable and contains Jordan cells.

To put it somewhat differently, one can say that the eigenstates of the quantum spin chain Hamiltonians correspond to the intersection points of two Lagrangian submanifolds in the phase space of the RS model. One of them is the hyperplane defined by fixing all the coordinates x_i while the other one is the Lagrangian submanifold obtained by fixing values (3.29) of the N integrals of motion in involution $\mathcal{H}_k^{\mathrm{RS}}$. In general, there are many such intersection points numbered by a finite set I, with coordinates, say $(x_1,\ldots,x_N,\ p_1^{(\alpha)},\ldots,p_N^{(\alpha)})$, $\alpha\in I$. The values of $p_j^{(\alpha)}$ give, through (3.21), the spectrum of $\mathbf{H}_j$:

$$H_j^{(\alpha)} = e^{-\eta p_j^{(\alpha)}}\prod_{k=1,\neq j}\frac{x_j-x_k+\eta}{x_j-x_k}\,.$$

However, we can not claim that all the intersection points correspond to the energy levels of the spin chain Hamiltonians. The example of $N=2$ considered below in detail suggests that some intersection points do not correspond to the energy levels of a given spin chain. Their meaning is to be clarified.

Anyway, the spectral problem for the non-local inhomogeneous spin chain Hamiltonians $\mathbf{H}_j$ in the subspace $\mathcal{V}(M)$ appears to be closely linked to the following *inverse spectral problem* for the RS Lax matrix Y^{RS} of the form (3.26). Let us fix the spectrum of the matrix Y^{RS} to be (3.28), where w_1, w_2 are eigenvalues of the (diagonal) twist matrix g. Then we ask what is the set of possible values of the H_j's allowed by these constraints. The eigenvalues H_j of the quantum Hamiltonians are contained in this set.

A similar correspondence between quantum and classical integrable systems was suggested in [12, 13], see also [14–16]. In a more general set-up, this assertion was derived [1, 3, 17, 18] as a corollary of the embedding of the spin chain into an infinite integrable hierarchy of non-linear PDE's. In [4], it was checked directly using the Bethe ansatz solution.

In order to find the characteristic polynomial of the matrix (3.26) explicitly, we use the well known fact that the coefficient in front of λ^{N-k} in the polynomial $\det_{N\times N}(\lambda\mathsf{I}+\mathsf{A})$ equals the sum of all diagonal $k\times k$ minors of the matrix A. All such minors can be found using decomposition (3.27) and the explicit expression for the determinant of the Cauchy matrix:

$$\det_{1\le i,j\le n}\frac{\eta}{x_i-x_j-\eta}=(-1)^n\prod_{1\le i<j\le n}\left(1-\frac{\eta^2}{(x_i-x_j)^2}\right)^{-1}.$$

The result is:

$$\det_{N\times N}(\lambda\mathsf{I}-\mathsf{Y}^{\mathrm{RS}})=\det_{N\times N}(\lambda\mathsf{I}+\mathsf{HC})=\sum_{n=0}^{N}\mathcal{J}_n\lambda^{N-n}, \tag{3.30}$$

where

$$\mathcal{J}_n=(-1)^n\sum_{1\le i_1<\cdots<i_n\le N}H_{i_1}\dots H_{i_n}\prod_{1\le\alpha<\beta\le n}\left(1-\frac{\eta^2}{(x_{i_\alpha}-x_{i_\beta})^2}\right)^{-1}. \tag{3.31}$$

In particular, the highest coefficient is given by the following simple formula:

$$\mathcal{J}_N=(-1)^N H_1H_2\dots H_N\prod_{i<j}\left(1-\frac{\eta^2}{(x_i-x_j)^2}\right)^{-1}.$$

For completeness, we point out that the integrals $\mathcal{H}_k$ introduced in the previous section are connected with the integrals $\mathcal{J}_k$ by the Newton's formula [33] $\sum_{k=0}^{N}\mathcal{J}_{N-k}\mathcal{H}_k=0$ (we have set $\mathcal{H}_0=\eta^{-1}\mathrm{tr}(\mathsf{Y}^{\mathrm{RS}})^0=N/\eta$).

Another way to write expressions (3.30), (3.31) is through a sum over $\epsilon_1,\dots,\epsilon_N$, with $\epsilon_i\in\{0,1\}$:

$$\det_{N\times N}(\lambda\mathsf{I}-\mathsf{Y}^{\mathrm{RS}})=\lambda^N\sum_{\{\epsilon_1,\dots,\epsilon_N\}\in\mathbb{Z}_2^N}\prod_{i=1}^{N}\left(-H_i/\lambda\right)^{\epsilon_i}\prod_{1\le j<k\le N}\left(1-\frac{\eta^2}{(x_j-x_k)^2}\right)^{-\epsilon_j\epsilon_k}. \tag{3.32}$$

The similarity of these expressions with tau-functions for N-soliton solutions to the KP hierarchy is not accidental. This point will be discussed elsewhere.

We conclude this section by writing down the system of algebraic equations for spectra of the operators $\mathbf{H}_i$. Combining (3.28) and (3.31), we obtain N polynomial equations for N unknown quantities $H_1,\dots,H_N$:

$$\sum_{1\le i_1<\cdots<i_n\le N}H_{i_1}\dots H_{i_n}\prod_{1\le\alpha<\beta\le n}\left(1-\frac{\eta^2}{(x_{i_\alpha}-x_{i_\beta})^2}\right)^{-1}=C_n(N,M), \tag{3.33}$$

where $C_n(N,M)=\frac{1}{2\pi i}\oint_{|z|=1}(1+zw_1)^{N-M}(1+zw_2)^M z^{-n-1}dz$, $n=1,2,\dots,N$. Let us emphasize that in contrast to the Bethe ansatz solution, the algebraic equations are written here not for some auxiliary quantities like Bethe roots but for the spectrum itself.

The state where all spins look up ($M = 0$) is an obvious eigenvector of the operators $\mathbf{H}_i$ with the eigenvalues

$$H_i = w_1 \prod_{j=1,\neq i}^{N} \Big(1 + \frac{\eta}{x_i - x_j}\Big). \tag{3.34}$$

One can check that these H_i's indeed solve the system (3.33) with $C_n(N, 0) = \frac{N! w_1^n}{n!(N-n)!}$.

3.5 Examples: $N = 1$ and $N = 2$

The case $N = 1$ is trivial. The only quantum Hamiltonian $\mathbf{H}_1$ is diagonal in the standard basis of $\mathbb{C}^2$ and coincides with the twist matrix, so we have two eigenvalues: $H_1 = w_1$ or $H_1 = w_2$. The one-particle RS model is the model of a free particle on the line, the Lax "matrix" is just the number $-\dot{x}_1$. Fixing it to be w_1 or w_2, as required by the QC duality, we obtain the two eigenvalues of $\mathbf{H}_1$ by the identification $H_i = -\dot{x}_i$, see (3.26).

The case $N = 2$ is meaningful and instructive. First, let us find the spectrum of the quantum Hamiltonians directly. The transfer matrix is:

$$\mathbf{T}(x) = \mathrm{tr}\left[\begin{pmatrix} w_1 & 0 \\ 0 & w_2 \end{pmatrix}\begin{pmatrix} (x-x_1)\mathbf{I} + \eta \mathbf{s}_1^{(1)} & \eta\, \mathbf{s}_-^{(1)} \\ \eta\, \mathbf{s}_+^{(1)} & (x-x_1)\mathbf{I} + \eta \mathbf{s}_2^{(1)} \end{pmatrix} \times \begin{pmatrix} (x-x_2)\mathbf{I} + \eta \mathbf{s}_1^{(2)} & \eta\, \mathbf{s}_-^{(2)} \\ \eta\, \mathbf{s}_+^{(2)} & (x-x_2)\mathbf{I} + \eta \mathbf{s}_2^{(2)} \end{pmatrix}\right]$$

A simple calculation gives the following explicit form of the Hamiltonians:

$$\mathbf{H}_1 = w_1 \mathbf{s}_1^{(1)} + w_2 \mathbf{s}_2^{(1)} + \frac{\eta w_1}{x_1 - x_2}(\mathbf{s}_1^{(1)}\mathbf{s}_1^{(2)} + \mathbf{s}_-^{(1)}\mathbf{s}_+^{(2)}) + \frac{\eta w_2}{x_1 - x_2}(\mathbf{s}_2^{(1)}\mathbf{s}_2^{(2)} + \mathbf{s}_+^{(1)}\mathbf{s}_-^{(2)}),$$

$$\mathbf{H}_2 = w_1 \mathbf{s}_1^{(2)} + w_2 \mathbf{s}_2^{(2)} + \frac{\eta w_1}{x_2 - x_1}(\mathbf{s}_1^{(1)}\mathbf{s}_1^{(2)} + \mathbf{s}_-^{(1)}\mathbf{s}_+^{(2)}) + \frac{\eta w_2}{x_2 - x_1}(\mathbf{s}_2^{(1)}\mathbf{s}_2^{(2)} + \mathbf{s}_+^{(1)}\mathbf{s}_-^{(2)}).$$

We see that $\mathbf{H}_1 + \mathbf{H}_2 = \mathbf{g}^{(1)} + \mathbf{g}^{(2)}$, as it should be. The space $\mathbb{C}^2 \otimes \mathbb{C}^2$ is decomposed into the direct sum of the one-dimensional space $\mathcal{V}(0)$ generated by the vector $|{+}{+}\rangle$ ($M = 0$), two-dimensional space $\mathcal{V}(1)$ generated by the vectors $|{+}{-}\rangle, |{-}{+}\rangle$ ($M = 1$) and one-dimensional space $\mathcal{V}(2)$ generated by the vector $|{-}{-}\rangle$ ($M = 2$). We have:

$$\mathbf{H}_1 |{+}{+}\rangle = w_1\Big(1 + \frac{\eta}{x_1 - x_2}\Big)|{+}{+}\rangle\,, \qquad \mathbf{H}_1 |{-}{-}\rangle = w_2\Big(1 + \frac{\eta}{x_2 - x_1}\Big)|{-}{-}\rangle\,,$$

$$\mathbf{H}_1\,|{+}{-}\rangle = w_1\,|{+}{-}\rangle + \frac{\eta w_1}{x_1-x_2}\,|{-}{+}\rangle\,,$$

$$\mathbf{H}_1\,|{-}{+}\rangle = w_2\,|{-}{+}\rangle + \frac{\eta w_2}{x_1-x_2}\,|{+}{-}\rangle\,.$$

Here we use the usual notation for the basis vectors in $\mathbb{C}^2\otimes\mathbb{C}^2$:

$$|{+}{+}\rangle = \begin{pmatrix}1\\0\end{pmatrix}\otimes\begin{pmatrix}1\\0\end{pmatrix}, \qquad |{+}{-}\rangle = \begin{pmatrix}1\\0\end{pmatrix}\otimes\begin{pmatrix}0\\1\end{pmatrix}, \quad \text{and so on.}$$

The vectors $|{+}{+}\rangle$ and $|{-}{-}\rangle$ are eigenvectors of $\mathbf{H}_1$. The rest part of the spectrum is found by diagonalizing the 2×2 matrix $\begin{pmatrix} w_1 & \frac{\eta w_1}{x_1-x_2} \\ \frac{\eta w_2}{x_1-x_2} & w_2\end{pmatrix}$. The two eigenvalues are $\frac{1}{2}\left(w_1+w_2\pm\sqrt{R}\right)$, where

$$R = (w_1-w_2)^2 + \frac{4\eta^2 w_1 w_2}{(x_1-x_2)^2}.$$

The final result for the joint spectrum of the operators $\mathbf{H}_i$ is as follows:

$$(H_1,H_2) = \begin{cases} \left(w_1+\dfrac{\eta w_1}{x_1-x_2},\ w_1-\dfrac{\eta w_1}{x_1-x_2}\right), & M=0,\\[2ex] \left(\dfrac{w_1+w_2+\sqrt{R}}{2},\ \dfrac{w_1+w_2-\sqrt{R}}{2}\right), & M=1,\\[2ex] \left(\dfrac{w_1+w_2-\sqrt{R}}{2},\ \dfrac{w_1+w_2+\sqrt{R}}{2}\right), & M=1,\\[2ex] \left(w_2+\dfrac{\eta w_2}{x_1-x_2},\ w_2-\dfrac{\eta w_2}{x_1-x_2}\right), & M=2. \end{cases} \tag{3.35}$$

Note that in the case of the periodic boundary condition $w_1=w_2=1$ the eigenvalue $H_1 = 1+\frac{\eta}{x_1-x_2}$ becomes 3-fold degenerate as it should be due to the $GL(2)$-invariance of the R-matrix.

Now consider the Lax matrix of the 2-particle RS model, where we substitute $\dot{x}_i = -H_i$:

$$\mathsf{Y} = \begin{pmatrix} H_1 & \dfrac{\eta H_1}{x_2-x_1+\eta} \\[2ex] \dfrac{\eta H_2}{x_1-x_2+\eta} & H_2 \end{pmatrix}$$

The characteristic equation $\det(\mathsf{Y}-\lambda\mathsf{I})=0$ reads $\lambda^2-(H_1+H_2)\lambda+\frac{x_{12}^2 H_1 H_2}{x_{12}^2-\eta^2}=0$, where $x_{12}\equiv x_1-x_2$ and the two eigenvalues are

$$\frac{1}{2}\left(H_1+H_2\pm\sqrt{(H_1+H_2)^2-\frac{4x_{12}^2\,H_1H_2}{x_{12}^2-\eta^2}}\right).$$

In the subspace with $M=0$ the eigenvalue of $\mathbf{H}_1+\mathbf{H}_2$ is $2w_1$ and the Lax matrix has the double eigenvalue w_1. This implies that the expression under the square root vanishes, i.e., we arrive at the system

$$\begin{cases} H_1+H_2=2w_1\\ H_1H_2=w_1^2\Big(1-\dfrac{\eta^2}{x_{12}^2}\Big)\end{cases}$$

which is a particular case $N=2$ of the general system (3.33). There are two solutions:

$$(H_1,\,H_2)=\left(w_1\pm\frac{\eta w_1}{x_1-x_2},\;\; w_1\mp\frac{\eta w_1}{x_1-x_2}\right),\qquad M=0.$$

The choice of the upper sign corresponds to the first line in (3.35). The meaning of the other solution is to be clarified. In a similar way, for $M=2$ we obtain two solutions

$$(H_1,\,H_2)=\left(w_2\pm\frac{\eta w_2}{x_1-x_2},\;\; w_2\mp\frac{\eta w_2}{x_1-x_2}\right),\qquad M=2,$$

of which the one with the upper sign corresponds to the last line in (3.35). Finally, at $M=1$ we have the system

$$\begin{cases} H_1+H_2=w_1+w_2\\ H_1H_2=w_1w_2\Big(1-\dfrac{\eta^2}{x_{12}^2}\Big).\end{cases}$$

There are two solutions which coincide with the second and the third lines in (3.35).

3.6 The Limit to the Quantum Gaudin Model and the Classical Calogero-Moser System

In the limit $\eta\to 0$ the QC duality discussed above becomes a correspondence (3.3) between the quantum Gaudin model and the classical Calogero-Moser system with inversely quadratic pair potential. Some details are given below.

The rational $GL(2)$ Gaudin model [10] is the $\eta \to 0$ limit of the inhomogeneous spin chain with the transfer matrix $\mathbf{T}(x; e^{\eta h}, \eta, \{x_j\})$. The expansion as $\eta \to 0$ gives:

$$\mathbf{T}(x; e^{\eta h}, \eta, \{x_j\}) = 2\mathbf{I} + \eta \left(\operatorname{tr} h + \sum_{i=1}^{N} \frac{1}{x - x_i} \right) \mathbf{I} + \eta^2 \left(\frac{1}{2} \operatorname{tr} h^2 \, \mathbf{I} + \sum_{i=1}^{N} \frac{\mathbf{H}_i^G}{x - x_i} \right) + O(\eta^3),$$

where $h = \begin{pmatrix} \omega_1 & 0 \\ 0 & \omega_2 \end{pmatrix}$ is the Gaudin analogue of the twist matrix, and

$$\mathbf{H}_i^G = \lim_{\eta \to 0} \frac{\mathbf{H}_i(\eta, e^{\eta h}, \{x_j\}) - \mathbf{I}}{\eta} = \mathbf{h}^{(i)} + \sum_{j \neq i} \frac{\mathbf{P}_{ij}}{x_i - x_j}$$
$$= \sum_{j \neq i} \frac{\mathbf{I}}{x_i - x_j} + \mathbf{h}^{(i)} + 2 \sum_{j \neq i} \frac{\vec{\mathbf{s}}^{(i)} \vec{\mathbf{s}}^{(j)}}{x_i - x_j} \tag{3.36}$$

are the Hamiltonians of the $GL(2)$-invariant Gaudin model. Here $\mathbf{h}^{(i)} = \frac{\omega_1 + \omega_2}{2} \mathbf{I} + (\omega_1 - \omega_2)\mathbf{s}_z^{(i)}$ is the twist matrix acting in the space $V_i \cong \mathbb{C}^2$ at the ith site. In the context of the Gaudin model, the parameters x_i (in general, complex numbers) are often called marked points of the Riemann sphere. Since the first two terms in the $\eta \to 0$ expansion of the $\mathbf{T}(x; e^{\eta h}, \eta, \{x_j\})$ are proportional to the identity operator and thus commute with everything, commutativity of the transfer matrices implies commutativity of the Gaudin Hamiltonians: $[\mathbf{H}_i^G, \mathbf{H}_j^G] = 0$. The Gaudin spectral problem consists in the simultaneous diagonalization of these operators and the operator $\mathbf{M}$ which has the same form as above: $\mathbf{H}_i^G \Psi = H_i^G \Psi$, $\mathbf{M}\Psi = M\Psi$. The Bethe ansatz solution is the $\eta \to 0$ limit of (3.18), (3.19):

$$H_j^G = \omega_1 + \sum_{k \neq j} \frac{1}{x_j - x_k} + \sum_{\alpha=1}^{M} \frac{1}{u_\alpha - x_j}, \tag{3.37}$$

where the Bethe roots u_α satisfy the system of equations

$$\omega_1 - \omega_2 + \sum_{k=1}^{N} \frac{1}{u_\alpha - x_k} = 2 \sum_{\beta=1, \neq \alpha}^{M} \frac{1}{u_\alpha - u_\beta}. \tag{3.38}$$

An alternative solution is achieved via the QC duality with the classical CM model with the Hamiltonian $\mathcal{H}^{\mathrm{CM}} = \frac{1}{2} \sum_{i=1}^{N} p_i^2 - \sum_{i<j} \frac{1}{(x_i - x_j)^2}$. The equations of motion are

$$\ddot{x}_i = -\sum_{k \neq i} \frac{2}{(x_i - x_k)^3}, \qquad i = 1, \ldots, N. \tag{3.39}$$

The CM model is known to be integrable, with the higher integrals of motion in involution being given by $\mathcal{H}_k^{\rm CM} = \frac{1}{k}\mathrm{tr}\,(\mathsf{Y}^{\rm CM})^k$ ($\mathcal{H}_1^{\rm CM}$ being the total momentum $\mathcal{P}^{\rm CM} = \sum_j p_j$ and $\mathcal{H}_2^{\rm CM} = \mathcal{H}^{\rm CM}$), where

$$\mathsf{Y}^{\rm CM}(\{x_i\};\{\dot{x}_i\}) = \begin{pmatrix} -\dot{x}_1 & \frac{1}{x_2-x_1} & \frac{1}{x_3-x_1} & \dots & \frac{1}{x_N-x_1} \\ \frac{1}{x_1-x_2} & -\dot{x}_2 & \frac{1}{x_3-x_2} & \dots & \frac{1}{x_N-x_2} \\ \vdots & \vdots & \vdots & \ddots & \vdots \\ \frac{1}{x_1-x_N} & \frac{1}{x_2-x_N} & \frac{1}{x_3-x_N} & \dots & -\dot{x}_N \end{pmatrix} \tag{3.40}$$

is the Lax matrix of the model. Its matrix elements are $\mathsf{Y}_{ij}^{\rm CM} = -\dot{x}_i\delta_{ij} - \dfrac{1-\delta_{ij}}{x_i-x_j}$.

Note that the CM model can be treated as a $\eta \to 0$ limit of the RS model meaning that

$$\mathsf{Y}^{\rm RS} = \mathsf{I} + \eta\mathsf{Y}^{\rm CM} + O(\eta^2)\,, \qquad \mathcal{H}_1^{\rm RS} = \frac{N}{\eta} + \mathcal{P}^{\rm CM} + \eta\tilde{\mathcal{H}}^{\rm CM} + O(\eta^2),$$

where $\tilde{\mathcal{H}}^{\rm CM} = \dfrac{1}{2}\sum_i \Big(p_i + \sum_{k\neq i}\dfrac{1}{x_i-x_k}\Big)^2 - \sum_{i<j}^N \dfrac{1}{(x_i-x_j)^2}$ differs from the $\mathcal{H}^{\rm CM}$ by a simple canonical transformation and leads to the same equations of motion.

The rules of the QC duality in this case are as follows [2, 4]. Consider the Lax matrix (3.40) of the N-particle CM model, where the x_i's are identified with the N marked points of the Gaudin model. Let us also substitute $\dot{x}_i = -H_i^G$:

$$\mathsf{Y}^{\rm CM}(\{x_i\};\{-H_i\}) = \begin{pmatrix} H_1^G & \frac{1}{x_2-x_1} & \frac{1}{x_3-x_1} & \dots & \frac{1}{x_N-x_1} \\ \frac{1}{x_1-x_2} & H_2^G & \frac{1}{x_3-x_2} & \dots & \frac{1}{x_N-x_2} \\ \vdots & \vdots & \vdots & \ddots & \vdots \\ \frac{1}{x_1-x_N} & \frac{1}{x_2-x_N} & \frac{1}{x_3-x_N} & \dots & H_N^G \end{pmatrix}. \tag{3.41}$$

The claim is that if the H_i^G's are eigenvalues of the Gaudin Hamiltonians in the invariant subspace $\mathcal{V}(M)$, then the first $N-M$ eigenvalues of this matrix coincide with eigenvalues of the twist matrix ω_1 while the rest M eigenvalues coincide with ω_2:

$$\mathrm{Spec}\,(\mathsf{Y}^{\mathrm{CM}}) = \Big(\underbrace{\omega_1, \dots, \omega_1}_{N-M}, \underbrace{\omega_2, \dots, \omega_2}_{M}\Big). \tag{3.42}$$

As it follows from the results of [34, 35], the characteristic polynomial of the matrix Y^{CM} can be represented in the form

$$\det_{N\times N}\Big(\lambda \mathsf{I} - \mathsf{Y}^{\mathrm{CM}}\Big) = \exp\Big(\sum_{i<j}^{N} \frac{\partial_{y_i}\partial_{y_j}}{(x_i - x_j)^2}\Big) \prod_{k=1}^{N}(\lambda - y_k)\Big|_{y_i = H_i^G}. \tag{3.43}$$

Therefore, the spectrum consists of the values $(H_1, H_2, \dots, H_N)$ such that the equality

$$\exp\Big(\sum_{i<j}^{N} \frac{\partial_{y_i}\partial_{y_j}}{(x_i - x_j)^2}\Big) \prod_{k=1}^{N}(\lambda - y_k)\Big|_{y_i = H_i^G} = (\lambda - w_1)^{N-M}(\lambda - w_2)^M \tag{3.44}$$

is satisfied identically in λ. As in the case of the XXX model, this is equivalent to N algebraic equations for N quantities H_i^G.

3.7 Concluding Remarks

The QC duality can be more or less straightforwardly extended to quantum inhomogeneous spin chains associated with $GL(n)$-invariant R-matrices. These models are solved by the nested Bethe ansatz (see [36]). On the classical side, the correspondence is with the same rational RS model, with eigenvalues of the Lax matrix being chosen (with some multiplicities) from the elements of the $n \times n$ diagonal twist matrix. The corresponding results can be found in [1, 3, 4]. In the present paper, we have restricted ourselves by the $GL(2)$ case only because of the notational simplicity.

An interesting possible generalization is the q-deformation of the QC duality which implies the anisotropic spin chains with trigonometric R-matrices (associated with $U_q(gl_n)$) on the quantum side. As is shown in [17], the classical side in this case is represented by the trigonometric RS model. However, some interesting details, including an accurate limit to the trigonometric Gaudin model, are still to be elaborated.

Among future perspectives we mention an extension to the supersymmetric $GL(n|m)$-invariant spin chains and to the spin chains with elliptic R-matrices. The latter case seems to be especially non-trivial because integrable magnets constructed with the help of elliptic R-matrices do not allow twisted boundary conditions with continuous parameters. That is why it is not clear how to fix values of the classical integrals of motion in the elliptic RS model which would be the most natural candidate for the classical part of the QC duality. Another difficulty is that the Lax matrix

for the elliptic RS model contains a spectral parameter. The role of this parameter in the context of the quantum-classical correspondence is not clear at the moment.

Acknowledgments Discussions with A. Alexandrov, A. Gorsky, V. Kazakov, S. Khoroshkin, I. Krichever, S. Leurent, M. Olshanetsky, A. Orlov, T. Takebe, Z. Tsuboi, and A. Zotov are gratefully acknowledged. Some of these results were reported at the International School and Workshop "Nonlinear Mathematical Physics and Natural Hazards" (November 28–December 2 2013, Sofia, Bulgaria). The author thanks the organizers and especially professors B. Aneva and V. Gerdzhikov for the invitation and support. This work was supported in part by RFBR grant 12-01-00525, by joint RFBR grants 12-02-91052-CNRS, 14-01-90405-Ukr and grant NSh-1500.2014.2 for support of leading scientific schools.

References

1. A. Alexandrov, V. Kazakov, S. Leurent, Z. Tsuboi, A. Zabrodin, Classical tau-function for quantum spin chains. JHEP **1309**, 064 (2013). arXiv:1112.3310
2. A. Alexandrov, S. Leurent, Z. Tsuboi, A. Zabrodin, The master T-operator for the Gaudin model and the KP hierarchy. Nucl. Phys. B **883**, 173–223 (2014). arXiv:1306.1111
3. A. Zabrodin, The master T-operator for inhomogeneous XXX spin chain and mKP hierarchy. SIGMA **10**, 006 (18 pp) (2014). arXiv:1310.6988
4. A. Gorsky, A. Zabrodin, A. Zotov, Spectrum of quantum transfer matrices via classical many-body systems. JHEP **01**, 070 (2014). arXiv:1310.6958
5. S.N.M. Ruijsenaars, H. Schneider, A new class of integrable systems and its relation to solitons. Ann. Phys. **170**, 370–405 (1986)
6. S.N.M. Ruijsenaars, Complete integrability of relativistic Calogero-Moser systems and elliptic function identities. Commun. Math. Phys. **110**, 191–213 (1987)
7. F. Calogero, Solution of the one-dimensional N -body problems with quadratic and/or inversely quadratic pair potentials. J. Math. Phys. **12**, 419–436 (1971)
8. J. Moser, Three integrable hamiltonian systems connected with isospectrum deformations. Adv. Math. **16**, 354–370 (1976)
9. M. Olshanetsky, A. Perelomov, Classical integrable finite dimensional systems related to Lie algebras. Phys. Rep. **71**, 313–400 (1981)
10. M. Gaudin, Diagonalisation d'une classe d'hamiltoniens de spin. J. de Phys. **37**(10), 1087–1098 (1976)
11. A. Givental, B.-S. Kim, Quantum cohomology of flag manifolds and Toda lattices. Commun. Math. Phys. **168**, 609–641 (1995). arXiv:hep-th/9312096
12. E. Mukhin, V. Tarasov, A. Varchenko, Gaudin Hamiltonians generate the Bethe algebra of a tensor power of vector representation of gl_N. St. Petersburg Math. J. **22**, 463–472 (2011). arXiv:0904.2131
13. E. Mukhin, V. Tarasov, A. Varchenko, Bethe algebra of Gaudin model, Calogero-Moser space and Cherednik algebra. Int. Math. Res. Not. **2014**(5), 1174–1204 (2014). arXiv:0906.5185
14. E. Mukhin, V. Tarasov, A. Varchenko, KZ characteristic variety as the zero set of classical Calogero-Moser Hamiltonians. SIGMA **8**, 072 (11 pp) (2012). arXiv:1201.3990
15. E. Mukhin, V. Tarasov, A. Varchenko, Bethe subalgebras of the group algebra of the symmetric group. arXiv:1004.4248
16. E. Mukhin, V. Tarasov, A. Varchenko, Spaces of quasi-exponentials and representations of the Yangian $Y(gl_N)$. arXiv:1303.1578
17. A. Zabrodin, The master T-operator for vertex models with trigonometric R-matrices as classical tau-function. Teor. Mat. Fys. **171**, 1, 59–76 (2013) (Theor. Math. Phys. **174**, 52–67 (2013)). arXiv:1205.4152

18. A. Zabrodin, Hirota equation and Bethe ansatz in integrable models. Suuri-kagaku J. (in Japanese) (Number **596**, 7–12 (2013))
19. E. Date, M. Jimbo, M. Kashiwara, T. Miwa, Transformation groups for soliton equations, in *Nonlinear Integrable Systems—Classical and Quantum*, ed. by M. Jimbo, T. Miwa (World Scientific, Singapore, 1983), pp. 39–120
20. M. Jimbo, T. Miwa, Solitons and infinite dimensional Lie algebras. Publ. RIMS Kyoto Univ. **19**, 943–1001 (1983)
21. N. Nekrasov, A. Rosly, S. Shatashvili, Darboux coordinates, Yang-Yang functional, and gauge theory. Nucl. Phys. Proc. Suppl. **216**, 69–93 (2011). arXiv:1103.3919
22. D. Gaiotto, P. Koroteev, On three dimensional quiver gauge theories and integrability. JHEP **05**, 126 (2013). arXiv:1304.0779
23. I. Krichever, O. Lipan, P. Wiegmann, A. Zabrodin, Quantum integrable models and discrete classical Hirota equations. Commun. Math. Phys. **188**, 267–304 (1997). arXiv:hep-th/9604080
24. A. Zabrodin, Discrete Hirota's equation in quantum integrable models. Int. J. Mod. Phys. **B11**, 3125–3158 (1997)
25. A. Zabrodin, Hirota equation and Bethe ansatz, Teor. Mat. Fyz. **116**, 54–100 (1998) (English translation: Theor. Math. Phys. **116**, 782–819 (1998)
26. V. Kazakov, A.S. Sorin, A. Zabrodin, Supersymmetric Bethe ansatz and Baxter equations from discrete Hirota dynamics. Nucl. Phys. B **790**, 345–413 (2008). arXiv:hep-th/0703147
27. A. Zabrodin, Bäcklund transformations for difference Hirota equation and supersymmetric Bethe ansatz. Teor. Mat. Fyz. **155**, 74–93 (2008) (English translation: Theor. Math. Phys. **155**, 567–584 (2008). arXiv:0705.4006
28. H. Bethe, Zur Theorie der Metalle. I. Eigenwerte und Eigenfunktionen der linearen Atomkette. Z. fur Phys. **71**, 205–226 (1931)
29. L. Faddeev, E. Sklyanin, L. Takhtajan, The quantum inverse problem method. I. Theor. Math. Phys. **40**, 688 (1980)
30. V.E. Korepin, N.M. Bogoliubov, A.G. Izergin, *Quantum Inverse Scattering Method and Correlation Functions*. Cambridge Monographs on Mathematical Physics (Cambridge University Press, Cambridge, 1997)
31. L. Faddeev, L. Takhtajan, The spectrum and scattering of excitations in the one-dimensional isotropic Heisenberg model. Zap. Nauch. Semin. LOMI **109**, 134–178 (1981)
32. K. Hikami, P. Kulish, M. Wadati, Construction of integrable spin systems with long-range interaction. J. Phys. Soc. Japan **61**, 3071–3076 (1992)
33. I. Macdonald, *Symmetric Functions and Hall Polynomials*, 2nd edn. (Oxford University Press, Oxford, 1995)
34. K. Sawada, T. Kotera, Integrability and a solution for the one-dimensional N-particle system with inversely quadratic pair potential. J. Phys. Soc. Jpn. **39**, 1614–1618 (1975)
35. S. Wojciechowski, New completely integrable Hamiltonian systems of N particles on the real line. Phys. Lett. A **59**, 84–86 (1976)
36. P. Kulish, N. Reshetikhin, Diagonalization of gl_N invariant transfer matrices and quantum N-wave system (Lee model). J. Phys. A **16**, L591–L596 (1983)

Chapter 4
Discriminantly Separable Polynomials and Their Applications

Vladimir Dragović and Katarina Kukić

Abstract Discriminantly separable polynomials by definition are polynomials which discriminants are factorized as the products of the polynomials in one variable. Motivating example for introducing such polynomials is Kowalevski top, one of the most celebrated integrable system, where the so called Kowalevski's fundamental equation appears to be such a polynomial. We introduced a whole class of systems which are based on discriminantly separable polynomials and on which the integration of the Kowalevski top may be generalized. We present also the role of the discriminantly separable polynomils in two well-known examples: the case of Kirchhoff elasticae and the Sokolov's case of a rigid body in an ideal fluid. Also we present the classification of the discriminantly separable polynomials of degree two in each of three variable and relate this classification to the classification of pencils of conics. Another application of discriminantly separable polynomials is in integrable quad-equations introduced by Adler, Bobenko and Suris. This paper presents a short review of our results concerning these polynomials.

4.1 Discriminantly Separable Polynomials—An Overview

The notion of *the discriminantly separable polynomials* has been introduced in [3], where one can see more about their properties. Here we briefly give outline of those notions.

V. Dragović (✉)
The Department of Mathematical Sciences, University of Texas at Dallas,
800 West Campbell Road, Richardson, TX 75080, USA
e-mail: Vladimir.Dragovic@utdallas.edu

V. Dragović
Mathematical Institute SANU, Kneza Mihaila 36, 11000 Belgrade, Serbia

K. Kukić
Faculty for Traffic and Transport Engineering, University of Belgrade,
Vojvode Stepe 305, 11000 Belgrade, Serbia
e-mail: k.mijailovic@sf.bg.ac.rs

B. Aneva and M. Kouteva-Guentcheva (eds.),
Nonlinear Mathematical Physics and Natural Hazards,
Springer Proceedings in Physics 163, DOI 10.1007/978-3-319-14328-6_4

Suppose that two conics C_1 and C_2 in general position are given by their tangential equations

$$C_1 : a_0w_1^2 + a_2w_2^2 + a_4w_3^2 + 2a_3w_2w_3 + 2a_5w_1w_3 + 2a_1w_1w_2 = 0; \quad (4.1)$$

$$C_2 : w_2^2 - 4w_1w_3 = 0. \quad (4.2)$$

We observe the pencil of conics $C(s) := C_1 + sC_2$ in which conics share four common tangents. Then the coordinate equation of the conics of the pencil is:

$$F(s, z_1, z_2, z_3) := \det M(s, z_1, z_2, z_3) = 0,$$

with the matrix M given in the next form:

$$M(s, z_1, z_2, z_3) = \begin{bmatrix} 0 & z_1 & z_2 & z_3 \\ z_1 & a_0 & a_1 & a_5 - 2s \\ z_2 & a_1 & a_2 + s & a_3 \\ z_3 & a_5 - 2s & a_3 & a_4 \end{bmatrix}. \quad (4.3)$$

The point equation of the pencil $C(s)$ is in the form of the quadratic polynomial in s

$$F := H + Ks + Ls^2 = 0$$

where H, K, and L are quadratic expressions in (z_1, z_2, z_3). After introducing a new system of coordinates in the plane, the Darboux coordinates (x_1, x_2) (see [1]), we rewrite its equation F in the form

$$F(s, x_1, x_2) = L(x_1, x_2)s^2 + K(x_1, x_2)s + H(x_1, x_2). \quad (4.4)$$

In the last formula L, K, and H are biquadratic polynomials of x_1, x_2 and the explicit formulae in terms of the coefficients of the conic C_1 may be seen in [3], and also detailed procedure of introducing the Darboux coordinates in the plane.

Here we emphasize one exceptional property that relates the equation of pencil of conics and the discriminants of the polynomial F.

The key algebraic property of the pencil equation written in the form (4.4) as a quadratic equation in each of three variables s, x_1, x_2 is: *all three of its discriminants are expressed as products of two polynomials in one variable each*:

$$\mathscr{D}_s(F)(x_1, x_2) = P(x_1)P(x_2), \ \mathscr{D}_{x_i}(F)(s, x_j) = J(s)P(x_j), i, j = c.p.1, 2,$$

where J and P are polynomials of degree 3 and 4 respectively. The explicit formulae for the polynomials P and J are

$$\begin{aligned} P(x) &= a_4x^4 - 4a_3x^3 + (4a_2 + 2a_5)x^2 - 4a_1x + a_0 \\ J(s) &= 4s^3 + 4(a_2 - a_5) + (a_5^2 - a_0a_4 + 4(a_1a_3 - a_2a_5))s \\ &\quad + a_0a_3^2 + a_2a_5^2 + a_4a_1^2 - a_0a_2a_4 - 2a_1a_3a_5. \end{aligned}$$

The elliptic curves

$$\Gamma_1 : y^2 = P(x), \quad \Gamma_2 : y^2 = J(s)$$

are isomorphic.

For better understanding of the correlation between pencils of conics and the discriminantly separable polynomials one can see [2, 3, 6, 8, 9].

The family of discriminantly separable polynomials in three variables of degree two in each of them, constructed from pencils of conics served as a motivation to introduce more general classes of **discriminantly separable polynomials**. Let us recall here the definitions from [3]: a polynomial $F(x_1, \dots, x_n)$ is *discriminantly separable* if there exist polynomials $f_i(x_i)$ such that for every $i = 1, \dots, n$

$$\mathscr{D}_{x_i} F(x_1, \dots, \hat{x}_i, \dots, x_n) = \prod_{j \neq i} f_j(x_j).$$

It is *symmetrically discriminantly separable* if $f_2 = f_3 = \cdots = f_n$, while it is *strongly discriminantly separable* if $f_1 = f_2 = f_3 = \cdots = f_n$. It is *weakly discriminantly separable* if there exist polynomials $f_i^j(x_i)$ such that for every $i = 1, \dots, n$: $\mathscr{D}_{x_i} F(x_1, \dots, \hat{x}_i, \dots, x_n) = \prod_{j \neq i} f_j^i(x_j)$.

The so-called *fundamental Kowalevski equation* (4.5) (see [10, 15]) appeared to be an example of a member of the family, as it has been observed in [3]:

$$Q(s, x_1, x_2) := (x_1 - x_2)^2(s - \frac{l_1}{2})^2 - R(x_1, x_2)(s - \frac{l_1}{2}) - \frac{1}{4}R_1(x_1, x_2) = 0, \quad (4.5)$$

where $R(x_1, x_2)$ and $R_1(x_1, x_2)$ are biquadratic polynomials in x_1 and x_2 given by

$$\begin{aligned} R(x_1, x_2) &= -x_1^2x_2^2 + 6l_1x_1x_2 + 2lc(x_1 + x_2) + c^2 - k^2 \\ R_1(x_1, x_2) &= -6l_1x_1^2x_2^2 - (c^2 - k^2)(x_1 + x_2)^2 - 4lcx_1x_2(x_1 + x_2) \\ &\quad + 6l_1(c^2 - k^2) - 4c^2l^2. \end{aligned}$$

The discriminant separability condition

$$\mathscr{D}_s(Q)(x_1, x_2) = P(x_1)P(x_2), \ \mathscr{D}_{x_i}(Q)(s, x_2) = J(s)P(x_j)$$

is satisfied with polynomials

$$J(s) = 4s^3 + (c^2 - k^2 - 3l_1^2)s - l^2c^2 + l_1^3 - l_1k^2 + l_1c^2$$
$$P(x_i) = -x_i^4 + 6l_1x_i^2 + 4lcx_i + c^2 - k^2,\ i = 1, 2.$$

Moreover, as it has been explained in [3], all the main steps of the Kowalevski integration procedure from [15] (see also [10]) now follow as easy and transparent logical consequences of the theory of discriminantly separable polynomials.

After we noticed these interesting properties of discriminantly separable polynomials, two natural questions appeared: the question of classification of such polynomials and the question of existence other integrable dynamical systems related to discriminantly separable polynomials. We answered on both questions in our papers: in [4] we presented new examples of dynamical systems obtained by replacing the Kowalevski fundamental equation by some other discriminantly separable polynomail in three variables degree two in each of them and we called such systems systems of Kowalevski type. In [5] we further developed theory of such systems, we obtained procedure for their explicit integration in theta functions of genus two by generalizing integration of Kowalevski top and we also found few examples of well known systems from theory of integrable dynamical systems that could be explicitly integrated by suggested procedure. In [6] we presented classification of discriminantly separable polynomials of three variables degree two in each of them modulo the group of Möbius transformations, as introduced in Corollary 3 of [3]:

$$x_1 \mapsto \frac{a_1x_1 + b_1}{c_1x_1 + d_1},\ x_2 \mapsto \frac{a_2x_2 + b_2}{c_2x_2 + d_2},\ w \mapsto \frac{a_3w + b_3}{c_3w + d_3}. \tag{4.6}$$

In [6] we also related discriminantly separable polynomials with quad-equations. In this review paper we give a brief overview of these results.

4.2 Classification of Strongly Discriminantly Separable Polynomials of Degree Two in Three Variables

In this section we present classification of strongly discriminantly separable polynomials $\mathscr{F}(x_1, x_2, x_3) \in C[x_1, x_2, x_3]$ which are of degree two in each variable, modulo a group of the Möbius transformations

$$x_1 \mapsto \frac{ax_1 + b}{cx_1 + d},\ x_2 \mapsto \frac{ax_2 + b}{cx_2 + d},\ x_3 \mapsto \frac{ax_3 + b}{cx_3 + d}. \tag{4.7}$$

Let

$$\mathscr{F}(x_1, x_2, x_3) = \sum_{i,j,k=0}^{2} a_{ijk}x_1^i x_2^j x_3^k \tag{4.8}$$

be a strongly discriminantly separable polynomial with

$$\mathscr{D}_{x_i}\mathscr{F}(x_j, x_k) = P(x_j)P(x_k), \quad (i, j, k) = c.p.(1, 2, 3). \tag{4.9}$$

Here, by $\mathscr{D}_{x_i}\mathscr{F}(x_j, x_k)$ we denote the discriminant of $\mathscr{F}$ considered as a quadratic polynomial in x_i.

Theorem 4.1 *The strongly discriminantly separable polynomials $\mathscr{F}(x_1, x_2, x_3)$ satisfying (4.9) modulo fractional linear transformations are exhausted by the following list depending on the structure of the roots of a non-zero polynomial $P(x)$:*

(A) P has four simple zeros, with the canonical form $P_A(x) = (k^2x^2 - 1)(x^2 - 1)$, the correspoding strongly discriminantly separable polynomial is

$$\begin{aligned}\mathscr{F}_A =& \frac{1}{2}(-k^2x_1^2 - k^2x_2^2 + 1 + k^2x_1^2x_2^2)x_3^2 + (1 - k^2)x_1x_2x_3 \\ &+ \frac{1}{2}(x_1^2 + x_2^2 - k^2x_1^2x_2^2 - 1),\end{aligned}$$

(B) P has two simple zeros and one double zero, with the canonical form $P_B(x) = x^2 - e^2$, $e \neq 0$,

$$\mathscr{F}_B = x_1x_2x_3 + \frac{e}{2}(x_1^2 + x_2^2 + x_3^2 - e^2)$$

(C) P has two double zeros, with the canonical form $P_C(x) = x^2$,

$$\mathscr{F}_{C_1} = \lambda x_1^2x_2^2 + \mu x_1x_2x_3 + \nu x_3^2, \quad \mu^2 - 4\lambda\nu = 1,$$

$$\mathscr{F}_{C_2} = \lambda x_1^2x_3^2 + \mu x_1x_2x_3 + \nu x_2^2, \quad \mu^2 - 4\lambda\nu = 1,$$

$$\mathscr{F}_{C_3} = \lambda x_2^2x_3^2 + \mu x_1x_2x_3 + \nu x_1^2, \quad \mu^2 - 4\lambda\nu = 1,$$

$$\mathscr{F}_{C_4} = \lambda x_1^2x_2^2x_3^2 + \mu x_1x_2x_3 + \nu, \quad \mu^2 - 4\lambda\nu = 1,$$

(D) P has one simple and one triple zero,with the canonical form $P_D(x) = x$,

$$\mathscr{F}_D = -\frac{1}{2}(x_1x_2 + x_2x_3 + x_1x_3) + \frac{1}{4}(x_1^2 + x_2^2 + x_3^2),$$

(E) P has one quadruple zero, with the canonical form $P_E(x) = 1$,

$$\mathscr{F}_{E_1} = \lambda(x_1 + x_2 + x_3)^2 + \mu(x_1 + x_2 + x_3) + \nu, \quad \mu^2 - 4\lambda\nu = 1,$$

$$\mathscr{F}_{E_2} = \lambda(x_2 + x_3 - x_1)^2 + \mu(x_2 + x_3 - x_1) + \nu, \quad \mu^2 - 4\lambda\nu = 1,$$

$$\mathscr{F}_{E_3} = \lambda(x_1 + x_3 - x_2)^2 + \mu(x_1 + x_3 - x_2) + \nu, \quad \mu^2 - 4\lambda\nu = 1,$$

$$\mathscr{F}_{E_4} = \lambda(x_1 + x_2 - x_3)^2 + \mu(x_1 + x_2 - x_3) + \nu, \quad \mu^2 - 4\lambda\nu = 1.$$

The proof of the theorem is computational and may be seen in [6]. There is a remarkable correspondence between this classification and the classification of pencils of conics. In the case of general position, the conics of a pencil intersect in four distinct points, and it corresponds to the case where the polynomial P has four simple zeros. In this case, the family of strongly discriminantly separable polynomials coincides with the family constructed above from a general pencil of conics. However, in the degenerate cases the above mentioned correspondence between the discriminantly separable polynomials and pencils of conics is much more delicate. It remains valid in all cases where the polynomial J has at least one simple zero (cases (B) and (D)). But this correspondence is broken in the other two cases, which are characterized by the fact that the polynomial J has multiple zeros only, cases (C) and (E). The more detailed this correspondence is explained in [6]. In the same paper we established correlation between discriminantly separable polynomials and quad-equations, but here we do not get into details of that correlation.

4.3 The Role of Discriminantly Separable Polynomials in Systems of Kowalevski Type

Motivated by the system of equation to which the Kowalevski top reduces and by discriminant separability of the Kowalevski fundamental (4.5), we introduced a new class of integrable systems and named them systems of Kowalevski type. Basically we replace the Kowalevski fundamental (4.5) by a discriminantly separable polynomial of the second degree in each of three variables

$$\mathscr{F}(x_1, x_2, s) := A(x_1, x_2)s^2 + 2B(x_1, x_2)s + C(x_1, x_2), \tag{4.10}$$

such that

$$\mathscr{D}_s(\mathscr{F})(x_1, x_2) = 4(B^2 - AC) = 4P(x_1)P(x_2),$$

and

$$\mathscr{D}_{x_1}(\mathscr{F})(s, x_2) = P(x_2)J(s)$$
$$\mathscr{D}_{x_2}(\mathscr{F})(s, x_1) = P(x_1)J(s).$$

Suppose, that a given system in variables $x_1,\ x_2,\ e_1,\ e_2,\ r,\ \gamma_3$, after some transformations reduces to

$$\begin{aligned} \dot{x}_1 &= -if_1, \quad \dot{e}_1 = -me_1, \\ \dot{x}_2 &= if_2, \quad \dot{e}_2 = me_2, \end{aligned} \tag{4.11}$$

where

$$f_1^2 = P(x_1) + e_1A(x_1, x_2), \quad f_2^2 = P(x_2) + e_2A(x_1, x_2). \tag{4.12}$$

Suppose additionally, that the first integrals and invariant relations of the initial system reduce to a relation

$$P(x_2)e_1 + P(x_1)e_2 = C(x_1, x_2) - e_1e_2A(x_1, x_2). \tag{4.13}$$

Instead of (4.13) we can assume that

$$\dot{x}_1\dot{x}_2 = -B(x_1, x_2) \tag{4.14}$$

where $B(x_1, x_2)$ is coefficient of polynomial (4.10). The equivalence of (4.13) and (4.14) under assumptions (4.11), (4.12) and (4.10) is shown in [5]. The equations for $\dot{r}$ and $\dot{\gamma}_3$ are not specified for the moment and m is a function of system's variables. If a system satisfies the above assumptions we will call it *a system of the Kowalevski type*. The Kowalevski top is an example of such systems. The following theorem is quite general, and gives the integration procedure for the whole new class of systems.

Theorem 4.2 *Given a system which reduces to* (4.11, 4.12, 4.13). *Then the system is linearized on the Jacobian of the curve*

$$y^2 = J(z)(z - k)(z + k),$$

where J is a polynomial factor of the discriminant of $\mathscr{F}$ as a polynomial in x_1 and k is a constant such that

$$e_1e_2 = k^2.$$

In the continuation of the paper we briefly present one already known system in the new light, as a system of Kowalevski type. It is about the system introduced by Sokolov in [14, 16, 17] given by the Hamiltonian

$$\hat{H} = M_1^2 + M_2^2 + 2M_3^2 + 2c_1\gamma_1 + 2c_2(\gamma_2M_3 - \gamma_3M_2) \tag{4.15}$$

on $e(3)$ with the Lie-Poisson brackets

$$\{M_i, M_j\} = \varepsilon_{ijk}M_k, \quad \{M_i, \gamma_j\} = \varepsilon_{ijk}\gamma_k, \quad \{\gamma_i, \gamma_j\} = 0 \tag{4.16}$$

where ε_{ijk} is the totally skew-symmetric tensor. In [14] a set of the separation variables for this case was given. We proved that this system belongs to the class of systems of the Kowalevski type by introducing slightly modified separation variables which further, as in Theorem 4.2, gave us possibility to explicitly integrate this system of equation. The Lie-Poisson bracket (4.16) has two well-known Casimir functions $\gamma_1^2 + \gamma_2^2 + \gamma_3^2 = a$ and $\gamma_1M_1 + \gamma_2M_2 + \gamma_3M_3 = b$. Following [14, 15] we introduce the new variables $z_1 = M_1 + iM_2$ and $z_2 = M_1 - iM_2$ and

$$e_1 = z_1^2 - 2c_1(\gamma_1 + i\gamma_2) - c_2^2 a - c_2(2\gamma_2 M_3 - 2\gamma_3 M_2 + 2i(\gamma_3 M_1 - \gamma_1 M_3)),$$
$$e_2 = z_2^2 - 2c_1(\gamma_1 - i\gamma_2) - c_2^2 a - c_2(2\gamma_2 M_3 - 2\gamma_3 M_2 + 2i(\gamma_1 M_3 - \gamma_3 M_1)).$$

The second integral of motion for the system (4.15) may be rewritten as $e_1 e_2 = k^2$. The equations of motion in the new variables z_i, e_i can be written in the form of (4.11) and (4.12), and this corresponds to the definition of the systems of the Kowalevski type. One can easily check that:

$$\dot{e}_1 = -4i M_3 e_1, \quad \dot{e}_2 = 4i M_3 e_2$$

and

$$-\dot{z_1}^2 = P(z_1) + e_1(z_1 - z_2)^2, \quad -\dot{z_2}^2 = P(z_2) + e_2(z_1 - z_2)^2 \tag{4.17}$$

where P is a polynomial of fourth degree given by

$$P(z) = -z^4 + 2Hz^2 - 8c_1 bz - k^2 + 4ac_1^2 - 2c_2^2(2b^2 - Ha) + c_2^4 a. \tag{4.18}$$

In order to prove that the Sokolov system belongs to the class of the systems of the Kowalevski type, we still need to show that a relation of the form (4.13) or equivalent (4.14) is satisfied and we have to relate it with certain discriminantly separable polynomial of the form of (4.10). After some calculations we obtained

Lemma 4.1 *The variables z_1, z_2, e_1, e_2 of the Sokolov system satisfy the following identity*:

$$(z_1 - z_2)^2[2F(z_1, z_2)(H + c_2^2 a) + (z_1 - z_2)^2(H + c_2^2 a)^2 - P(z_1)e_2 - P(z_2)e_1 - e_1 e_2(z_1 - z_2)^2] + F^2(z_1, z_2) - P(z_1)P(z_2) = 0.$$

where $F(z_1, z_2) = -\frac{1}{2}\left(P(z_1) + P(z_2) + (z_1^2 - z_2^2)^2\right)$.

So we conclude that the Sokolov system is a system of the Kowalevski type. It can be explicitly integrated in the theta-functions of genus 2, as we did in [7].

Another already known system that can be integrated with the help of the properties of the discriminantly separable polynomials as stated in Theorem 4.2 is the classical Kirchhoff problem of elasticae. In [11], Jurdjevic connected deformations of the Kowalevski top introduced by Komarov in [12, 13], with the classical Kirchhoff problem of elasticae. In [5] we derived the explicit solutions in genus two theta-functions of these systems and also presented one more way to get those systems. We showed that discriminantly separable polynomials induced by these systems and the Kowalevski fundamental equation are equivalent by using simple linear transformation.

4.4 Conclusion

Discriminantly separable polynomials clearly have a significant role in a certain type of integrable systems. Their role is visible also in the class of discrete integrable systems in the case of quad-equation. Their geometric background gives us a possibility to relate these integrable systems with pencils of conics in certain sence. The list of the integrable systems in which one can find a discriminantly separable polynomials in some varibles is still supplementing and that is our current assignment.

Acknowledgments The research was partially supported by the Serbian Ministry of Science and Technological Development, Project 174020 *Geometry and Topology of Manifolds, Classical Mechanics and Integrable Dynamical Systems*. One of the authors (K.K.) uses the opportunity to thanks to professor Boyka Aneva for hospitallity during the conference *Nonlinear Mathematical Physics and Natural Hazards*, held in Sofia in November 2013, and also to the ICTP—SEENET-MTP Project PRJ09 "Cosmology and Strings" in frame of the Southeastern European Network in Theoretical and Mathematical Physics.

References

1. G. Darboux, *Principes de géométrie analytique* (Gauthier-Villars, Paris, 1917), p. 519
2. V. Dragović, Poncelet-Darboux curves, their complete decomposition and Marden theorem. Int. Math. Res. **15**, 3502–3523 (2011)
3. V. Dragović, Generalization and geometrization of the Kowalevski top. Commun. Math. Phys. **298**(1), 37–64 (2010)
4. V. Dragović, K. Kukić, New examples of systems of the Kowalevski type. Regul. Chaotic Dyn. **16**(5), 484–495 (2011)
5. V. Dragović, K. Kukić, Systems of the Kowalevski type and discriminantly separable polynomials. Regul. Chaotic Dyn. **19**(2), 162–184 (2014)
6. V. Dragović, K. Kukić, Discriminantly separable polynomials and quad-equations. J. Geom. Mech. **6**(3), 319–333 (2014)
7. V. Dragović, K. Kukić, The Sokolov case, integrable Kirchhoff elasticae, and genus 2 theta-functions via discriminantly separable polynomials. Proc. Steklov Inst. Math. **286**(1), 224–239 (2014)
8. V. Dragović, M. Radnović, Poncelet porisms and beyond (Springer, Basel, 2011)
9. V. Dragović, M. Radnović, Billiard algebra, integrable line congruences and DR-nets J. Nonlinear Math. Phys. **19**(3), 300–317 (2012)
10. V.V. Golubev, *Lectures on the integration of motion of a heavy rigid body around a fixed point* (Israel program for scintific literature, English translation, 1960). (Gostechizdat, Moscow, 1953 [in Russian])
11. V. Jurdjevic, Integrable Hamiltonian systems on Lie Groups: Kowalevski type. Ann. Math. **150**, 605–644 (1999)
12. I.V. Komarov, Kowalevski top for the hydrogen atom. Theor. Math. Phys. **47**(1), 67–72 (1981)
13. I.V. Komarov, V.B. Kuznetsov, Kowalevski top on the Lie algebras $o(4)$, $e(3)$ and $o(3, 1)$. J. Phys. A **23**(6), 841–846 (1990)
14. I.V. Komarov, V.V. Sokolov, A.V. Tsiganov, Poisson maps and integrable deformations of the Kowalevski top. J. Phys. A **36**, 8035–8048 (2003)
15. S. Kowalevski, Sur la probleme de la rotation d'un corps solide autour d'un point fixe. Acta Math. **12**, 177–232 (1889)

16. V.V. Sokolov, A new integrable case for Kirchoff equation. Theor. Math. Phys. **129**(1), 1335–1340 (2001)
17. V.V. Sokolov, Generalized Kowalevski Top: New Integrable Cases on $e(3)$ and $so(4)$, ed. by V.B. Kuznetsov. The Kowalevski Poperty (CRM Proceedings and Lecture Notes, AMS, 2002), p. 307

Chapter 5
MKdV-Type of Equations Related to $B_2^{(1)}$ and $A_4^{(2)}$

V.S. Gerdjikov, D.M. Mladenov, A.A. Stefanov and S.K. Varbev

Abstract We have derived two systems of mKdV-type equations which can be related to the affine Lie algebras $B_2^{(1)}$ and $A_4^{(2)}$ respectively. They are integrable via the inverse scattering method and possess soliton solutions and a hierarchy of Hamiltonian structures.

5.1 Introduction

This work can be considered as an extension of our recent publications [12, 13] and the classical paper by Drinfeld and Sokolov [4]. Many of the important ideas in the field of completely integrable infinite dimensional systems were introduced there. These include: (i) the importance of the graded algebras for deriving their Lax representation; (ii) the importance of the automorphisms of Coxeter type to construct the Kac-Moody algebras; (iii) the recursion operators and the bi-Hamiltonian formulation of the integrable systems.

Each of those ideas deserve separate and detailed exposition which often varies due to the system considered. These ideas can naturally be combined with a deeper study of the spectral properties of the relevant Lax operators, which most often

V.S. Gerdjikov (✉)
Institute of Nuclear Research and Nuclear Energy, Bulgarian Academy of Sciences,
72 Tsarigradsko chausee, 1784 Sofia, Bulgaria
e-mail: gerjikov@inrne.bas.bg

D.M. Mladenov · A.A. Stefanov · S.K. Varbev
Theoretical Physics Department, Faculty of Physics,
Sofia University "St. Kliment Ohridski", 5 James Bourchier Blvd,
1164 Sofia, Bulgaria
e-mail: dimitar.mladenov@phys.uni-sofia.bg

A.A. Stefanov
e-mail: astefanov@phys.uni-sofia.bg

S.K. Varbev
e-mail: stanislavvarbev@phys.uni-sofia.bg

B. Aneva and M. Kouteva-Guentcheva (eds.),
Nonlinear Mathematical Physics and Natural Hazards,
Springer Proceedings in Physics 163, DOI 10.1007/978-3-319-14328-6_5

leads to the interpretation of the inverse scattering method (ISM) [2, 5, 11, 21] as a generalized Fourier transform [1, 6, 7]. The completion of all these tasks is a still a challenge which, we believe, must be met.

The present paper is an attempt to provide a detailed explanation of how some of the simplest mKdV-type equations related to the Lie algebra $so(5) \simeq B_2^{(1)}$ and to the twisted affine Kac-Moody algebra $A_4^{(2)}$ can be derived. Both systems involve two functions of two variables. Although they look similar they are inequivalent because they correspond to inequivalent Kac-Moody algebras.

In Sect. 5.2 we have given some basic preliminaries, including the grading introduced by the Coxeter automorphism. Section 5.3 is devoted to the recursion relations and the recursion operators [6, 10, 11, 18] that we will use to derive the corresponding systems of equations. The considerations here demonstrate that the recursion operators [1, 11, 18, 19], known to generate the NLEE and their Hamiltonian hierarchies, factorize. Sections 5.4 and 5.5 contain the derivation of the equations for the $B_2^{(1)}$ and $A_4^{(2)}$ algebras respectively. We also find the Hamiltonians of the two equations which are equivalent to the ones in [4]. We end the paper in Sect. 5.6 with some concluding remarks.

5.2 Preliminaries

We assume that the reader is familiar with the theory of the simple Lie algebras [14] and of the Kac-Moody algebras [3, 15]. The mKdV equations admit a Lax representation $[L,\ M] = 0$ and can be written as the commutativity condition of two ordinary differential operators of the type

$$\begin{aligned} L\psi &\equiv i\frac{\partial\psi}{\partial x} + U(x,t,\lambda)\psi = 0, \\ M\psi &\equiv i\frac{\partial\psi}{\partial t} + V(x,t,\lambda)\psi = \psi\Gamma(\lambda). \end{aligned} \tag{5.1}$$

In our case $U(x,t,\lambda)$, $V(x,t,\lambda)$ are polynomials of the spectral parameter λ taking values in the simple Lie algebra $\mathfrak{g}$ and $\Gamma(\lambda)$ is a matrix independent of x and t. We request also that the Lax pair (5.1) possesses appropriate reduction group [16], for example if the reduction group is $\mathbb{Z}_h$ then the reduction condition is

$$C\big(U(x,t,\lambda)\big) = U(x,t,\omega\lambda), \qquad C\big(V(x,t,\lambda)\big) = V(x,t,\omega\lambda). \tag{5.2}$$

Since the potentials are polynomial in λ, this implies that its coefficients must take values in a graded Lie algebra, where the grading is introduced by the automorphism C of order h

$$C^h(X) = X, \qquad X \in \mathfrak{g}\,. \tag{5.3}$$

Obviously C introduces a grading in $\mathfrak{g}$ by

$$\mathfrak{g} = \bigoplus_{k=0}^{h} \mathfrak{g}^{(k)}, \qquad C(X^{(k)}) = \omega^k X^{(k)}, \qquad X^{(k)} \in g^{(k)}, \tag{5.4}$$

where $\omega^h = 1$ and ω^k are the eigenvalues of C. The grading condition also holds

$$\left[\mathfrak{g}^{(k)}, \mathfrak{g}^{(l)}\right] \subset \mathfrak{g}^{(k+l)}, \tag{5.5}$$

where $k + l$ is taken modulo h.

In our case the automorphism is a Coxeter automorphism, i.e. an automorphism of order h, where h is called the Coxeter number. We would like to note, that if the underlying algebra is not $D_{2r}^{(1)}$ and the grading is done using a Coxeter automorphism then for each eigenspace we have

$$\dim(\mathfrak{g}^{(k)}) = \begin{cases} r & \text{if } k \text{ is not an exponent,} \\ r+1 & \text{if } k \text{ is an exponent,} \end{cases} \tag{5.6}$$

where r is the rank of $\mathfrak{g}$.

We start with a Lax pair that is polynomial in λ

$$\begin{aligned} L &= i\partial_x + Q(x,t) - \lambda J, \\ M &= i\partial_t + \sum_{k=0}^{n-1} \lambda^k V^{(k)}(x,t) - \lambda^n K, \end{aligned} \tag{5.7}$$

where

$$Q(x,t) \in \mathfrak{g}^{(0)}, \quad V^{(k)}(x,t) \in \mathfrak{g}^{(k)}, \quad K \in \mathfrak{g}^{(n)}, \quad J \in \mathfrak{g}^{(1)}. \tag{5.8}$$

Here J and K are some properly chosen constant matrices. In order to get a set of MKdV equations, we have chosen $V(x,t,\lambda)$ to be cubic polynomial of λ. For technical reasons the Lax pair (5.7) is slightly different from the one used in [4].

The Lax pair must commute, i.e.

$$\left[L, M\right] = 0 \tag{5.9}$$

for every λ, which will lead to a set of recursion relations. Solving them we will get explicit expressions for $V^{(k)}(x,t)$ in terms of $Q(x,t)$ and finally will obtain the equations as constraints for the potential $Q(x,t)$.

Below we denote the Killing-Cartan form on $\mathfrak{g}$ by $\langle\ ,\ \rangle$. By ad_J below we mean the linear operator defined by

$$\mathrm{ad}_J(X) = \left[J, X\right]. \tag{5.10}$$

This operator has a kernel and can only be inverted on its image. We denote that inverse by ad_J^{-1}. From its spectral properties it follows that ad_J^{-1} can be expressed as a polynomial of ad_J. By e_{ij} we denote a matrix with one at the i-th row and j-th column and zeros everywhere else, i.e. $(e_{ij})_{mn} = \delta_{im}\delta_{jn}$.

5.3 Recursion Relations and Recursion Operators

Here we adapt the theory of the recursion operators [6, 10, 11, 18] to the special choices of the Lax operator (5.7). For simplicity we assume that n in (5.7) is $n \le h$ and n is an exponent of $\mathfrak{g}$. The commutativity condition (5.9) implies the following recursion relations

$$\begin{aligned}
&\lambda^{n+1}: && \big[J, K\big] = 0,\\
&\lambda^{n}: && \big[J, V^{(n)}(x,t)\big] + \big[Q(x,t), K\big] = 0,\\
&\lambda^{s}: && i\frac{\partial V^{(s)}}{\partial x} + \big[Q(x,t), V^{(s)}(x,t)\big] - \big[J, V^{(s-1)}(x,t)\big] = 0,\\
&\lambda^{0}: && -i\frac{\partial Q}{\partial x} + i\frac{\partial V^{(0)}}{\partial x} + \big[Q(x,t), V^{(0)}(x,t)\big] = 0.
\end{aligned} \tag{5.11}$$

Each element splits into "orthogonal" and "parallel" parts

$$\begin{aligned}
&V^{(s)}(x,t) = V_\perp^{(s)}(x,t) + V_\parallel^{(s)}(x,t), \quad \mathrm{ad}_J\left(V_\parallel^{(s)}(x,t)\right) = 0,\\
&V_\parallel^{(s)}(x,t) = \begin{cases} 0 & \text{if } s \text{ is not an exponent,}\\ c_s^{-1} J^s \big\langle V_s, J^{h-s}\big\rangle & \text{if } s \text{ is an exponent,}\end{cases}
\end{aligned} \tag{5.12}$$

where $c_s = \langle J^{n-s}, J^{h-n+s}\rangle$.

From (5.11) we can see that

$$\begin{aligned}
&V_\perp^{(s-1)}(x,t) = \mathrm{ad}_J^{-1}\left(i\frac{\partial V^{(s)}}{\partial x} + \big[Q(x,t), V_\perp^{(s)}(x,t)\big] + \big[Q(x,t), V_\parallel^{(s)}(x,t)\big]\right),\\
&i\frac{\partial V_\parallel^{(s)}}{\partial x} = \big[Q(x,t), V_\perp^{(s)}(x,t)\big]_\parallel.
\end{aligned} \tag{5.13}$$

Integrating the second equation we see that

$$\begin{aligned}
V_\parallel^{(s)}(x,t) &= -i(\partial_x)_\pm^{-1}\left(\big[Q(x,t), V_\perp^{s}(x,t)\big]_\parallel\right)\\
&= -c_s^{-1} J^s i(\partial_x)^{-1}\Big\langle \big[Q(x,t), V_\perp^{s}(x,t)\big], J^{h-s}\Big\rangle,
\end{aligned} \tag{5.14}$$

where $(\partial_x)_{\pm}^{-1} = \int_{\pm\infty}^{x} dy$ and we have set any constants of integration to be equal to zero. Thus the formal solution of the recurrent relations takes the form

$$V_{\perp}^{(s)}(x,t) = \Lambda_s V_{\perp}^{(s+1)}(x,t). \tag{5.15}$$

If s is not an exponent, then

$$\Lambda_s X = \mathrm{ad}_J^{-1}\left(i\frac{\partial X}{\partial x} + \big[Q(x,t), X\big]\right), \tag{5.16}$$

otherwise

$$\Lambda_s X = \mathrm{ad}_J^{-1}\left(i\frac{\partial X}{\partial x} + \big[Q(x,t), X\big] - ic_s^{-1}\big[Q(x,t), J^s\big](\partial_x)_{\pm}^{-1}\Big\langle\big[Q(x,t), X\big], J^{h-s}\Big\rangle\right). \tag{5.17}$$

The corresponding NLEE can be written as

$$i\ \mathrm{ad}_J^{-1}\frac{\partial Q}{\partial t} - a\Lambda_0 V^{(0)} = 0 \tag{5.18}$$

and Λ_0 is given by (5.16).

5.4 Equations Related to $B_2^{(1)}$

The underlying Kac-Moody algebra is $B_2^{(1)}$, its rank is 2, the Coxeter number is 4 and the exponents are 1 and 3. The Coxeter automorphism is given by

$$C_4(X) = c_4 X c_4^{-1}, \tag{5.19}$$

where

$$c_4 = \begin{pmatrix} \omega^2 & 0 & 0 & 0 & 0 \\ 0 & \omega^1 & 0 & 0 & 0 \\ 0 & 0 & 1 & 0 & 0 \\ 0 & 0 & 0 & \omega^{-1} & 0 \\ 0 & 0 & 0 & 0 & \omega^{-2} \end{pmatrix} \tag{5.20}$$

and $\omega = \exp(2\pi i/4)$. The inverse of ad_J is

$$\mathrm{ad}_J^{-1} = \frac{1}{16}(6\,\mathrm{ad}_J^3 + \mathrm{ad}_J^7). \tag{5.21}$$

A basis compatible with the grading of $B_2^{(1)}$ is given by

$$\begin{aligned}
&\mathfrak{g}^{(0)}: \quad E_1^{(0)} = e_{11} - e_{55}, \quad E_2^{(0)} = e_{22} - e_{44}, \\
&\mathfrak{g}^{(1)}: \quad E_1^{(1)} = e_{12} + e_{45}, \quad E_2^{(1)} = e_{23} + e_{34}, \quad E_3^{(1)} = e_{41} + e_{52}, \\
&\mathfrak{g}^{(2)}: \quad E_1^{(2)} = e_{13} - e_{35}, \quad E_2^{(2)} = e_{31} - e_{53}, \\
&\mathfrak{g}^{(3)}: \quad E_1^{(3)} = e_{21} + e_{54}, \quad E_2^{(3)} = e_{32} + e_{43}, \quad E_3^{(3)} = e_{14} + e_{25}.
\end{aligned} \tag{5.22}$$

The coefficients of the potentials in the Lax pair are parameterized by

$$\begin{aligned}
Q(x,t) &= \frac{1}{2}\left(q_1(x,t)E_1^{(0)} + q_2(x,t)E_2^{(0)}\right), \\
V^{(2)}(x,t) &= v_1^{(2)}(x,t)E_1^{(2)} + v_2^{(2)}(x,t)E_2^{(2)}, \\
V^{(1)}(x,t) &= v_1^{(1)}(x,t)E_1^{(1)} + v_2^{(1)}(x,t)E_2^{(1)} + v_3^{(1)}(x,t)E_3^{(1)}, \\
V^{(0)}(x,t) &= v_1^{(0)}(x,t)E_1^{(0)} + v_2^{(0)}(x,t)E_2^{(0)}, \\
K &= aE_1^{(3)} + 2aE_2^{(3)} + aE_3^{(3)}, \\
J &= E_1^{(1)} + E_2^{(1)} + E_3^{(1)}.
\end{aligned} \tag{5.23}$$

To simplify the notation we will omit writing the dependence on x and t. Using the recursion operators (5.15), we get for the coefficients of the potentials

$$v_1^{(2)} = \frac{a}{2}(q_1 + q_2), \qquad v_2^{(2)} = \frac{a}{2}(q_1 - q_2), \tag{5.24}$$

$$\begin{aligned}
v_1^{(1)} &= -\frac{a}{4}\left(\frac{1}{4}q_1^2 + q_1q_2 + 2i\frac{\partial q_1}{\partial x} + i\frac{\partial q_2}{\partial x} + \frac{1}{4}q_2^2\right), \\
v_2^{(1)} &= \frac{a}{4}\left(\frac{3}{4}q_1^2 + i\frac{\partial q_2}{\partial x} - \frac{1}{4}q_2^2\right), \\
v_3^{(1)} &= -\frac{a}{4}\left(\frac{1}{4}q_1^2 - q_1q_2 - 2i\frac{\partial q_1}{\partial x} + i\frac{\partial q_2}{\partial x} + \frac{1}{4}q_2^2\right),
\end{aligned} \tag{5.25}$$

$$\begin{aligned}
v_1^{(0)} &= \frac{a}{32}\left(q_1^3 - 3q_2^2q_1 - 16\frac{\partial^2 q_1}{\partial x^2} + 12iq_1\frac{\partial q_2}{\partial x}\right), \\
v_2^{(0)} &= \frac{a}{32}\left(q_2^3 - 3q_1^2q_2 + 8\frac{\partial^2 q_2}{\partial x^2} - 12iq_1\frac{\partial q_1}{\partial x}\right).
\end{aligned} \tag{5.26}$$

Finally, the λ-independent terms in the Lax representation provide the equations

$$\begin{aligned}\alpha\frac{\partial q_1}{\partial t} &= -\frac{\partial^3 q_1}{\partial x^3} + i\frac{3}{4}\left[\left(\frac{\partial q_1}{\partial x}\right)\left(\frac{\partial q_2}{\partial x}\right) + q_1\left(\frac{\partial^2 q_2}{\partial x^2}\right)\right] \\ &\quad + \frac{3}{16}\left(q_1^2 - q_2^2\right)\left(\frac{\partial q_1}{\partial x}\right) - \frac{3}{8}q_1 q_2\left(\frac{\partial q_2}{\partial x}\right), \\ \alpha\frac{\partial q_2}{\partial t} &= \frac{1}{2}\frac{\partial^3 q_2}{\partial x^3} - i\frac{3}{4}\left[\left(\frac{\partial q_1}{\partial x}\right)^2 + q_1\left(\frac{\partial^2 q_1}{\partial x^2}\right)\right] \\ &\quad + \frac{3}{16}\left(q_2^2 - q_1^2\right)\left(\frac{\partial q_2}{\partial x}\right) - \frac{3}{8}q_1 q_2\left(\frac{\partial q_1}{\partial x}\right),\end{aligned} \tag{5.27}$$

where $\alpha = 1/a$. The (5.27) allow a Hamiltonian formulation

$$\frac{\partial q_i}{\partial t} = \frac{\partial}{\partial x}\frac{\delta H}{\delta q_i}, \tag{5.28}$$

where

$$H = \frac{1}{64\alpha}\left(q_1^4 + q_2^4 - 6q_1^2 q_2^2 + 32\left(\frac{\partial q_1}{\partial x}\right)^2 - 16\left(\frac{\partial q_2}{\partial x}\right)^2 + i24q_1^2\left(\frac{\partial q_2}{\partial x}\right)\right). \tag{5.29}$$

After the following transformation

$$q_1 \mapsto iu_1\,, \qquad q_2 \mapsto -iu_2\,, \qquad x \mapsto 2x\,, \qquad t \mapsto \frac{t}{64\alpha} \tag{5.30}$$

the Hamiltonian (5.29) coincides with the one in Table 5 in [4].

5.5 Equations Related to $A_4^{(2)}$

The underlying algebra is $A_4^{(2)}$ which is one of the twisted Kac-Moody algebras. Its rank is 2, the Coxeter number is 10 and the exponents are 1, 3, 7, 9. The Coxeter automorphism is given by

$$C_5(X) = -c_5 S X^T S c_5^{-1}, \tag{5.31}$$

where

$$c_5 = \begin{pmatrix} \omega^4 & 0 & 0 & 0 & 0 \\ 0 & \omega^2 & 0 & 0 & 0 \\ 0 & 0 & 1 & 0 & 0 \\ 0 & 0 & 0 & \omega^{-2} & 0 \\ 0 & 0 & 0 & 0 & \omega^{-4} \end{pmatrix}, \quad S = \begin{pmatrix} 0 & 0 & 0 & 0 & 1 \\ 0 & 0 & 0 & -1 & 0 \\ 0 & 0 & 1 & 0 & 0 \\ 0 & -1 & 0 & 0 & 0 \\ 1 & 0 & 0 & 0 & 0 \end{pmatrix} \tag{5.32}$$

and $\omega = \exp(2\pi i/10)$. The inverse of ad_J is

$$\mathrm{ad}_J^{-1} = \frac{2^8}{5^5}(5^4\,\mathrm{ad}_J^9 + 2^8\,\mathrm{ad}_J^{19}). \tag{5.33}$$

A basis compatible with the grading of the twisted Kac-Moody algebra $A_4^{(2)}$ is given by

$$\begin{aligned}
\mathfrak{g}^{(0)}: &\quad E_1^{(0)} = \frac{1}{2}(h_1 + h_4), && E_2^{(0)} = \frac{1}{2}(h_2 + h_3), \\
\mathfrak{g}^{(1)}: &\quad E_1^{(1)} = \frac{1}{2}(e_{14} - e_{25}), && E_2^{(1)} = \frac{1}{2}(e_{31} + e_{53}), && E_3^{(1)} = e_{42}, \\
\mathfrak{g}^{(2)}: &\quad E_1^{(2)} = \frac{1}{2}(e_{12} + e_{45}), && E_2^{(2)} = \frac{1}{2}(e_{23} + e_{34}), \\
\mathfrak{g}^{(3)}: &\quad E_1^{(3)} = \frac{1}{2}(e_{21} - e_{54}), && E_2^{(3)} = \frac{1}{2}(e_{32} - e_{43}), && E_3^{(3)} = e_{15}, \\
\mathfrak{g}^{(4)}: &\quad E_1^{(4)} = \frac{1}{2}(e_{13} - e_{35}), && E_2^{(4)} = \frac{1}{2}(e_{41} + e_{52}), \\
\mathfrak{g}^{(5)}: &\quad E_1^{(5)} = \frac{1}{2}(h_1 - h_4), && E_2^{(5)} = \frac{1}{2}(h_2 - h_3), \\
\mathfrak{g}^{(6)}: &\quad E_1^{(6)} = \frac{1}{2}(e_{14} + e_{25}), && E_2^{(6)} = \frac{1}{2}(e_{31} - e_{53}), \\
\mathfrak{g}^{(7)}: &\quad E_1^{(7)} = \frac{1}{2}(e_{12} - e_{45}), && E_2^{(7)} = \frac{1}{2}(e_{23} - e_{34}), && E_3^{(7)} = e_{51}, \\
\mathfrak{g}^{(8)}: &\quad E_1^{(8)} = \frac{1}{2}(e_{21} + e_{54}), && E_2^{(8)} = \frac{1}{2}(e_{32} + e_{43}), \\
\mathfrak{g}^{(9)}: &\quad E_1^{(9)} = \frac{1}{2}(e_{13} + e_{35}), && E_2^{(9)} = \frac{1}{2}(e_{41} - e_{52}), && E_3^{(9)} = e_{24},
\end{aligned} \tag{5.34}$$

where $h_i = e_{ii} - e_{i+1,i+1}$. The potential is parameterized by

$$\begin{aligned}
Q(x,t) &= q_1(x,t)E_1^{(0)} + (q_2(x,t) + q_1(x,t))E_2^{(0)}, \\
V^{(2)}(x,t) &= v_1^{(2)}(x,t)E_1^{(2)} + v_2^{(2)}(x,t)E_2^{(2)}, \\
V^{(1)}(x,t) &= v_1^{(1)}(x,t)E_1^{(1)} + v_2^{(1)}(x,t)E_2^{(1)} + v_3^{(1)}(x,t)E_3^{(1)}, \\
V^{(0)}(x,t) &= v_1^{(0)}(x,t)E_1^{(0)} + v_2^{(0)}(x,t)E_2^{(0)}, \\
K &= -aE_1^{(3)} + 2aE_2^{(3)} - aE_3^{(3)}, \\
J &= E_1^{(1)} + E_2^{(1)} + E_3^{(1)}.
\end{aligned} \tag{5.35}$$

Again we will omit writing the dependence on x and t. Using the recursion operators (5.15), we get for the coefficients of the potentials

$$v_1^{(2)} = 2aq_1, \qquad v_2^{(2)} = a(q_1 - q_2), \tag{5.36}$$

$$\begin{aligned} v_1^{(1)} &= a\left(2i\frac{\partial q_1}{\partial x} - 4i\frac{\partial q_2}{\partial x} - 2q_2^2 - 2q_1^2 + 5q_2q_1\right), \\ v_2^{(1)} &= a\left(3q_2^2 - 8i\frac{\partial q_1}{\partial x} + 6i\frac{\partial q_2}{\partial x} - 2q_1^2\right), \\ v_3^{(1)} &= a\left(12i\frac{\partial q_1}{\partial x} - 4i\frac{\partial q_2}{\partial x} - 2q_2^2 + 3q_1^2\right). \end{aligned} \tag{5.37}$$

$$\begin{aligned} v_1^{(0)} &= \frac{a}{5}\left(16\frac{\partial^2 q_1}{\partial x^2} - 12\frac{\partial^2 q_2}{\partial x^2} + i\,(12q_2 - 6q_1)\,\frac{\partial q_2}{\partial x} - 3q_2^2q_1 + 2q_1^3\right), \\ v_2^{(0)} &= \frac{a}{5}\left(4\frac{\partial^2 q_1}{\partial x^2} - 8\frac{\partial^2 q_2}{\partial x^2} + i\,(6q_1 - 12q_2)\,\frac{\partial q_1}{\partial x} + i\,(12q_2 - 6q_1)\,\frac{\partial q_2}{\partial x}\right. \\ &\quad \left. - 3q_1^2q_2 - 3q_2^2q_1 + 2q_1^3 + 2q_2^3\right). \end{aligned} \tag{5.38}$$

From the λ-independent terms in the Lax representation we get the equations

$$\begin{aligned} \alpha\frac{\partial q_1}{\partial t} &= 16\frac{\partial^3 q_1}{\partial x^3} - 12\frac{\partial^3 q_2}{\partial x^3} + i\left[-6\left(\frac{\partial q_1}{\partial x}\right)\left(\frac{\partial q_2}{\partial x}\right) + 12\left(\frac{\partial q_2}{\partial x}\right)^2\right. \\ &\quad \left. - 6\,(q_1 - 2q_2)\left(\frac{\partial^2 q_2}{\partial x^2}\right)\right] + \left(6q_1^2 - 3q_2^2\right)\left(\frac{\partial q_1}{\partial x}\right) - 6q_1q_2\left(\frac{\partial q_2}{\partial x}\right), \end{aligned} \tag{5.39}$$

$$\begin{aligned} \alpha\frac{\partial q_2}{\partial t} &= -12\frac{\partial^3 q_1}{\partial x^3} + 4\frac{\partial^3 q_2}{\partial x^3} + i\left[-12\left(\frac{\partial q_1}{\partial x}\right)\left(\frac{\partial q_2}{\partial x}\right) + 6\left(\frac{\partial q_1}{\partial x}\right)^2\right. \\ &\quad \left. + 6\,(q_1 - 2q_2)\left(\frac{\partial^2 q_1}{\partial x^2}\right)\right] + \left(6q_2^2 - 3q_1^2\right)\left(\frac{\partial q_2}{\partial x}\right) - 6q_1q_2\left(\frac{\partial q_1}{\partial x}\right), \end{aligned}$$

where $\alpha = 5/a$.

The corresponding Hamiltonian is

$$\begin{aligned} H = \frac{1}{2\alpha}\Bigg[&q_1^4 + q_2^4 - 3q_1^2q_2^2 - 16\left(\frac{\partial q_1}{\partial x}\right)^2 - 4\left(\frac{\partial q_2}{\partial x}\right)^2 \\ &- i6q_1^2\left(\frac{\partial q_2}{\partial x}\right) - i12q_2^2\left(\frac{\partial q_1}{\partial x}\right) + 24\left(\frac{\partial q_1}{\partial x}\right)\left(\frac{\partial q_2}{\partial x}\right)\Bigg]. \end{aligned} \tag{5.40}$$

After the following transformation

$$q_1 \mapsto iu_2, \qquad q_2 \mapsto -iu_1, \qquad x \mapsto 2x, \qquad t \mapsto \frac{t}{2\alpha} \tag{5.41}$$

the Hamiltonian (5.40) coincides with the one in Table 5 in [4].

5.6 Discussion and Conclusions

We have repeated the work done in [4]. Having derived the equations we are in a position to analyze the effect of the "twisting".

The fundamental difference is hidden in the gradings of the two algebras. In the first case we introduce a grading in $so(5)$ using the Coxeter automorphism c_4 (5.20) which is of order 4. Therefore each of the subspaces $\mathfrak{g}^{(k)}$ is spanned by the root vectors E_α corresponding to the roots of height k mod(4). Along with $\mathfrak{g}^{(0)} \simeq \mathfrak{h}$ we have split $so(5)$ into 5 linear subspaces.

In the second case we introduce a grading in $sl(5)$ using the Coxeter automorphism c_5 (5.32) composed with the external automorphism of $sl(5)$. But now the Coxeter automorphism is of order 5. Note that the external automorphism of $sl(5)$ has as a subalgebra $so(5)$. Using the grading introduced by c_5 we split $so(5)$ into 5 linear subspaces: $\mathfrak{g}^{(0)}$ isomorphic to the Cartan subalgebra of $so(5)$ and $\mathfrak{g}^{(k)}$ spanned by the root vectors E_α of $so(5)$ corresponding to the roots of height k mod(5). The rest of the algebra $sl(5)\backslash so(5)$ is also splited by c_5 into 5 linear subspaces. Thus our grading now contains 10 linear subspaces.

This accounts for the inequivalence not only of the gradings but also of the resulting mKdV equations.

Further steps in analyzing these equations will be:

- to find their soliton solutions. It is most natural to use the dressing method discovered and developed by Zakharov, Shabat and Mikhailov [16, 17, 20, 21].
- to analyze the spectral properties of the corresponding Lax operators, see [8–10, 16]. They are determined by the eigenvalues of the corresponding matrices J. In the case of $so(5)$ the eigenvalues are $\exp(2\pi ki/4), k = 0, \ldots, 3$, so the continuous spectrum of L fills up 4 straight lines passing through the origin enclosing equal angles $\pi/4$. For the second case the eigenvalues of J are $\exp(2\pi ki/10)$, $k = 0, \ldots, 9$ so the continuous spectrum of L fills up 10 straight lines passing through the origin and closing equal angles $\pi/10$.
- to use the recursion operators [1, 8, 11, 18] for constructing the hierarchy of Hamiltonian structures.

These results will be published elsewhere.

Acknowledgments The work is supported in part by the ICTP—SEENET-MTP project PRJ-09.

References

1. M.J. Ablowitz, D.J. Kaup, A.C. Newell, H. Segur, The inverse scattering transform–Fourier analysis for nonlinear problems. Stud. Appl. Math. **53**, 249–315 (1974)
2. F. Calogero, A. Degasperis, *Spectral Transform and Solitons*, vol. I (North Holland, Amsterdam, 1982)
3. R. Carter, *Lie Algebras of Finite and Affine Type* (Cambridge University Press, Cambridge, 2005)

4. V.V. Drinfel'd, V.G. Sokolov, Lie algebras and equations of Korteweg-de Vries type. Itogi Nauki i Tekhniki, Seriya Sovremennye Problemy Matematiki (Noveishie Dostizheniya) **24**, 81–180 (1984)
5. L.D. Faddeev, L.A. Takhtadjan, *Hamiltonian Methods in the Theory of Solitons* (Springer, Berlin, 1987)
6. V.S. Gerdjikov, Generalised Fourier transforms for the soliton equations. Gauge covariant formulation. Inverse Prob. **2**, 51–74 (1986)
7. V.S. Gerdjikov, Algebraic and analytic aspects of N-wave type equations. Contemp. Math. **301**, 35–68 (2002)
8. V.S. Gerdjikov, Derivative nonlinear schrödinger equations with $\mathbb{Z}_N$ and $\mathbb{D}_N$ reductions. Rom. J. Phys. **58**, 573–582 (2013)
9. V.S. Gerdjikov, A.B. Yanovski, Completeness of the eigenfunctions for the Caudrey-Beals-Coifman system. J. Math. Phys. **35**, 3687–3725 (1994)
10. V.S. Gerdjikov, A.B. Yanovski, On soliton equations with $\mathbb{Z}_h$ and $\mathbb{D}_h$ reductions: conservation laws and generating operators. J. Geom. Symmetry Phys. **31**, 57–92 (2013)
11. V.S. Gerdjikov, G. Vilasi, A.B. Yanovski, *Integrable Hamiltonian Hierarchies. Spectral and Geometric Methods*. Lecture Notes in Physics, vol. 748 (Springer, New York, 2008)
12. V.S. Gerdjikov, D.M. Mladenov, A.A. Stefanov, S.K. Varbev, *MKdV-type of equations related to* $\mathfrak{sl}(N, \mathbb{C})$ *algebra* (Cambridge Scholar Publishing, 2014), pp. 335–344
13. V.S. Gerdjikov, D.M. Mladenov, A.A. Stefanov, S.K. Varbev, *On an one-parameter family of MKdV equations related to the* $\mathfrak{so}(8)$ *Lie algebra* (Cambridge Scholar Publishing, 2014), pp. 345–365
14. S. Helgasson, *Differential Geometry, Lie Groups and Symmetric Spaces* (Academic Press, New York, 1978)
15. V. Kac, *Infinite-Dimensional Lie Algebras*, 3rd edn. (Cambridge University Press, Cambridge, 1994)
16. A.V. Mikhailov, The reduction problem and the inverse scattering problem. Physica D **3D**, 73–117 (1981)
17. A.V. Mikhailov, V.E. Zakharov, On the integrability of classical spinor models in two-dimensional space-time. Commun. Math. Phys. **74**, 21–40 (1980)
18. A. Yanovski, Recursion operators and expansions over adjoint solutions for the Caudrey-Beals-Coifman system with $\mathbb{Z}_p$ reductions of Mikhailov type. J. Geom. Symm. Phys. **30**, 105–119 (2013)
19. A. Yanovski, G. Vilasi, Geometric theory of the recursion operators for the generalized Zakharov-Shabat system in pole gauge on the algebra $sl(n, C)$: with and without reductions. SIGMA **8**, 87–110 (2012)
20. V.E. Zakharov, A.V. Mikhailov, Relativistically invariant two-dimensional models of field theory which are integrable by means of the inverse scattering problem method. Sov. Phys. JETP **47**, 1017–1027 (1978)
21. V.E. Zakharov, S.V. Manakov, S.P. Novikov, L.I. Pitaevskii, *Theory of Solitons: The Inverse Scattering Method* (Plenum, New York, 1984)

Chapter 6
Chaotic Versus Regular Behavior in Yang-Mills Theories

A. Nicolaidis

Abstract We consider spatially uniform $SU(2)$ color fields. At the classical level the system exhibits almost exclusively chaotic behavior. To include quantum effects, we introduce a renormalization-group improved effective action, where the fixed coupling constant g is replaced by a running coupling constant g, depending upon the color magnetic field. The effective Lagrangian gives rise to invariant tori which occupy a significant portion of the phase space and sustain ordered behavior. For some energy values, stable periodic orbits exist, with the corresponding gluon field being color neutral.

6.1 Introduction

Quantum chromodynamics (QCD) has proved to be a very efficient tool for analyzing and understanding hadronic phenomena. The smallness of the coupling constant at large momentum transfer (short distances) makes it possible to study "hard processes" using familiar perturbative techniques. However, the most important aspects of hadronic physics (color confinement, chiral symmetry, hadronic spectroscopy) are determined by the low energy (long distances) regime of QCD, where the coupling constant is large and nonlinearities manifest. A meaningful approximation consists in adopting some assumptions, which, while simplifying the calculations, retain the qualitative features expected of the full theory. An important step along these lines has been initiated in [1–3], where classical Yang-Mills fields, homogeneous in space, were investigated. Fields, depending solely on time, originate in the long wavelength limit of the theory and they are important in the description of the ground state of QCD. In this paper we examine how the quantum corrections modify the classical picture. We find out that these corrections introduce novel features, bearing upon color confinement.

A. Nicolaidis (✉)
Theoretical Physics Department, Aristotle University of Thessaloniki, Thessaloniki, Greece
e-mail: nicolaid@auth.gr

B. Aneva and M. Kouteva-Guentcheva (eds.),
Nonlinear Mathematical Physics and Natural Hazards,
Springer Proceedings in Physics 163, DOI 10.1007/978-3-319-14328-6_6

Let us summarize the findings of [1–3]. Consider an $SU(2)$ pure Yang-Mills system described by the Lagrangian

$$L = -\frac{1}{4g^2} F^{\alpha}_{\mu\nu} F^{\alpha}_{\mu\nu} \tag{6.1}$$

where

$$F^{\alpha}_{\mu\nu} = \partial_\mu A^{\alpha}_{\nu} - \partial_\nu A^{\alpha}_{\mu} + \epsilon^{\alpha bc} A^{b}_{\mu} A^{c}_{\nu}. \tag{6.2}$$

Assuming that the non-Abelian fields depend only on time, i.e., $A^{\alpha}_{i} = A^{\alpha}_{i}(t)$, and selecting the gauge $A^{\alpha}_{0} = 0$ we obtain the classical equations of motion [1–3]

$$\ddot{A}^{\alpha}_{i} + \left(A^{\alpha}_{i} A^{b}_{j} - A^{\alpha}_{j} A^{b}_{i} \right) A^{b}_{j} = 0 \tag{6.3}$$

supplemented by a constraint (Gauss law). With the ansatz

$$A^{\alpha}_{i} = O^{\alpha}_{i} f^{\alpha}(t) \quad (a \text{ not summed}) \tag{6.4}$$

where O^{α}_{i}, are constant orthogonal matrices obeying

$$O^{\alpha}_{i} O^{b}_{i} = \delta^{\alpha b}, \tag{6.5}$$

the Gauss law is automatically satisfied and the equations of motion are reproduced from the Hamiltonian $\left(f^1 = x,\, f^2 = y,\, f^3 = z\right)$

$$H = \frac{1}{2}\left(\dot{x}^2 + \dot{y}^2 + \dot{z}^2\right) + \frac{1}{2}\left[x^2 y^2 + z^2 x^2 + y^2 z^2\right]. \tag{6.6}$$

Extensive studies [2–5] have been presented for the simplified case with $z = 0$, which may be viewed as the motion of a "particle" under the influence of the potential $V(x, y) = \frac{1}{2} x^2 y^2$. The motion is bounded by the hyperbola $xy = \pm (2E)^{1/2}$ (E is the energy of the particle). Escape solutions to infinity exist only along the axes $x = 0$ and $y = 0$ (Abelian solutions, $\ddot{x} = 0$ and $\dot{x} \neq 0$ or $\ddot{y} = 0$ and $\dot{y} \neq 0$). In general a particle moving in one of the four "channels" surrounding the coordinate axes and limited by the hyperbolas will return after a finite time to the central region $x \simeq y$. There, after a complicated motion, the particle enters another channel. We observe that a large color amplitude gradually decreases and it is replaced by a large amplitude in another color direction. These color flips take place in a random fashion [2, 5]. Of special interest is the symmetric solution $x = y = J$, where J is an analytic function (Jacobi elliptic cosine) [1]. However the solution is unstable. The overall dynamical features of the potential $V = \frac{1}{2} x^2 y^2$ have been studied also in [6]. There it was conjectured that the system is completely chaotic. Small islands of regular motion around a stable periodic orbit of period 11 have been located, however, in [7].

6.2 Quantum Corrections

It is highly interesting to explore how the above picture changes when quantum corrections are included. Infrared instabilities of the Yang-Mills system are expected to generate a quantum ground state which may have little to do with the minima of the classical action. Phenomena such as color confinement, gluon condensation, and chiral symmetry breaking are viewed as dynamical manifestations of the full quantum theory. General renormalization group arguments suggest that an effective Lagrangian L_{eff} incorporating quantum corrections can be defined by replacing the fixed coupling g by a running coupling $\bar{g}$, which runs with the color fields [8–11]. The evolution of $\bar{g}$ is controlled by the β function

$$\mu \frac{d\bar{g}}{d\mu} = \beta(\bar{g}) \tag{6.7}$$

where the scale μ, depends upon the Yang-Mills fields (to be determined later). The usual perturbative one-loop result for the β function, $\beta = -b\bar{g}^3 \left(b = \frac{11}{24\pi^2}\right)$, provides

$$\bar{g}^2(\mu) = \frac{1}{b \ln\left(\frac{\mu^2}{\Lambda^2}\right)}. \tag{6.8}$$

The above expression gives rise to uncontrolled growth for $\bar{g}(\mu)$ as μ approaches Λ (Landau pole). It is believed that $\bar{g}(\mu)$ will saturate at small μ and calculations in a nonperturbative background [12] indicate such a behavior. In [12] an expression for $\bar{g}(\mu)$, positive for all values of μ, is suggested:

$$\bar{g}^2(\mu) = \frac{1}{b \ln\left(\frac{\mu^2+\sigma^2}{\Lambda^2}\right)}. \tag{6.9}$$

The parameter σ ($\sigma > \Lambda$) is related to the QCD string tension. On the other hand, calculations of the effective action in the presence of a constant chromomagnetic field [8, 10] generate logarithms of the chromomagnetic field which can be absorbed in a renormalized coupling constant. We infer that the scale μ, can be identified with the chromomagnetic field and under assumptions similar to the outlined classical case we are led to [13]

$$\bar{g}^2(\mu) = \frac{1}{b \ln\left(\frac{x^2y^2+\sigma^2}{\Lambda^2}\right)}. \tag{6.10}$$

The effective Lagrangian looks like

$$L_{eff} = \frac{b}{2} \ln\left(\frac{x^2y^2+\sigma^2}{\Lambda^2}\right)\left[\dot{x}^2 + \dot{y}^2 - x^2y^2\right]. \tag{6.11}$$

We consider the above Lagrangian as a classical model that incorporates features of the full quantum problem. The Lagrangian (6.11) transforms to the Hamiltonian

$$H_{eff} = \left(p_x^2 + p_y^2\right) / (2b \ln u) + \frac{b}{2} x^2 y^2 \ln u, \tag{6.12}$$

where

$$u = \frac{\sigma^2 + x^2 y^2}{\Lambda^2} \tag{6.13}$$

and

$$p_x = b\dot{x} \ln u, \qquad p_y = b\dot{y} \ln u. \tag{6.14}$$

Since H is an integral of motion, for every constant value $H = E$ the zero-velocity curves which bound the motion in the xy-configuration space are the hyperbolas

$$xy = c\,(E)\,, \tag{6.15}$$

where c is defined by the equation

$$c^2 \ln\left(\frac{\sigma^2 + c^2}{\Lambda^2}\right) = 2\frac{E}{b}. \tag{6.16}$$

We define the Poincare section in the usual manner (e.g., [14], p. 17), i.e.,

$$H = E = const, \quad y = 0, \quad p_y > 0.$$

In the corresponding Poincare map p_x^2 is bounded by the relation

$$p_x^2 < 2Eb \ln\left(\frac{\sigma^2}{\Lambda^2}\right). \tag{6.17}$$

Since $\frac{b}{2}$ in (6.11) is a mere multiplicative constant, its numerical value does not affect the qualitative features of the system. In the following we fix $b = \frac{1}{4}$ by a suitable choice of the unit of energy.

The Hamiltonian (6.12) possesses also the symmetric periodic solution $x = y$. This solution in the classical case is always unstable and supports in its vicinity chaotic orbits, which eject through the channels along the two axes, in the fashion described above. Numerical results show that this solution for the new Hamiltonian (6.12) is stable for values of σ, Λ and in E in suitable open domains.

In Fig. 6.1, the surface of section for $\Lambda = 1$ and $E = 15$ is shown, for different values of σ. The horizontal x axis runs from -1 to 1 while p_x runs from 0 to 1.5. In all cases, a horizontal line represents the boundary (6.17). Because of the symmetry of Hamiltonian (6.12), all figures are symmetric both with respect to the x and p_x axes. Figure 6.1a corresponds to $\sigma = 1.09$. The symmetric solution $x = y$

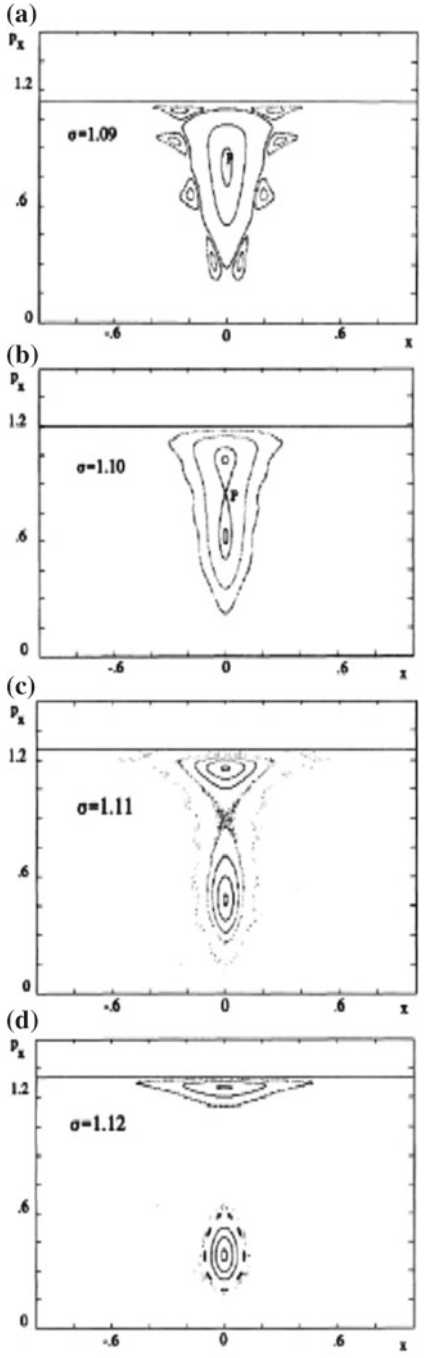

Fig. 6.1 The Poincare sections for $\Lambda = 1, \quad E = 15$ for varying σ

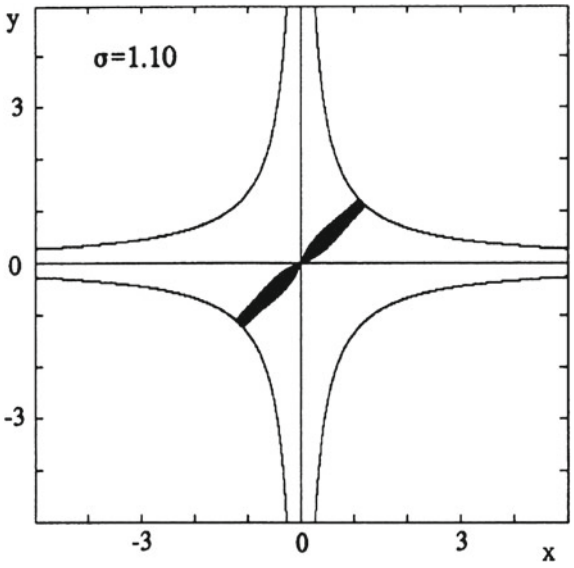

Fig. 6.2 Bounded motion in the vicinity of $x = y$ for $\sigma = 1.10$

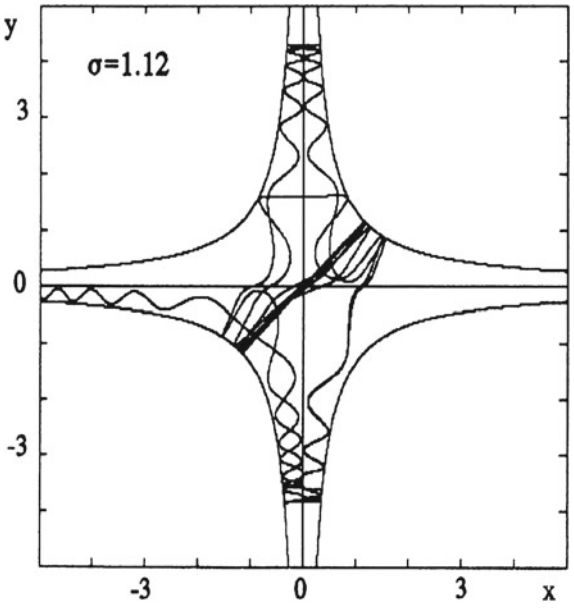

Fig. 6.3 A chaotic motion for $\sigma = 1.12$

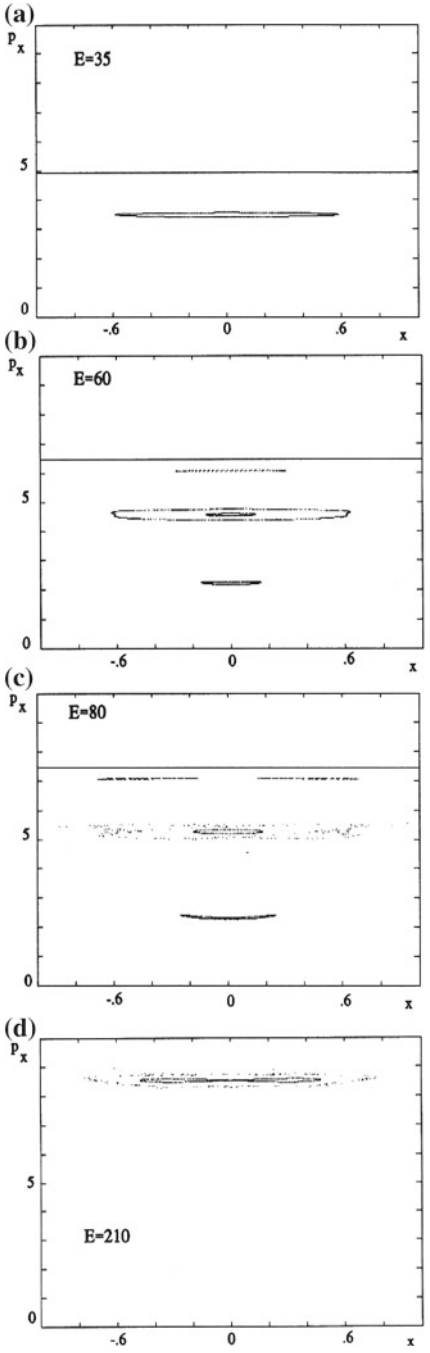

Fig. 6.4 The Poincare sections for $\Lambda = 1, \sigma = 2$ for varying E

is stable and its corresponding point P on the section is surrounded by invariant circles which support quasiperiodic motions, while two island chains around two periodic orbits in 1/4 resonance may be seen. In Fig. 6.1b, $\sigma = 1.10$ and the periodic solution $x = y$ has become unstable by undergoing a pitchfork bifurcation. Two stable periodic orbits, centered at the two islands on the p_x axis, have appeared. The motion in the vicinity of the symmetric solution is weakly chaotic, but is bounded by invariant circles which restrict it in the central area $x \simeq y$, as may be seen in Fig. 6.2. For $\sigma = 1.11$, the chaotic character of the motion near $x = y$ is apparent (Fig. 6.1c). No invariant circle bounding this chaotic orbit has been found, so the motion may eventually diffuse slowly to the channels. In Fig. 6.1d ($\sigma = 1.12$), the chaotic motion around $x = y$ is unbounded, but the two stable periodic motions on the p_x axis persist. The orbits in the vicinity of $x = y$ show a strong sensitivity on the initial conditions. For very slight differences in the selected initial point, the corresponding orbits evolve in a very different manner. Such a chaotic orbit is shown in Fig. 6.3. This motion resembles the previously described classical case. Figure 6.4 corresponds to $\Lambda = 1$, $\sigma = 2$, while the energy varies. The p_x axis runs in this case from 0 to 10. We start with $E = 35$ in Fig. 6.4a and the straight-line solution $x = y$ is stable. The relative area, however, filled in with ordered motions is very small in comparison to the previous case (see Fig. 6.1a). In Fig. 6.4b, for $E = 60$, two additional stable orbits have appeared, which become unstable for $E = 80$ as is shown in Fig. 6.4c, but the symmetric orbit remains stable up to $E = 210$ (Fig. 6.4d) and then becomes unstable, again by a pitchfork bifurcation.

6.3 Conclusions

We studied spatially uniform $SU(2)$ color fields, using a phenomenological effective Lagrangian which includes quantum corrections [13]. While our ansatz is not unique, we believe that our approach is justified. Similar techniques have been largely applied to the opposite case: time-independent color fields (see [11] and references therein). Comparing the classical and quantum description we discover similarities and distinct differences. The classical Hamiltonian is scale invariant and for all nonzero energies displays the same chaotic behavior. On the other hand, the quantum corrections introduce new scales, scale invariance is lost and for different values of the energy the effective quantum Hamiltonian gives different qualitative behaviors. For small energies such that $xy \leq c < \sigma$, the logarithm in (6.12) varies little, the quantum Hamiltonian resembles the classical one, and we encounter chaos. However, for larger values of the energy, ordered behavior appears. What is most interesting is that the symmetric solution $x = y$, which is unstable at the classical level, becomes stabilized at the quantum level. Preliminary numerical calculations show that a stable symmetric solution $x = y = z$ exists in the full three-dimensional problem. The solution $x = y = z$ represents a color neutral gluonic field. We feel that our findings bear on confinement. Vacuum polarization, responsible for the running coupling constant, creates color charges which induce screening, thus stabilizing the color

neutral solution. Related results, albeit in different context, have been obtained in [15]. There a classical strong color charge leads to instabilities and color screening. Following our analysis we are led to the conclusion that for appropriate energies, a nonperturbative color neutral gluonic field arises. Such a dynamical object might be important in hadronic phenomenology.

Acknowledgments I would like to thank Prof. Boyka Aneva for a warm hospitality and perfect organization.

References

1. G. Baseyan, S. Matinyan, G. Savvidi, Pis'ma Zh. Eksp. Teor. Fiz. **29**, 641 (1979) (JETP Lett. **29**, 587 (1979))
2. S. Matinyan, G. Savvidi, N. Ter-Arutyunan-Savvidi, Zh. Eksp. Teor. Fiz. **80**, 830 (1981) (Sov. Phys. JETP **53**, 421 (1981))
3. G. Savvidy, Nucl. Phys. B **246**, 302 (1984)
4. E. Nikolaevskii, L. Shur, Pis'ma Zh. Eksp. Teor. Fiz. **36**, 176 (1982) (JETP Lett. **36**, 218 (1982))
5. S.J. Chang, Phys. Rev. D **29**, 259 (1984)
6. A. Carnegie, I. Percival, J. Phys. A **17**, 801 (1984)
7. P. Dahlquist, G. Russberg, Phys. Rev. Lett. **65**, 2837 (1990)
8. S. Matinyan, G. Savvidy, Nucl. Phys. B **134**, 539 (1978)
9. H. Pagels, E. Tomboulis, Nucl. Phys. B **143**, 485 (1978)
10. L. Maiani, G. Martinelli, G. Rossi, M. Testa, Nucl. Phys. B **273**, 275 (1986)
11. S. Adler, T. Piran, Rev. Mod. Phys. **56**, 1 (1984)
12. Y. Simonov, Perturbative theory in the nonperturbative QCD vacuum, Heidelberg Report No. HD-THEP-93-16 (unpublished)
13. A. Nicolaidis, S. Ichtiaroglou, G. Voyatzis, Phys. Rev. D **52**, 3700 (1984)
14. A.J. Lichtenberg, M.A. Lieberman, *Regular and Stochastic Motion* (Springer, New York, 1995)
15. J. Mandula, Phys. Lett. **67B**, 175 (1977)

Part II
Seismic Hazard and Risk

Chapter 7
A New Probabilistic Shift Away from Seismic Hazard Reality in Italy?

A. Nekrasova, A. Peresan, V.G. Kossobokov and G.F. Panza

Abstract Objective testing is a key issue in the process of revision and improvement of seismic hazard assessments. Therefore we continue the rigorous comparative analysis of past and newly available hazard maps for the territory of Italy against the seismic activity observed in reality. The final Global Seismic Hazard Assessment Program (GSHAP) results and the most recent version of Seismic Hazard Harmonization in Europe (SHARE) project maps, along with the reference hazard maps for the Italian seismic code, all obtained by probabilistic seismic hazard assessment (PSHA), are cross-compared to the three ground shaking maps based on the duly physically and mathematically rooted neo-deterministic approach (NDSHA). These eight hazard maps for Italy are tested against the available data on ground shaking. The results of comparison between predicted macroseismic intensities and those reported for past earthquakes (in the time interval 1000–2014) show that models provide rather conservative estimates, which tend to over-estimate seismic hazard at the ground shaking levels below the MCS intensity IX. Only exception is represented by the neo-deterministic maps associated with a fixed return period of 475 or 2475 years, which provide a better fit to observations, at the cost of model consistent 10 % or 2 % cases of exceedance respectively. In terms of the Kolmogorov-Smirnov

A. Nekrasova · V.G. Kossobokov
Institute of Earthquake Prediction Theory and Mathematical Geophysics, Russian Academy of Sciences, Moscow, Russian Federation

A. Nekrasova · A. Peresan · V.G. Kossobokov · G.F. Panza
The Abdus Salam International Centre for Theoretical Physics, SAND Group, Trieste, Italy

A. Peresan (✉) · G.F. Panza
Department of Mathematics and Geosciences, University of Trieste, Trieste, Italy
e-mail: aperesan@units.it

V.G. Kossobokov
Institut de Physique du Globe de Paris, Paris, France

A. Peresan · V.G. Kossobokov · G.F. Panza
International Seismic Safety Organization (ISSO), Arsita, Italy
http://www.issoquake.org

G.F. Panza
Institute of Geophysics, China Earthquake Administration, Beijing, People's Republic of China

B. Aneva and M. Kouteva-Guentcheva (eds.),
Nonlinear Mathematical Physics and Natural Hazards,
Springer Proceedings in Physics 163, DOI 10.1007/978-3-319-14328-6_7

goodness of fit criterion, although all of the eight hazard maps differ significantly from the distribution of the observed ground shaking reported in the available Italian databases, the NDSHA approach appears to outscore significantly the PSHA one.

7.1 Introduction

A reliable and comprehensive characterization of expected seismic ground shaking, in a anticipatory perspective, is essential in order to develop effective risk mitigation strategies, including the adequate engineering design of earthquake-resistant structures.

A common belief is that a probabilistic assessment of the seismic hazard (PSHA), accounting for the probability of occurrence of a given ground shaking within a specified time interval, is needed for any rational decision making and for optimal allocation of resources [11]. However, since data are often insufficient to constrain the probability models and to test them, ground shaking probabilities turn out highly uncertain and unreliable, particularly for the large, sporadic and most destructive earthquakes. Comparison of observed numbers of fatalities with those calculated based on expected ground shaking from GSHAP maps [9, 23], show that seismic hazard maps based on the standard probabilistic method do not allow to reliably estimate the risk to which the population is exposed due to large earthquakes in many regions worldwide.

Although testing should be a necessary step in any scientific process of seismic hazard assessment, it is not a standard practice and there is not yet a commonly agreed procedure for models evaluation and comparison. Mak et al. [10] pointed out that, depending on the limited time span of available observations (compared with the selected return period of PSHA map), the probability of failing to reject an inadequate model can be high. Even if formal testing does not guarantee the adequacy of a model, a quantitative analysis of performances may allow comparing different models and spotting out possible problems. Objective testing, in fact, may have different purposes, ranging from purely scientific verification of model distributions and parameters to the assessment of maps predictive capability for moderate to extreme shaking, which may require specific metrics and tests.

In spite of the evidenced shortcomings and of its poor performances (see [17] for an in depth discussion), PSHA is still widely applied in the framework of several large scale projects at regional and global scale (e.g. Global Earthquake Model). Most of such attempts in improving seismic hazard maps, however, basically rely on the collection and revision of the input data and, so far, did not include a formal procedure to assess the improved capability of the revised maps in describing ground shaking. By analogy with medicine testing, in fact, the adequacy of the proposed maps should be established before their publication and control should be performed by the proponents as a primary test of reliability of the new results.

A possible alternative to the conventional PSHA approach is provided by the Neo-Deterministic Seismic Hazard Assessment, NDSHA [14–16], a methodology that allows for the consideration of a wide range of possible seismic sources as the starting point for deriving scenarios via full waveforms modeling. Besides the standard NDSHA maps, which provide reliable estimates of maximum seismic ground motion from a wide set of possible scenario earthquakes, the flexibility of NDSHA allows to account for earthquake recurrence and it permits to compute ground shaking maps at specified return periods [18]. A systematic comparative analysis was carried out for the territory of Italy between the NDSHA and PSHA maps (the last is at the base of current seismic regulation), investigating their performances with respect to past earthquakes, so as to better understand the performances and possible limits of the two different approaches to seismic hazard assessment [13].

In this study the comparative analysis is extended to additional hazard maps for the Italian territory, which are available from large scale projects (i.e. GSHAP), including the most recent probabilistic map, which has been compiled for the territory of Europe in the framework of Seismic Hazard Harmonization in Europe (SHARE) project [5]. The new European Seismic Hazard Map (ESHM13), in fact, has been released recently by [6] with the following declared intent:

> SHARE's main objective is to provide a community-based seismic hazard model for the Euro-Mediterranean region with update mechanisms. The project aims to establish new standards in Probabilistic Seismic Hazard Assessment (PSHA) practice by a close cooperation of leading European geologists, seismologists and engineers.

Regretfully, the new SHARE map does not seem to address most of the limits of the PSHA approach (e.g. [17, 22]) and repeats the errors of its predecessors, possibly (mis)leading to unexpected economic and human life losses from future earthquakes.

7.2 Data

In this study we consider ground shaking estimates for the territory of Italy within the boundaries from 36°N to 48°N and from 6°E to 20°E provided by the following eight seismic hazard assessment maps.

(a) The final Global Seismic Hazard Assessment Program (GSHAP) map that depicts peak ground acceleration (PGA) values with a 10 % chance of exceedance of in 50 years (GSHAP10%) corresponding to a return period of 475 years.

The GSHAP PGA values obtained by the probabilistic seismic hazard analysis (PSHA) methodology and presented as the final Global Seismic Hazard Map [4, 19] and Table (GSHPUB.dat, http://www.seismo2009.ethz.ch/GSHAP/) are provided on a $0.1° \times 0.1°$ regular grid for seismically active regions of the Globe, including the territory of Italy.

(b) The SHARE PGA values as defined by a 10 % chance of exceedance in 50 years (SHARE10%) corresponding to a return period of 475 years.
(c) The SHARE PGA values for a probability of exceedance of 2 % in 50 years (SHARE2%) associated with a 2475-year return period.

The SHARE PGA values, obtained by the, claimed, improved PSHA methodology, are given at the grid points of a regular $0.1^\circ \times 0.1^\circ$ mesh, which data can be downloaded from http://www.efehr.org:8080/jetspeed/portal/hazard.psml.

(d) The current Italian official seismic hazard map PGA values as defined by a 10 % chance of exceedance of in 50 years (PGA10%) corresponding to a return period of 475 years
(e) The Italian official seismic hazard map PGA values for a 2 % probability of exceedance in 50 years (PGA2%) associated with a return period of 2475 years.

Both the official seismic hazard maps for Italy are based on PSHA ([12] the data file http://esse1.mi.ingv.it/d2.html) at the grid points of a regular $0.2^\circ \times 0.2^\circ$ mesh.

(f) The maximum design ground acceleration (DGA) map for Italy, estimated by the standard NDSHA approach.
(g) The NDSHA DGA values estimated for a return period of 475 years, corresponding to a 10 % chance of exceedance of in 50 years (DGA10%).
(h) The NDSHA DGA values estimated for a return period of 2475 years, corresponding to a 2 % chance of exceedance of in 50 years (DGA2%).

The three design ground acceleration (DGA) maps are based on the neo-deterministic seismic hazard assessment, NDSHA ([15] and references therein), which provides ground shaking estimates at the grid points of a regular $0.2^\circ \times 0.2^\circ$ mesh. From the complete synthetic seismograms associated to each grid point, the DGA estimates are extracted, which can be compared to PGA [24]. The DGA map defined by the standard NDSHA method does not depend on temporal properties of earthquakes occurrence, whereas the DGA10% and DGA2% maps are obtained by incorporating earthquake recurrence information into NDSHA [2, 18], and correspond to return periods of 475 and 2475 years, respectively (i.e. same as considered in compilation of the PSHA maps). The application of NDSHA variant that computes ground shaking at a fixed return period implies additional requirements to the input data, which are not fulfilled in the parts of the Italian territory delineated as blank areas in Fig. 7.1g, h. In turn, the limits of available data in adequately constraining ground shaking recurrence, as evidenced by NDSHA analysis [18], cast doubts on the meaning and validity of PSHA values given for these blank areas, if based on the same data.

For the purpose of comparison between different grids we enhance the regular $0.2^\circ \times 0.2^\circ$ mesh into a $0.1^\circ \times 0.1^\circ$ one, so that each PGA value from the original grid point is attributed to four points on the fine grid (i.e. the original point, plus its three nearest neighbors to the east, south, and south-east).

The observed seismic activity data are taken from the SHARE European Earthquake Catalogue (SHEEC), as reported by Stucchi et al. [21] for historical events in 1000–1899 and by Grünthal et al. [7] for earthquakes in 1900–2006.

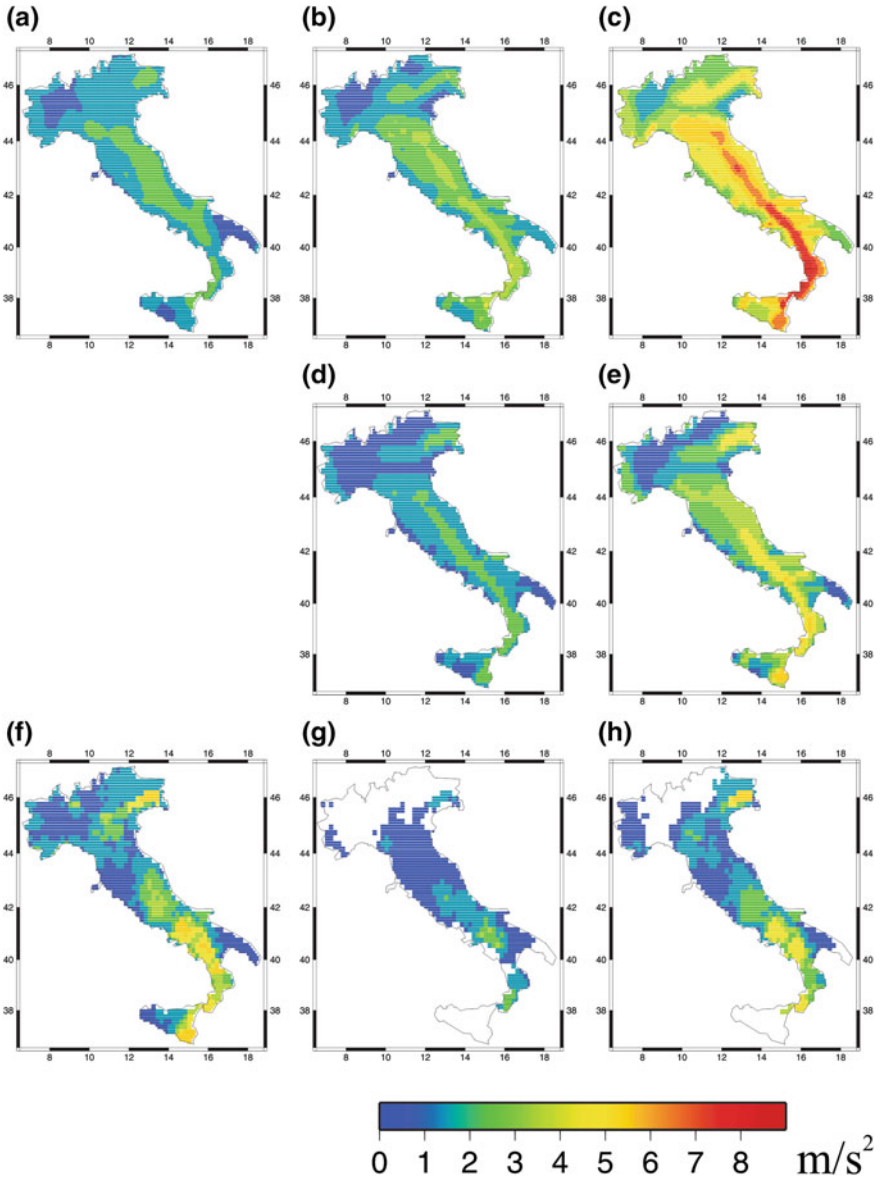

Fig. 7.1 Comparison of model ground acceleration maps: **a** GSHAP corresponding to a return period of 475 years; **b** SHARE10% corresponding to a return period of 475 years; **c** SHARE2% corresponding to a return period of 2475 years; **d** PGA10% corresponding to a return period of 475 years; **e** PGA2% corresponding to a return period of 2475 years; **f** DGA not depending on time; **g** DGA10% corresponding to a return period of 475 years; **h** DGA2% corresponding to a return period of 2475 years

The data set covering more than a millennium (a time interval about ten times longer than that available in most of the regions worldwide), with a completeness level satisfactory for this kind of analysis, is quite a unique property of the territory of Italy and fully warrants the following analysis. The SHEEC data provides records on macroseismic intensity at epicenter, I_0. In our analysis we have used integer values of I_0, attributing the upper limit when in SHEEC the reported I_0 is a range. This is a conservative natural choice of seismic hazard estimate, adequate to analysis aimed at the largest possible ground shaking. The observed intensity map, I_{obs}, is compiled by attributing to a grid point of a regular $0.1° \times 0.1°$ mesh the maximum of I_0 for earthquakes from SHEEC within the 0.25°-side square centered at this grid point. This resulting map of the observed ground shaking intensity gives us an opportunity for a quantitative comparison of the eight seismic hazard maps of the Italian territory with the seismic reality.

7.3 Cross-Comparison of the PGA Maps for Italy

We repeat the analysis reported in [13], expanding the comparison to the probabilistic seismic hazard maps for the Italian territory obtained in the framework of large scale projects: the Global Seismic Hazard Assessment Programme (GSHAP) map published 15 years ago [3], and its new offspring for Europe (SHARE), which became available recently [5, 6].

Table 7.1 gives an overall summary on the PGA values for each of the eight SHA maps (Fig. 7.1). Evidently, the SHARE maps increase dramatically both the lower and the upper limits of the expected seismic hazard in Italy. In particular, the minimum of the SHARE PGA is about 2 and 4 times larger than the corresponding estimates of the earlier probabilistic SHA. In comparison to the NDSHA maps the minimum values of ground shaking by the SHARE maps are about 5 and 10 times larger. The increase of the maximum PGA on the SHARE maps accounts to about 10–50 % of the corresponding previously suggested values.

Table 7.2 provides a more refined comparison, based upon the percentage of PGA values ratio at a grid point (mGA1/mGA2), for a number of pairs of model maps mGA1 and mGA2. SHARE map values at a grid point exceed those of the previous maps by a factor of 2 or more in 4 % of cases, for the GSHAP map, in 17 and 40 % of cases, for the corresponding national PSHA maps, and to up to more than 75 % of cases, for the NDSHA estimates. The SHARE estimate is less than any previous hazard estimates in 2–3 % of grid points. Specifically, as can be concluded from the maps of the ratio of the PGA values for different pairs of models, a selection being provided in Fig. 7.2, just about 2 % of the grid points of the Italian official SHA maps have higher PGA values than that of SHARE; these are all located in the Friuli-Venezia-Giulia region (Fig. 7.2c, d). In comparison to the previous hazard maps, the SHARE PGA values corresponding to a return period of 475 years increase by a factor of 2 or more in the regions of Trentino, Lombardia, Eastern Sicily, and Puglia; for Liguria PGA increases more than 4 times. The misfit of the SHARE maps with

Table 7.1 The parameters of the eight SHA ground acceleration maps for Italian territory

Map	GSHAP	SHARE10%	SHARE2%	PGA10%	PGA2%	DGA	DGA10%	DGA2%
Number of points	3,066	3,066	3,066	3,044	3,044	3,066	1,739	2,266
min(mGA) (m/s^2)	0.39	0.74	1.72	0.30	0.43	0.20	0.16	0.18
max(mGA) (m/s^2)	2.97	4.19	8.82	2.71	5.98	5.83	3.74	5.83

Table 7.2 The percentage of the grid points from different ranges of the ratio mGA1/mGA2 of the PGA values from selected pairs of SHA maps

mGA1	GSHAP	SHARE10%	SHARE10%	SHARE2%	SHARE10%	SHARE10%	SHARE2%
mGA2 range	PGA10%	GSHAP	PGA10%	PGA2%	DGA	DGA10%	DGA2%
≥4	–	–	0.26	1.25	4.04	30.82	39.81
≥2	6.73	4.21	17.05	40.31	26.65	75.79	78.60
≥1	78.58	85.32	97.40	97.96	65.04	97.99	97.04
<1	21.42	14.68	2.60	2.04	34.96	2.01	2.96

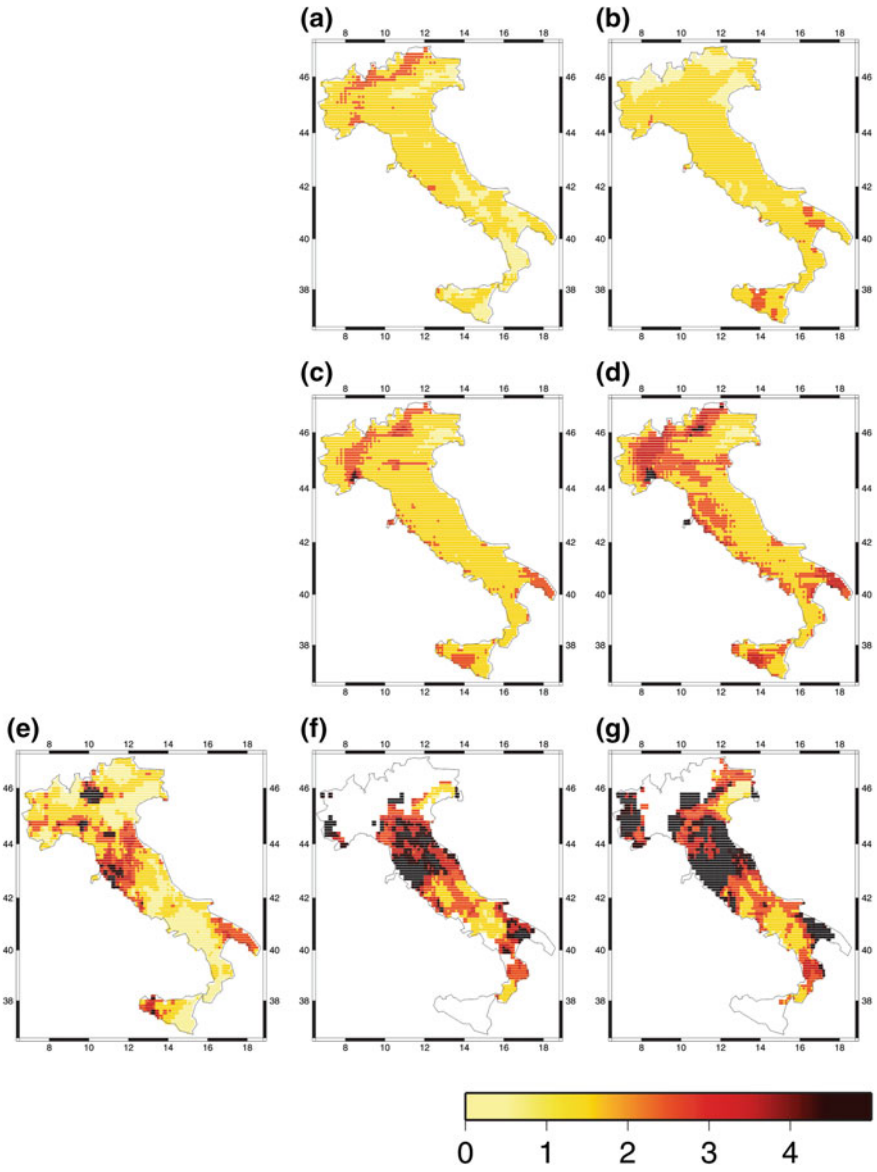

Fig. 7.2 Selected maps of the ratio between PGA values from different pairs of SHA maps: **a** GSHAP divided by PGA10%; **b** SHARE10% divided by GSHAP; **c** SHARE10% divided by PGA10%; **d** SHARE2% divided by PGA2%; **e** SHARE10% divided by DGA; **f** SHARE10% divided by DGA10%; **g** SHARE2% divided by DGA2%

respect to the NDSHA ones is even more dramatic (Fig. 7.2e–g): e.g. the SHARE2% values are larger than the DGA2% by a factor of 4 or more in about 40 % of the Italian territory.

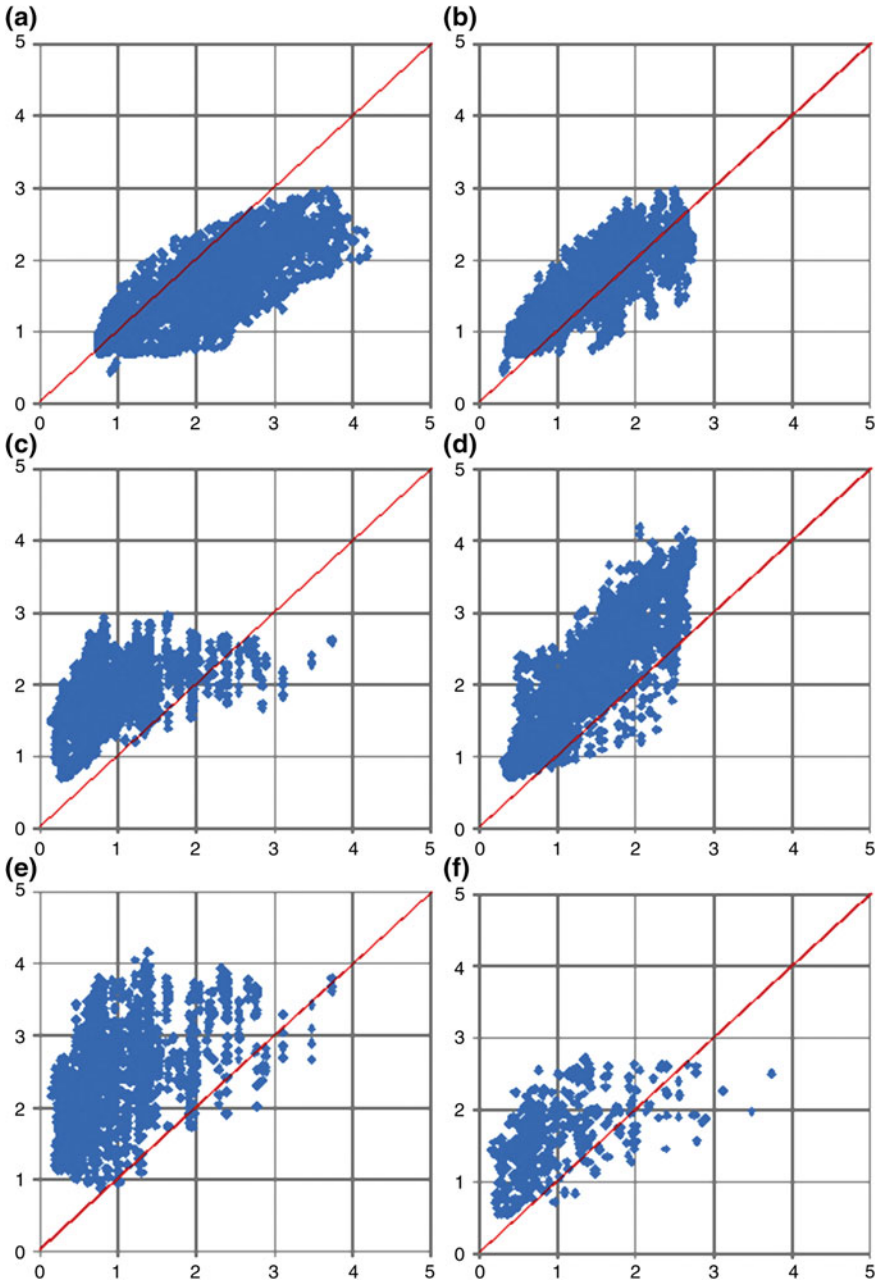

Fig. 7.3 Correlation diagrams of the PGA values (in m/s^2) on the four hazard maps of Italy corresponding to a return period of 475 years: **a** GSHAP (ordinate) versus SHARE10% (abscissa); **b** GSHAP versus PGA10%; **c** GSHAP versus DGA10%; **d** SHARE10% versus PGA10%; **e** SHARE10% versus DGA10%; **f** PGA10% versus DGA10%. These are all possible pairs of maps corresponding to a return period of 475 years (i.e. probabilistic GSHAP, SHARE10%, PGA10%, and adjusted neo-deterministic DGA10%)

Each of the six graphs in Fig. 7.3 shows the correlation diagram between a pair of seismic hazard maps of Italy, displaying the PGA values on a grid point of one map versus the PGA values on the same grid point of another map. These are all possible pairs of maps corresponding to a return period of 475 years (i.e. probabilistic GSHAP, SHARE10%, PGA10%, and neo-deterministic DGA10%). It is evident that the most recent map reviewed by the probabilistic approach to seismic hazard assessment (SHARE10%) evidently provides a gross overestimation of PGA values, compared to all of the other maps. The neo-deterministic map (DGA10%) is the most optimistic in providing low PGA values, under 1 m/s^2, but conservative in expecting high accelerations, above 2 m/s^2.

Of course, any cross-comparison of the maps obtained by different models and/or series of correlation diagrams does not answer to the key question of a model adequacy to reality. In the next section we address this pivotal question in hazard assessment by comparisons of the model maps with the available observations.

7.4 Comparison of the Hazard Maps for Italy Against Registered Ground Shaking

The two currently official seismic hazard maps for Italy PGA10 % and PGA2 % and the three neo-deterministic maps DGA, DGA10 % and DGA2 % were already subject of comparison in [13]. Here we update and expand the comparison with the observed ground shaking to the European Seismic Hazard Maps 2013—SHARE10 % and SHARE2 %, issued recently [6], along with their predecessor, GSHAP map [3]. Table 7.3 lists the conversion rules between PGA and MCS for the territory of Italy after Indirli et al. [8]. These rules are used to convert the estimated ground shaking from SHARE10 %, SHARE2 %, PGA10 %, PGA2 %, DGA, DGA10 %, DGA2 % into the corresponding macroseismic intensity MCS values. Figure 7.4 shows the eight model intensity maps subject to comparison along with the map I_{obs} compiled from the SHEEC reported data. All the nine intensity maps refer to the same regular $0.1^\circ \times 0.1^\circ$ mesh within the borders of Italy. For the purposes of comparison the recurrence adjusted DGA10 % and DGA2 % neo-deterministic maps were expanded to the grid points of no recurrence determination, following the empirical linear regression equation that links the DGA map values and the existing estimates on the DGA2 % and DGA10 % maps. The resulting model intensity maps are DGA2 %* and DGA10 %*, respectively.

Table 7.3 Relation between I_{MCS} and model ground motion, mGA, after Indirli et al. [8]

I_{MCS}	VI	VII	VIII	IX	X	XI
mGA (g)	0.01–0.02	0.02–0.04	0.04–0.08	0.08–0.15	0.15–0.3	0.3–0.6

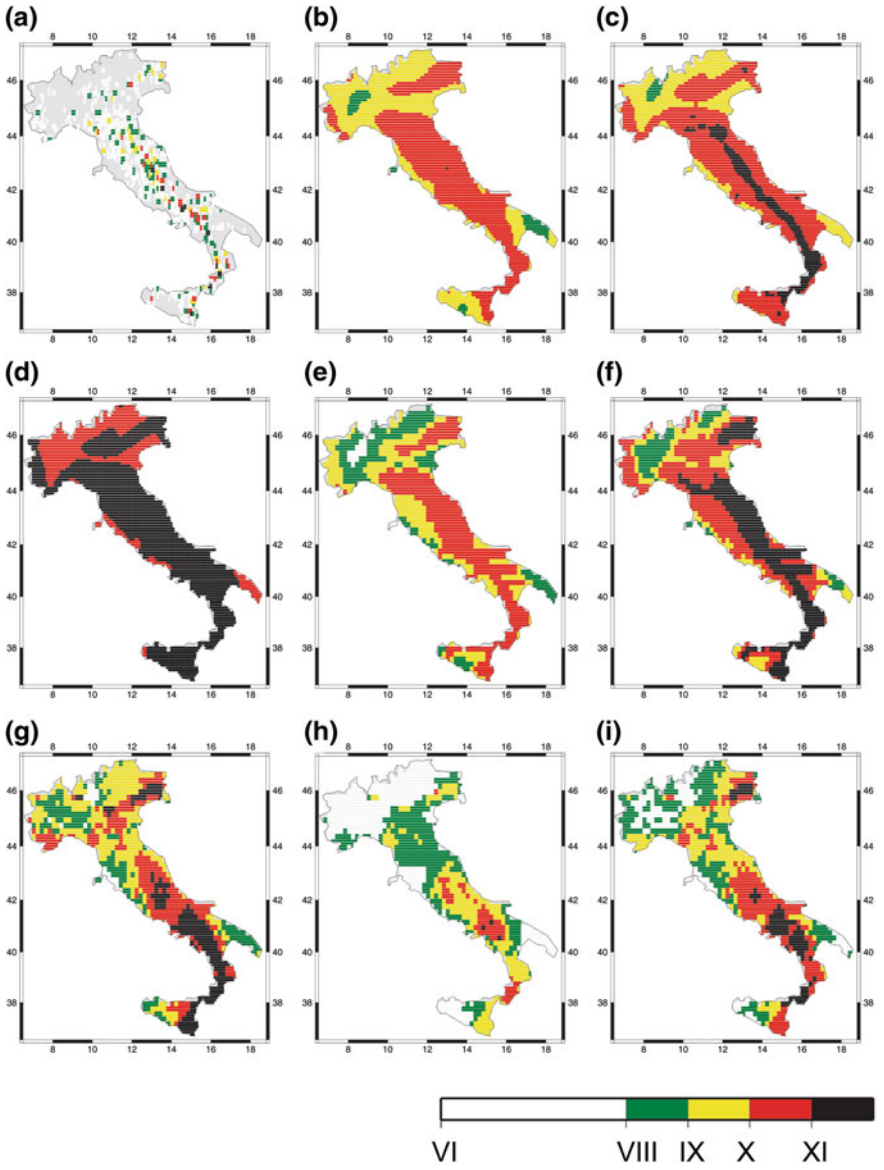

Fig. 7.4 The intensity maps under comparison: **a** I_{obs} map obtained from the reported seismicity data in 1000–2006; model intensity corresponding to PGA maps—**b** GSHAP, **c** SHARE10 %, **d** SHARE2 %, **e** PGA10 %, **f** PGA2 %, **g** DGA, **h** DGA10 %*, and **i** DGA2 %*

Figure 7.4 presents the eight intensity maps obtained (i) from the real seismicity I_{obs} (Fig. 7.4a) as well as (ii) from the ground motion estimates $I_{\mathrm{SHARE10\%}}$, $I_{\mathrm{SHARE2\%}}$, $I_{\mathrm{PGA10\%}}$, $I_{\mathrm{PGA2\%}}$, I_{DGA}, $I_{\mathrm{DGA10\%*}}$, $I_{\mathrm{DGA2\%*}}$ (Fig. 7.4b–h, respectively).

The percentage of the points with intensity VI or more for each of these maps is summarized in Table 7.3. Remarkably, the SHARE2 % assigns all the territory to "extreme" ground shaking of intensity X or larger, while the I_{obs} map of macroseismic intensities reports such intensity, in about 2000 years of observations, for less than 12 % of the territory. At this "extreme" level of ground shaking the DGA10%* with its 8 % appear to be the nearest to I_{obs}, and, in general, the neo-deterministic maps are closer to reality than all the probabilistic ones but PGA10%, which predicts (about 45 % of intensity X) for a return period of 475 years similar values to those of the time unlimited DGA. Similar situation exists at the "severe", intensity VIII level of ground shaking: it is attributed to 100 % of the Italian territory by all the probabilistic maps except PGA10%, which attributes it to 98 % of the territory, still too large in comparison to 42 % of I_{obs}. Once again the DGA10%* with its 61.42 % is the closest to I_{obs}.

More rigid comparison with respect to the I_{obs} map can be performed by applying the Kolmogorov-Smirnov test that quantifies the distance between the empirical distribution functions. The maximum absolute difference between the empirical distributions is commonly used in the Kolmogorov-Smirnov two-sample criterion to distinguish whether or not the values from the two samples are drawn from the same statistical distribution of independent variables. We apply the two sample Kolmogorov-Smirnov statistic λ_{K-S} to the empirical distribution functions of MCS values on a model map and the observed SHEEC reported data map:

$$\lambda_{\mathrm{K-S}}(D, n, m) = [nm/(n+m)]^{1/2} D,$$

where $D = \max|F_i(I) - F_0(I)|$ is the maximum of the absolute difference between the empirical distributions of the ith model map $F_i(I)$ and the I_{obs} map $F_0(I)$, whose sample sizes are n and m, respectively; I = VI, VII, VIII, IX, X, XI, XII. Figure 7.5a shows the empirical distribution functions used in the comparison. For the

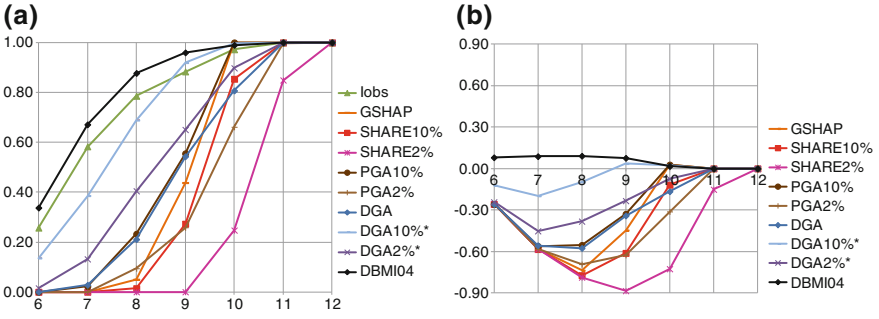

Fig. 7.5 The empirical probability functions of macroseismic intensity (**a**) and the difference between a model and the real intensities $F_i(I) - F_0(I)$ (**b**)

purposes of additional testing and qualitative uncertainty estimation, the empirical distribution function of the MCS values from the publicly available database of direct macroseismic observations DBMI04 [20] is also object of comparison with the I_{obs} map. Figure 7.5b shows the nine differences $F_i(I) - F_0(I)$ and it illustrates the departure of a model from the zero-line of reality; the departure of direct MCS observations from DBMI04 characterizes the realistic dispersion of the real data. Table 7.4 summarizes the results of the comparison in terms of computed D and λ_{K-S}.

The K-S test results confirm quantitatively the conclusions that could have been already reached from Table 7.3: the values of seismic intensity assigned by any of the models considered and reported in SHEEC do not come from the same distribution. The λ_{K-S} for the two representatives of the observed ground shaking, i.e. at epicenter (the I_{obs} map) and at site of direct observation (the DBMI04 data), provides an empirical estimate of admissible departure of real intensity distributions as a reference for claiming consistency of a model. Nekrasova et al. [13] have shown that the DGA10 % map appears to be "the best fit" among the five model intensity maps for Italy (i.e., the two official and the three neo-deterministic maps). The investigation expanded to the eight model maps confirms this conclusion. Moreover, it becomes evident that the GSHAP and most recent SHARE maps for Italy are hardly consistent with observations and overestimate dramatically the seismic hazard in the region. Apparently the SHARE maps keep moving away from reality, even more than GSHAP.

Tables 7.5 and 7.6 disclose the quality of a model map in predicting the maximum of the macroseismic intensity, in particular, the expectation of "a 10 or 2 % chance of exceedance in 50 years". Table 7.5 indicates clearly that for SHARE maps the number of exceedances, by a unit of MCS intensity or larger, is by far smaller than one should expect from the number of trials represented by the intensity VIII or larger records in DBMI04. Once again the fit of the adjusted neo-deterministic DGA10 %* and DGA2 %* (11.6 and 1.9 % exceedances, correspondingly) is more consistent with expectations than that of the probabilistic maps, both for a return period of 475 years (GSHAP is exceeded in 4.4 %, SHARE10 % in 0.1 % and PGA10 % in 4.5 % of cases, respectively) and for a return period of 2475 years (SHARE2 % and PGA2 % are never exceeded, thus it is 0.0 %). The small sample of $I_0 \geq$ VIII earthquakes from SHEEC (Table 7.6) does not permit, although does not contradict, the conclusion on a model map consistency, as clear as with the macroseismic records from DBMI04 (Table 7.7).

Table 7.4 The percentage of I_{MCS} from different ranges in real observation map (I_{obs}) and in the model intensity maps corresponding to the eight hazard maps considered

I_{MCS} range	I_{obs}	GSHAP	SHARE10 %	SHARE2 %	PGA10 %	PGA2 %	DGA	DGA10 %*	DGA2 %*
≥XI	2.76	0.03	14.58	75.28	–	33.84	19.28	0.39	10.21
≥X	11.63	56.20	72.70	100	44.48	74.15	45.66	8.06	34.93
≥IX	21.40	94.98	98.56	100	76.74	90.57	78.90	31.12	59.52
≥VIII	41.69	100	100	100	97.77	100	97.23	61.42	86.82
≥VII	74.27	100	100	100	100	100	100	86.43	98.47
≥VI	100								

Table 7.5 The Kolmogorov-Smirnov two-sample statistic λ_{K-S} applied to a model map and the real seismic intensity map (I_{obs}, sample size 1,341)

Statistic	Model seismic intensity map								
	GSHAP	SHARE10%	SHAE2%	PGA10%	PGA2%	DGA	DGA10%*	DGA2%*	DBMI04
Sample size	3,066	3,066	3,066	3,044	3,044	3,066	3,066	3,066	19,713
D	0.74	0.77	0.88	0.56	0.69	0.57	0.20	0.45	0.09
λ_{K-S}	22.47	23.57	26.99	17.11	21.10	17.56	6.03	13.79	1.82

Sample size indicates the number of grid points analysed

Table 7.6 Number of earthquakes with $I_0 \geq$ VIII from SHEEC for which the difference Δ, between I_0 and the maximum of the model map values at the distance of 1/8° or less, has been computed

Model	GSHAP	SHARE10%	SHARE2%	PGA10%	PGA2%	DGA	DGA10%*	DGA2%*
Total	42	42	42	42	42	42	42	42
$\Delta = 2$	0	0	0	0	0	0	3	1
$\Delta = 1$	2	0	0	1	0	1	5	1
$\Delta = 0$	8	2	0	9	1	5	8	5
$\Delta = -1$	12	10	4	13	9	9	19	12
$\Delta = -2$	20	16	9	19	16	13	6	14
$\Delta = -3$	0	14	18	0	16	14	1	9
$\Delta = -4$	0	0	11	0	0	0	0	0

Table 7.7 Number of grid points where the difference Δ, between the intensity $I \geq$ VIII records in DBMI04 and the maximum of the model map values at the distance of 1/8° or less, has been computed

Model	GSHAP	SHARE10%	SHARE2%	PGA10%	PGA2%	DGA	DGA10%*	DGA2%*
Total	4,421	4,421	4,421	4,421	4,421	4,421	4,421	4,421
$\Delta = 2$	1	0	0	0	0	0	81	6
$\Delta = 1$	193	3	0	200	0	9	434	76
$\Delta = 0$	589	236	0	620	189	276	1,194	430
$\Delta = -1$	1,562	706	257	1,611	633	963	1,444	1,125
$\Delta = -2$	2,009	1,790	914	1,990	1,670	1,616	1,049	1,557
$\Delta = -3$	67	1,686	1,711	0	1,924	1,557	213	1,227
$\Delta = -4$	0	0	1,539	0	5	0	0	0

7.5 Conclusions

The comparison of the model intensity maps against the real seismic activity in Italy, made over a time interval of more than a millennium, reveals many discrepancies in several aspects of the models seismic ground shaking distribution in space and size.

We did repeat the analysis reported in [13] and expanded it to the Global Seismic Hazard Assessment Programme (GSHAP) map and its new offspring for Europe (SHARE), which became available recently [6]. The results of the analysis described in this paper confirm the following conclusions:

- the estimates of seismic intensity attributed by any of the eight models considered, including the official and most recent SHARE seismic hazard maps, and those reported in the Italian databases of empirical observations could hardly arise from the same distribution;
- models (except for the recurrence adjusted neo-deterministic DGA10 % and DGA2 %, at the cost of model consistent 10 % or 2 % cases of exceedance) generally provide rather conservative estimates with respect to reality. They tend to over-estimate seismic hazard particularly at the levels below violent (MCS intensity IX) ground shaking events and yet most of them do not guarantee avoiding underestimations for the largest earthquakes;
- probabilistic maps have a higher tendency to overestimate the hazard, with respect to the corresponding deterministic maps and reality; in particular, the newly published SHARE maps assign all the territory of Italy to extreme ground shaking of intensity $I \geq$ IX;
- in terms of the goodness of fit measured by the Kolmogorov-Smirnov two-sample statistic, the NDSHA models appear to outscore the probabilistic ones and might be a better representation of the real seismicity. In particular, the minimum value of λ_{K-S} obtained for DGA10 %* is 3–4 times smaller than for any of the probabilistic models, while it is 3 times larger than for the reference misfit of the observed ground shaking at epicenters and at sites of direct observations.

The study of the statistical significance of the detected inconsistencies between model and observed intensities and their interpretation should be addressed in further investigation of earthquake phenomenon, in particular for the predictability of the maximum ground shaking.

What is often the problem with probabilistic approaches is that probability is a purely mathematical concept and, by the law of large numbers, the frequency approaches the probability only in an infinite collection of independent identically distributed random occurrences. It is clear, therefore, that all methods that mix these two terms (frequency and probability) without computing the deviations with sufficient number of moments are bound to fail sooner or later. As expected, an oversimplified model computation of the minimum time interval required for reliable occurrence rate estimates with reasonable uncertainty for a return period of 475 years [1, 10] suggests the geological time span of 12,000 years. In the case of Italy, on account of the millennial earthquake catalogue available, a reliable and physically sound

alternative is represented by NDSHA hazard estimations, which in their standard definition do not depend on the probability of earthquake occurrence, but can be adjusted by recurrence if the data allow.

The obtained results might be indicative of a fundamental misfit of the generally accepted uniform rules of homogeneous smoothing applied to observations on top the naturally fractal system of blocks-and-faults with evidently heterogeneous structure and rheology. Any model for SHA aimed, presumably, at predicting disastrous ground shaking that would actually occur must pass series of rigid testing against the available real seismic activity data before being suggested as a practical seismic hazard and risk estimation. Otherwise, similar to medical malpractice, although at much higher level of simultaneous losses [23], the use of untested seismic hazard maps would eventually mislead to crime of negligence.

Acknowledgments This paper was completed during the visit of A.K. Nekrasova at the Structure and Nonlinear Dynamics of the Earth (SAND) Group of the Abdus Salam International Centre for Theoretical Physics, Miramare—Trieste, Italy. AKN and VGK acknowledge the support from the Russian Foundation for Basic Research (RFBR grants №13-05-91167 and №14-05-92691).

References

1. C. Beauval, P.-Y. Bard P-Y, S. Hainzl, P. Guguen, Can strong motion observations be used to constrain probabilistic seismic hazard estimates? Bull. Seismol. Soc. Am. **98**(2), 509–520 (2008)
2. G. Folladore, Neo-deterministic seismic hazard assessment and earthquake recurrence, Master Thesis, Università degli studi di Trieste, Facoltà di Scienze Matematiche, Fisiche e Naturali (2010)
3. D. Giardini, G. Grünthal, K.M. Shedlock, P. Zhang, The GSHAP global seismic hazard map. Ann. Geofis. **42**(6), 1225–1228 (1999)
4. D. Giardini, G. Grünthal, K.M. Shedlock, P. Zhang, The GSHAP Global Seismic Hazard Map, in *International Handbook of Earthquake and Engineering Seismology, International Geophysics Series 81 B*, ed. by W. Lee, H. Kanamori, P. Jennings, C. Kisslinger (Academic Press, Amsterdam, 2003), pp. 1233–1239
5. D. Giardini, J. Woessner, L. Danciu, F. Cotton, H. Crowley, G. Grünthal, R. Pinho, G. Valensise, S. Akkar, R. Arvidsson, R. Basili, T. Cameelbeck, A. Campos-Costa, J. Douglas, M.B. Demircioglu, M. Erdik, J. Fonseca, B. Glavatovic, C. Lindholm, K. Makropoulos, C. Meletti, R. Musson, K. Pitilakis, A. Rovida, K. Sesetyan, D. Stromeyer, M. Stucchi, Seismic hazard harmonization in Europe (SHARE) (2013). doi:10.12686/SED-00000001-SHARE
6. D. Giardini, J. Woessner, L. Danciu, Mapping Europe's seismic hazard. Eos Trans. AGU, Eos **95**(29) (2014)
7. G. Grünthal, R. Wahlström, D. Stromeyer, The SHARE European earthquake catalogue (SHEEC) for the time period 1900–2006 and its comparison to the European mediterranean earthquake catalogue (EMEC). J. Seismolog. **17**(4), 1339–1344. (2013) doi:10.1007/s10950-013-9379-y
8. M. Indirli, H. Razafindrakoto, F. Romanelli, C. Puglisi, L. Lanzoni, E. Milani, M. Munari, S. Apablaza, Hazard evaluation in Valparaiso: the MAR VASTO Project. Pure Appl. Geophys. **168**(3–4), 543–582 (2011)
9. V.G. Kossobokov, A.K. Nekrasova, Global seismic hazard assessment program maps are erroneous. Seismic Instrum. **48**(2) (2012), http://dx.doi.org/10.3103/S0747923912020065. (Allerton Press Inc, pp. 2012162–2012170)

10. S. Mak, R.A. Clements, D. Schorlemmer, The statistical power of testing probabilistic seismic-hazard assessments. Seismol. Res. Lett. **85**(4), 781–783 (2014)
11. W. Marzocchi, Seismic hazard and public safety. Eos **94**(27), 240–241 (2013)
12. C. Meletti, V. Montaldo, Stime di pericolosità sismica per diverse probabilità di superamento in 50 anni: valori di ag. http://esse1.mi.ingv.it/d2.html, Deliverable D2 (2007)
13. A. Nekrasova, V. Kossobokov, A. Peresan, A. Magrin, The comparison of the NDSHA. PSHA seismic hazard maps and real seismicity for the Italian territory. Nat. Hazards **70**(1), 629–641 (2014). doi:10.1007/s11069-013-0832
14. G.F. Panza, F. Romanelli, F. Vaccari, Seismic wave propagation in laterally heterogeneous anelastic media: theory and applications to seismic zonation. Adv. Geophys. **43**, 1–95 (2001)
15. G.F. Panza, C. La Mura, A. Peresan, F. Romanelli, F. Vaccari, Seismic Hazard Scenarios as Preventive Tools for a Disaster Resilient Society, in *Advances in Geophysics*, ed. by R. Dmowska (Elsevier, London, 2012), pp. 93–165
16. G.F. Panza, A. Peresan, C. La Mura, Seismic Hazard and Strong Ground Motion: An Operational Neo-deterministic Approach from National to Local Scale, in *Encyclopedia of Life Support Systems (EOLSS), Geophysics and Geochemistry, Developed under the Auspices of the UNESCO*, ed. by UNESCO-EOLSS Joint Commitee (Eolss Publishers, Oxford, 2013), pp. 1–49
17. G.F. Panza, V. Kossobokov, A. Peresan, A. Nekrasova, Why are the standard probabilistic methods of estimating seismic hazard and risks too often wrong? in *Earthquake Hazard, Risk, and Disasters* (Chapter 12), ed. by M. Wyss (2014), pp. 309–357, http://dx.doi.org/10.1016/B978-0-12-394848-9.00012-2
18. A. Peresan, A. Magrin, A. Nekrasova, V.G. Kossobokov, G.F. Panza, Earthquake Recurrence and Seismic Hazard Assessment: A Comparative Analysis Over the Italian Territory, in *Proceedings of the ERES 2013 Conference. WIT Transactions on The Built Environment*, vol. 132 (2013), pp. 23–34. doi:10.2495/ERES130031, ISSN 1743-3509 (on-line)
19. K.M. Shedlock, D. Giardini., G. Grünthal, P. Zhang, The GSHAP global deismic hazard Map. Seismol. Res. Lett. **71**(6), 679–686 (2000)
20. M. Stucchi, R. Camassi, A. Rovida, M. Locati, E. Ercolani, C. Meletti, P. Migliavacca, F. Bernardini, R. Azzaro, DBMI04, il database delle osservazioni macrosismiche dei terremoti italiani utilizzate per la compilazione del catalogo parametrico CPTI04. Quad. Geof. **49**, 38 (2007), http://emidius.mi.ingv.it/DBMI04/
21. Stucchi et al., The SHARE European earthquake catalogue (SHEEC) 1000–1899. J. Seismolog. (2012). doi:10.1007/s10950-012-9335-2
22. S. Stein, R. Geller, M. Liu, Why earthquake hazard maps often fail and what to do about it. Tectonophysics **562–563**, 1–25 (2012)
23. M. Wyss, A. Nekrasova, V. Kossobokov, Errors in expected human losses due to incorrect seismic hazard estimates. Nat. Hazards **62**, 927–935 (2012)
24. E. Zuccolo, F. Vaccari, A. Peresan, G.F. Panza, Neo-deterministic and probabilistic seismic hazard assessments: a comparison over the Italian territory. Pure Appl. Geophys. **168**, 69–83 (2011)

Chapter 8
Steps in Seismic Risk Mapping for Romania Capital City

E.F. Manea, D. Toma-Danila, C.O. Cioflan and Gh. Marmureanu

Abstract Bucharest, capital of Romania, is one of the most seismically vulnerable cities in Europe. The earthquakes affecting the city have their origin in the Vrancea intermediate-depth source. In the last century, major earthquakes (November 10, 1940, *Mw* = 7.7; March 4, 1977, *Mw* = 7.4; August 30, 1986, *Mw* = 7.1; May 30, 1990, *Mw* = 6.9) produced significant effects for this area. This study's objective is to highlight the seismic risk of Bucharest nowadays by estimating the possible building and human losses, for relevant scenarios—based on real data and neodeterministic approach. The building loss estimates were obtained through the Improved Displacement Coefficient Analytical Method. In order to provide a balanced input that can also reflect different damage states in the risk analysis, for the hazard data we used real data from seismic stations for August 30, 1986 and May 30, 1990 earthquakes and microzonation map for the maximum possible earthquake that can be produced in Vrancea intermediate-depth source (M_w = 7.8 and depth 150 km). The spectral content was used for peak ground acceleration (PGA) and spectral acceleration at 0.3 and 1 seconds. For the vulnerability assessment, data obtained from the "Danube Cross-Border system for Earthquakes Alert" (DACEA) Project and a database with classification of the buildings in 1999 were used. The analysis is performed at sector level (6 in total). We computed the probability of damage for the buildings and human casualties in terms of different injury types with SELENA Software.

E.F. Manea (✉) · D. Toma-Danila · C.O Cioflan · Gh. Marmureanu
Department of Engineering Seismology, National Institute for Earth Physics,
P.O. BOX MG-2, 12 Calugareni Str., 077125 Magurele, Bucharest, Romania
e-mail: elena.manea@infp.ro

E.F. Manea
Faculty of Physics, Department of Atmospheric Physics, University of Bucharest,
P.O. BOX MG-11, Bucharest, Romania

D. Toma-Danila
Faculty of Geography, University of Bucharest, Bucharest, Romania

B. Aneva and M. Kouteva-Guentcheva (eds.),
Nonlinear Mathematical Physics and Natural Hazards,
Springer Proceedings in Physics 163, DOI 10.1007/978-3-319-14328-6_8

8.1 Introduction

The city of Bucharest, capital of Romania, is an extremely vulnerable capital in Europe. Bucharest comprises around 2 million inhabitants and a considerable number of buildings expected to collapse during a future major earthquake (373 out of 2,563 were classified in the seismic risk class 1 after individual expert evaluation; but the building stock consists of more than 1,13,900 buildings).

The major earthquakes affecting the city have their origin in the Vrancea region located at the curvature of the Carpathian Mountains, where the East European Plate and the Intra-Alpine and Moesic Subplates are in contact (continental collision). Vrancea seismic source presents a high concentration of events in a well-defined volume located at intermediate depth ($60 < h < 200$ km), where 2–3 events with $M_w > 7.0$ are generated each century [1]. Although situated at more than 170 Km away from the focal intermediate-depth source in Vrancea, Bucharest experienced significant damage to past earthquakes with magnitude M_w over 7.0 [2].

The last major earthquakes (November 10, 1940, $M_w = 7.7$; March 4, 1977, $M_w = 7.4$; August 30, 1986, $M_w = 7.1$; May 30, 1990, $M_w = 6.9$, May 31, 1990, $M_w = 6.4$, October 27, 2004, $M_w = 6$) (see their locations in Fig. 8.1) claimed in total more than 1,700 lives. The earthquake on March 4, 1977 ($M_w = 7.4$) especially was the most damaging seismic shock in recent history.

In Romania, a high number of human casualties were recorded: 1,570 deaths and over 11,300 injured, and most of them: 1,424 deaths and around 7,598 injured people were in Bucharest. The total number of the buildings that were destroyed and seriously damage was 33,000 and 1,82,000 with lesser damage. The total cost of damage was over 2 billion US dollars [3].

8.2 Methods

For the buildings and population damage assessment, we used SELENA Software (SEimic Loss EstimatioN using a logic tree Approach, ©NORSAR). SELENA is a tool based on the methodology of HAZUS (©FEMA) [4], that adapted it to the European conditions (new GMPE's), added new analytical methods (MADRS, I-DCM) [5] and replaced the ArcGis dependencies with open-source processing environments or Matlab.

SELENA computes the probability of damage in each one of the four damage states (slight, moderate, extensive and complete) for the given building types. This probability is subsequently used with the inventory data to express the results in terms of damaged area or number of damaged buildings [5].

The methodology used in this study relies on the Improved Displacement Coefficient analytical Method (I-DCM), which is also currently used within the Near Real-Time System for Estimating the Seismic Damage of Romania [6].

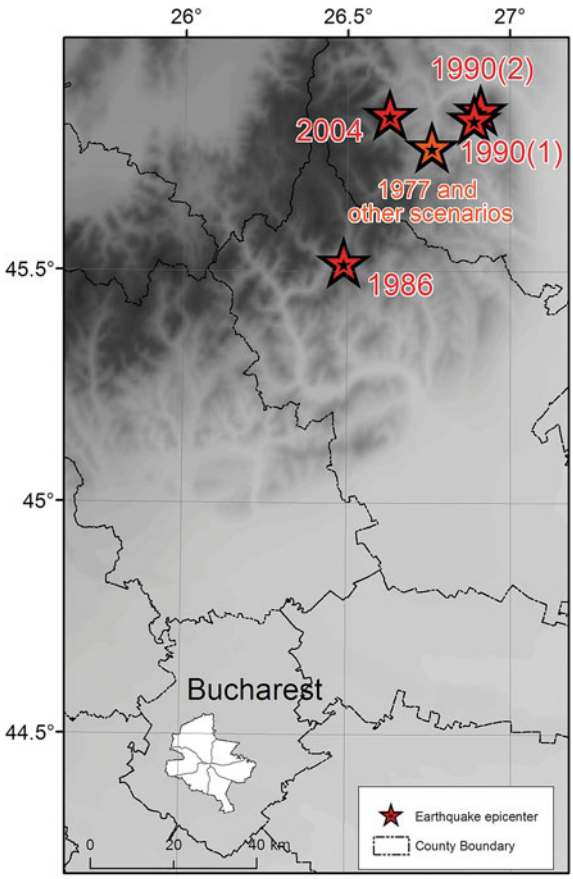

Fig. 8.1 Map showing the epicenters of recent major earthquakes in the Vrancea area and location of Bucharest

I-DCM is based on the idea that any building (defined as a single degree of freedom system—SDOF) is structurally damaged by the spectral displacement (and not by the spectral acceleration itself).

For each building, the inter-story drift is a function of the applied lateral force that can be analytically determined and transformed into building capacity curves, based on yield or ultimate points [7].

Differently from other capacity-spectrum methods (like CSM or MADRS), I-DCM modifies the displacement demand of the equivalent SDOF by multiplying it by a series of coefficients in order to generate an estimate of the maximum displacement demand of the nonlinear oscillator, as shown in Fig. 8.2 [5].

In order to express the probability distributions of the damage, fragility functions (curves) are used. Usually, the damage is characterized by specific damage states, like none, slight, moderate, extensive and complete (as in FEMA [4]). For each building typology, a specific damage probability is obtained by plotting on the fragility functions the spectral displacement coordinates of the target displacement point (δt).

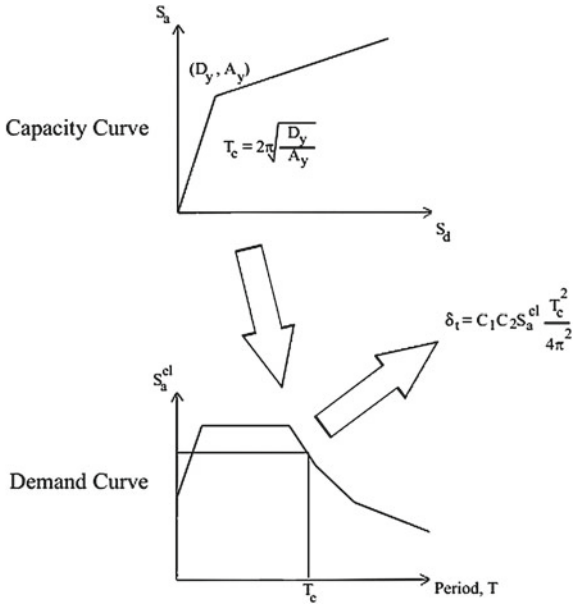

Fig. 8.2 Schematic illustration of I-DCM process which is used to compute the target displacement demand of a nonlinear oscillator for a given capacity *curve* and response spectrum (from Molina et al. [5])

The social losses are computed afterwards, using an empirical formula (8.1) based on the number of buildings in different damage states and the casualty rates for each building type and damage level (formula 2). This casualty rates are generally derived from past events.

Kij = Population per building * Number of damaged buildings in damage state j * Casualty Rate for severity level i and damage state j. (8.1)

8.3 Input Data

For the estimation of loss, two categories of input data are necessary: hazard data and building vulnerability data.

For defining a proper input for the risk analysis we used real data from August 30, 1986, $M_w = 7.1$ and May 30, 1990(1), $M_w = 6.9$ earthquakes (see Fig. 8.3). The values recorded at the seismic stations inside and near Bucharest were interpolated using the Inverse Interpolation Method, and a mean for each sector was calculated. The resulted values were used in the analysis. For the microzonation map there was no need for interpolation.

In order to include in the risk analysis a simulation with detailed hazard parameters calculated for Bucharest, we use a recent microzonation map of Marmureanu et al. [8], for the maximum predicted Vrancea earthquake (M_w7.8). This map (showed

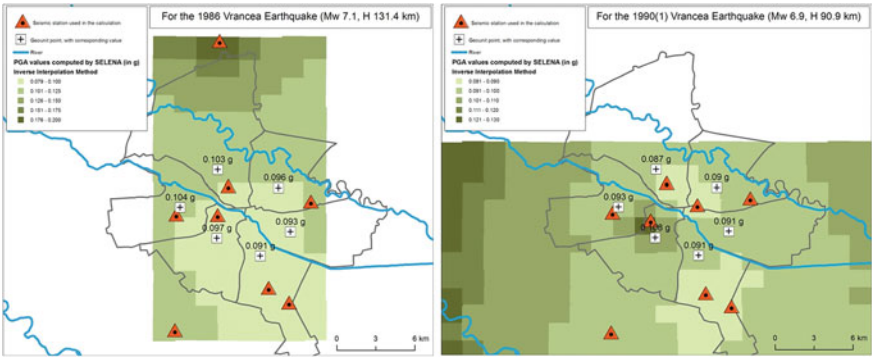

Fig. 8.3 Interpolation map used by SELENA in the calculation for geounit values, based on real recordings from the 1986 (*left*) and 1990(1) earthquakes (*right*)

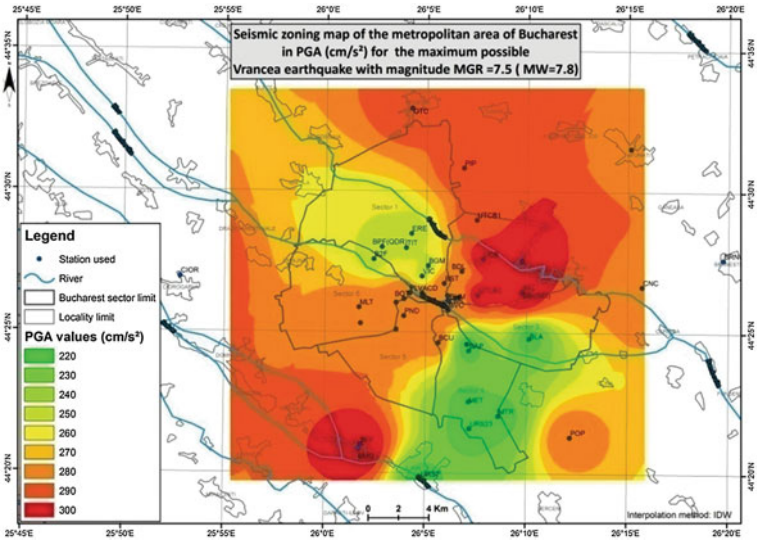

Fig. 8.4 Microzonation map of Bucharest for the maximum possible earthquake produced in Vrancea zone (M_w7.8) [8]

in Fig. 8.4) provides PGA values calculated at different boreholes, based on non-linear seismic response evaluation to a synthetic signal from a point source with a mechanism similar to the one of the 1940 earthquake. For this earthquake, we used the Eurocode8—type 2 design spectrum method to calculate the spectral response acceleration of this earthquake.

The characteristics of the building database compiled in the DACEA Project ("Danube Cross-Border system for Earthquakes Alert") [9] were used, such as capacity and fragility curves for 48 main building typologies in Romania (see Table 8.1). The building and population database for Bucharest was at the level of

Table 8.1 Structure of the buildings database and associated vulnerability curves (48 in total)

	Construction matarial	Material code	Height class	Construction code	Vulnerability curves
MAW	Adobe	M2	L	PC, LC, MC, HC	URM-L-PC[a]
	Unreinforced masonry bearing walls with flexible floors	M3_1	L	PC, LC, MC	URM-L-PC[a]
	Unreinforced masonry bearing walls with flexible floors	M3_1	M, H	PC, LC, MC	URM-M-PC[a]
	Unreinforced masonry bearing walls with rigid floors	M3_2	L	PC, LC, MC	URM-L-LC[a]
	Unreinforced masonry bearing walls with rigid floors	M3_2	M, H	PC, LC, MC	URM-M-LC[a]
	Reinforced or confined masonry bearing walls or retrofitted (overall strengthened) masonry buildings	M4	L, M, H	HC	M7-2, M 7-4, M7-6[b]
	Wood structures	W	L	PC, LC, MC, HC	W1-PC(LC, MC, HC)[a]

(continued)

Table 8.1 (continued)

	Construction matarial	Material code	Height class	Construction code	Vulnerability curves
RC	Concrete shear walls	RC2	L, M, H	PC, LC, MC, HC	C2-L(M,H)-PC(LC,MC,HC) fragility curve[a] + modified capacity curve (by UTCB)
	Concrete frame with unreinforced masonry infill walls	RC3	L, M, H	PC, LC, MC, HC	C3-L(M,H)-PC(LC,MC,HC) fragility curve[a] + modified capacity curve (by UTCB)
	Precast concrete walls	RC5	L, M, H	PC, LC, MC, HC	PC2-L(M,H)-PC(LC,MC,HC)[a]
Height class abbreviations	L = Low—1–2 stories	M = Medium—3–5 stories	H = High—6+ stories		
code abbreviations	PC = PreCode—older than 1963 MC = Moderate Code—1978–1991	LC = LowCode—1963–1977 HC = High Code—1991–1999			

[a] HAZUS-MH FEMA (2003) [4]
[b] Cattari et al. (2004) [10]

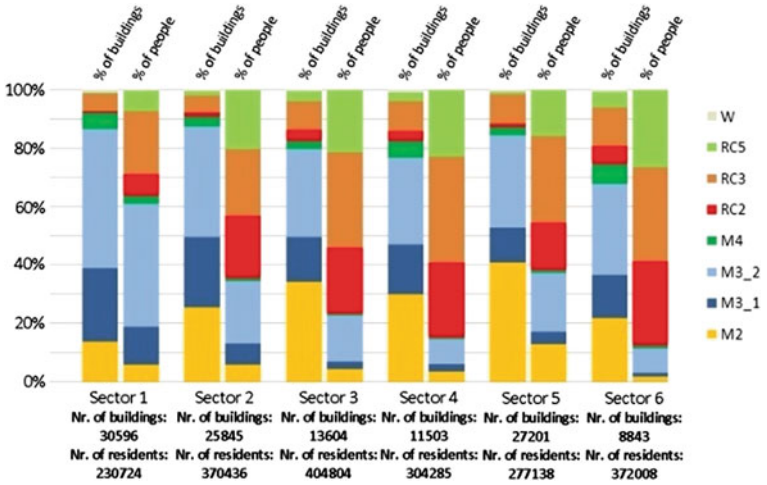

Fig. 8.5 The percentage of buildings and residents as a function of the building material typologies

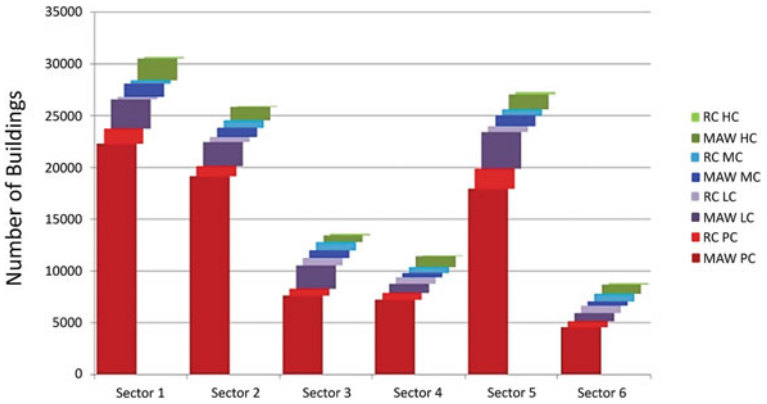

Fig. 8.6 Number of buildings for each sector, depending on major material type and age (seismic code)

1999, however newer buildings are not expected to be significantly damaged and not many old buildings were rehabilitated or demolished, so the database is relevant. The resolution of the available data was the sector level (6 in total).

In Figs. 8.5 and 8.6 are represented the characteristics of the database used in this study, according to the classification in Table 8.1. It can be seen that more than 50 % of the building stock is represented by masonry buildings and a high number of people

live in flats made from reinforced concrete. Also, a large amount of building (mostly from masonry) are older than 1963 and considered before seismic code regulation, therefore the main risk is expected to come from these buildings.

8.4 Results

The results obtained after the analysis are presented using two indicators:

- estimated number of buildings with complete damage, expressed as percentage from the total number of buildings (Fig. 8.7)
- estimated number of severe injuries, which represent a sum of severity grades 3—severe injuries and 4—deaths (Fig. 8.8).

The error bars show the 16 and 84 % percentiles.

As expected, there is a major difference between the simulations with real data and the simulation of the maximum possible. The 1986 and 1990(1) earthquakes did not produce in reality major damage; the last one producing 2 deaths in Bucharest in Colentina area (sector 2) [11]. The estimates for the maximum possible scenario show important damage not to be desired in reality, but considering however the focal distance to Vrancea Area and other situations worldwide (a good comparison is with the Mexico City earthquake [12]), the range seems to be credible.

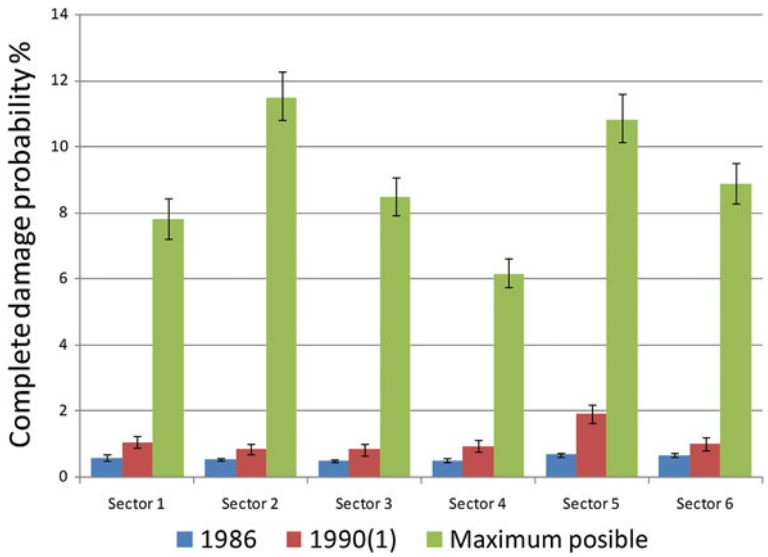

Fig. 8.7 Probability of completely damaged buildings for all 6 Bucharest sectors, for 1986 and 1990(1) and maximum possible earthquakes

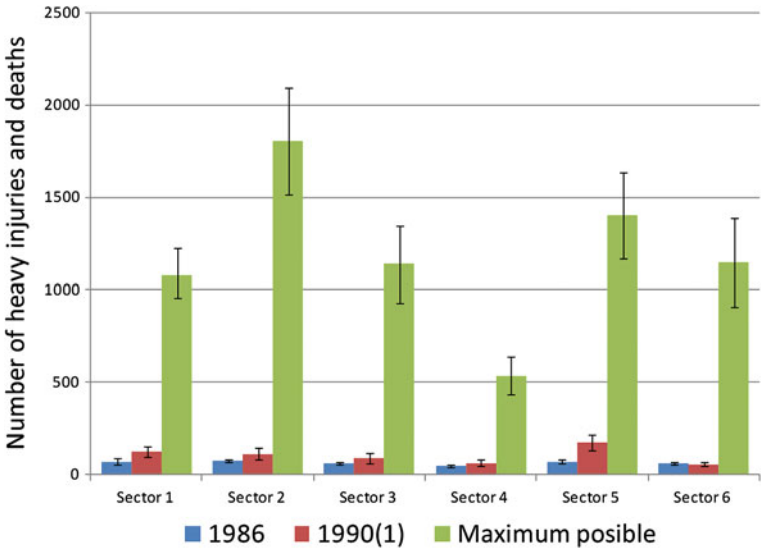

Fig. 8.8 Estimated number of cumulated human casualties and severe injuries

8.5 Conclusions

In this study the objective was to make an improvement in the estimation of loss scenarios and seismic risk computations using different scenarios based on real data and microzonation map for the city of Bucharest, capital of Romania. As a basis for these computations we used the available information on seismic hazard and vulnerability assessment of buildings for the city of Bucharest.

The loss estimates are greater than reality but still they are not very far considering the nature of the seismic risk. A very influent factor is the vulnerability function of the masonry buildings. There is a normal correlation between sectors with most damaged buildings and number of severe injuries—with sectors 2 and 5 being the most risky.

The impact comes mostly from the vulnerability of the building stock, rather than the site effects, in the analysis. Further investigations are needed to be considered, also taking into account the hysteresis aspects of the buildings.

Acknowledgments This study was made in the framework of the project BIGSEES: "BrInging the Gap between Seismology and Earthquake Engineering: from the Seismicity of Romania towards a refined implementation of seismic action EN1998-1 in earthquake resistant design of buildings" 72/2012, Poseizon PN 09–30 03 06 and PhD projects of Elena Florinela Manea and Dragos Toma-Danila.

References

1. M. Radulian, F. Vaccari, N. Mandrescu, G.F. Panza, C.L. Moldoveanu, Seismic hazard of Romania: deterministic approach. PAGEOPH **157**, 221–247 (2000)
2. Mărmureanu Gh. (coordonator), Cercetări privind hazardul seismic la nivel naţional şi local. Hărţi de hazard seismic general şi local (microzonare); Ed. Tehnopress, Iaşi (2009)
3. S. Balan et al., *Cutremurul de Pamant din Romania de la 4 Martie*, 1977. Ed. Academiei, Bucharest, Romania (1982)
4. Federal Emergency Management Agency (FEMA), *HAZUS-MH - Multi-hazard Loss Estimation Methodology, Earthquake Model* (Advanced Engineering Building Module, FEMA, Washington DC, 2004)
5. S. Molina, D.H. Lang, C.D. Lindholm, F. Lingvall, User Manual for the Earthquake Loss Estimation Tool: SELENA (2010)
6. D. Toma-Danila, C.O. Cioflan, S.F. Balan, E.F. Manea Characteristics and results of the near real-time system for estimating the seismic damage of Romania. Proceedings of the 5th national conference of earthquake engineering and the 1st national conference on earthquake engineering and seismology, Bucharest, Romania, 19–20 June 2014, pp 411–418
7. E. Erduran, D. Toma-Danila, A. Aldea et al., in *Real Time Earthquake Damage Assessment in Romanian-Bulgarian Border, 15 World Conference on Earthquake Engineering*, Lisbon, Portugal
8. G. Marmureanu, C.O. Cioflan, A. Marmureanu, *Researches on Local Seismic Hazard (Microzonation) for Metropolitan Bucharest Area*. (Tehnopress, Iasi, 2010) Accredited by ANCS, Code 89, ISBN: 978-973-702-809-9, p. 470
9. DACEA project (Danube Cross-border System for Earthquake Alert): http://quakeinfo.eu/en/
10. S. Cattari, E. Curti, S. Giovinazzi, S. Lagomarsino, S. Parodi, A. Penna, Un modello meccanico per l'analisi di vulnerabilita del costruitoin muratura a scala urbana, 11thConference "L'ingegneria Sismica in Italia". Genoa, Italy (2004)
11. GEM consequence database: http://gemecd.org/event/171
12. http://seismo.berkeley.edu/blog/seismoblog.php/2008/09/19/title

Chapter 9
Romanian Seismic Network Since 1980 to the Present

Mihaela Popa, Mircea Radulian, Daniela Ghica, Cristian Neagoe and Eduard Nastase

Abstract National Institute for Earth Physics is responsible for seismic monitoring of Romania. For this purpose, a dense seismic network is now operating covering almost the entire surface of the country. At present, the Real Time Seismic Network consists of 96 sites with seismic digital equipment, of which 3 in Republic of Moldova, and two seismic arrays: Bucovina (BURAR) and Plostina (PLOR). BURAR array is a high performance seismic monitoring system consisting of 3 broad-band and 9 short period stations distributed over a 5 km^2 area. Plostina seismo-acoustic array has been recently deployed in the Vrancea epicentral area for monitoring local microseismic activity and infrasound sources. All the stations are sending data in real time to the National Data Center (NDC) in Magurele. A strong motion network of 120 stations, equipped with accelerometer (EpiSensor—2g full scale) sensors was installed to record strong ground motion. 101 stations are sending data in real-time and 19 are offline stations. Most of the accelerometers are co-located with the seismic sensors. 23 of the accelerometers are operating in Bucharest city. Recently, 32 seismic stations were installed along the Danube River in the framework of the DACEA cross-border project. The goal of this network is to set an Early Warning System for the earthquakes in Romania and Bulgaria which affect the targeted area. To measure the ground motion deformation, a GPS network was developed mainly in the last years. NDC is exchanging data with other national and international seismological centers.

M. Popa (✉) · M. Radulian · D. Ghica · C. Neagoe · E. Nastase
National Institute for Earth Physics, 12 Calugareni St., Magurele, llfov, Romania
e-mail: mihaela@infp.ro

M. Radulian
e-mail: mircea@infp.ro

D. Ghica
e-mail: daniela@infp.ro

C. Neagoe
e-mail: cristian.neagoe@infp.ro

E. Nastase
e-mail: eduard-nastase@infp.ro

B. Aneva and M. Kouteva-Guentcheva (eds.),
Nonlinear Mathematical Physics and Natural Hazards,
Springer Proceedings in Physics 163, DOI 10.1007/978-3-319-14328-6_9

9.1 Introduction

The National Institute for Earth Physics (NIEP) operates a real-time seismic network designated to monitor seismic activity occurred across Romania's territory. The seismicity in Romania is dominated by the intermediate-depth earthquakes of the Vrancea region, with hypocentral depths between 50 and 200 km (Fig. 9.1). The crustal earthquakes occur more scattered and infrequent, but clustered activities can be defined in several epicentral areas such as: Vrancea, Fagaras-Campulung, Sinaia, Oltenia, Crisana and Maramures, Banat, Moldova, South and North Dobrogea [5].

The first network installed between 1980 and 1982, after the major earthquake of March 4, 1977 (M_w 7.4), was primarily designated to survey the Vrancea seismic region, located at the Carpathian arc bend. Despite the concentration of the focal volume, the rate of destroying events is high (3–4 events per century), affecting large areas in Europe. The initial network consisted of 18 short-period stations (S13 seismometers, one second natural period), 14 of them located in the outer part of Carpathians and 4 in the inner part of the Carpathians. Data were telemetered to NIEP, in Magurele.

In parallel with the telemetered network, NIEP operated, at that time, a free-field strong motion network consisting of 21 SMA-1 accelerometers designed to record strong and moderate Vrancea earthquakes. An important step forward was the development in 1995–1997 of the strong ground motion network by installing

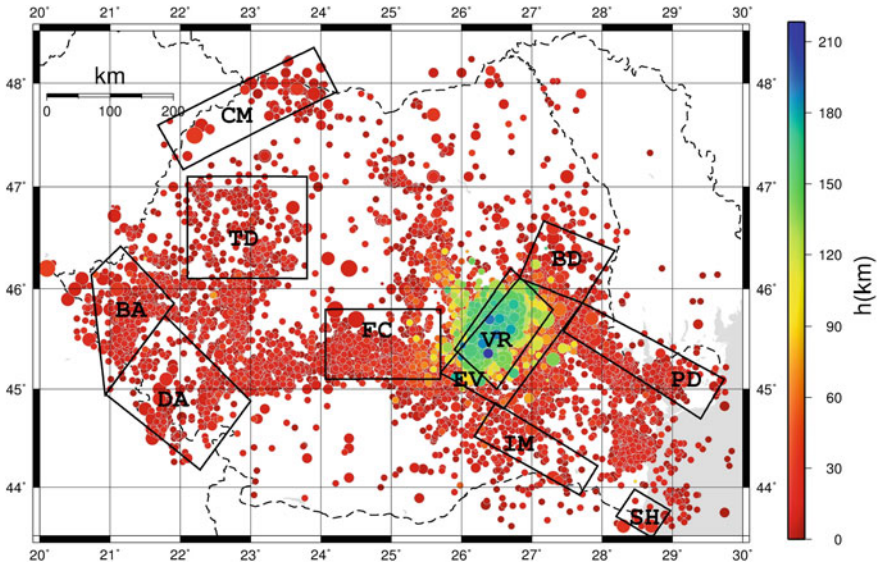

Fig. 9.1 Geographical distribution of the seismogenic zones (polygons) and Romania's seismicity. *VR* Vrancea, *EV* East Vrancea, *BD* Barlad Depression, *PD* Predobrogean Depression, *IM* Intramoesian Fault, *SH* Shabla, *FC* Fagaras-Campulung, *DA* Danubian Zone, *BA* Banat, *CM* Crisana-Maramures, *TD* Transylvanian Depression

36 K2 seismic stations, in cooperation with the University of Karlsruhe, Germany, in the framework of the Project "Strong Earthquakes: A Challenge for Geosciences and Civil Engineering" [1]. The new digital network was centered on the Vrancea seismic zone, covering an area with a diameter of up to 500 km.

9.2 Overview of the Present Status of the Romania's Seismic Network

The Romania's Seismic Network (RSN) consists of stand-alone stations and 8 observatories distributed all over the country (Fig. 9.2). At the beginning, the observatory had seismic equipment with analog, mechanical and photo recorders. Starting with 2002, the seismic network modernization was based on the installation of new and advanced equipment like acceleration (EpiSensor) and velocity sensors (broad-band: CMG3ESP, CMG40T, KS2000, KS54000, KS2000, CMG3T, STS2 and short-period instruments: SH-1, S13, Mark l4c, Ranger, GS21, L22_vel).

Since 1994, a high performance seismic system (Quanterra data logger, GPS timing broadband velocity sensors, three components and more than 7 days buffer for the data storage) has been installed at the Muntele Rosu (MLR) observatory (Fig. 9.3), in the framework of the cooperation with the GEOFON Network (Germany). MLR station was included in the auxiliary seismic network of the International Monitoring System (IMS) coordinated by CTBTO (Comprehensive Nuclear-Test-Ban Treaty

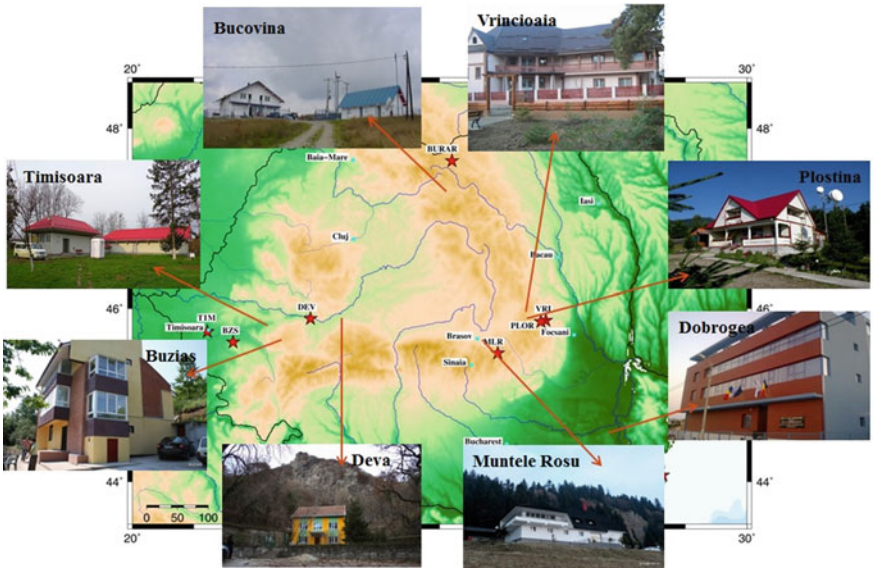

Fig. 9.2 Seismological observatories in Romania

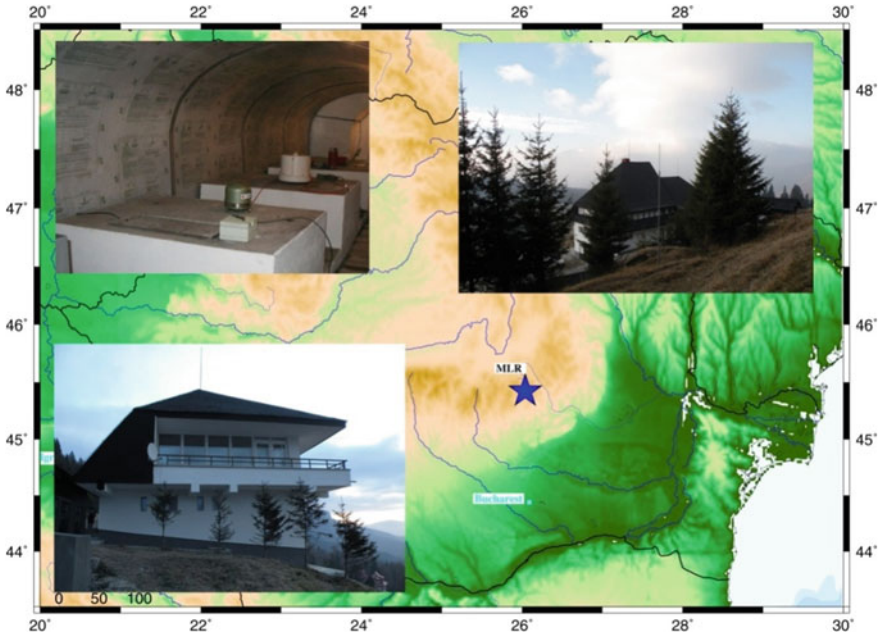

Fig. 9.3 Muntele Rosu (MLR) observatory

Organization). In order to ensure Romania's technical participation to the CTBTO activities and to maintain the station at the operational standards required by the Treaty, since 1999, an important upgrade has been carried out both at the seismic station MLR and at the NDC, involving technical cooperation with the Government of Japan and technical assistance from the CTBT Organization [3]. The data were continuously recorded and transmitted in real-time to the NDC in Magurele and IDC in Vienna.

Vrincioaia Observatory (Fig. 9.4), located in the North-Eastern part of Vrancea epicentral area, was built in 1956 for seismic monitoring and for measuring various precursor factors in correlation with the seismic activity. The personal from the Observatory has also in charge the maintenance of 10 seismic stations from the North-Eastern part of the country. Data from all this stations are transmitted in real-time to the NDC in Magurele.

Plostina seismo-acoustic array is located in Vrancea region, close to the Vrincioaia Observatory (Fig. 9.5). The array deployment started in 2007, when four seismic elements (PLOR1, PLOR2, PLOR3 and PLOR4) were installed. In 2009, two more seismic sites (PLOR5 and PLOR6) were added, and the infrasound array deployment was initiated, by placing of three infrasonic instruments (IPH4, IPH5 and IPH6), collocated with the corresponding seismic locations. In 2010, another seismo-acoustic element (PLOR7 and IPH7) was added and during 2012, sites 2 and 3 where equipped

Fig. 9.4 Vrincioaia (VRI) observatory and the nearby stations under administration

with infrasound sensors. Plostina seismo-acoustic array is currently distributed over an area of 3.5 km^2, inter-element distance varies between 450 and 2,450 m.

Presently, at Plostina, NIEP operates an integrated system (Fig. 9.5) which includes advanced technologies such as: seismic and infrasound arrays, strong motion sensors, magnetic field and electric field monitoring, soil temperature measuring, and a weather station. The main applications of this system are: monitoring of the local microseismic activity, acoustic measurement (infrasound monitoring of explosions, mine and quarry blasts, volcanic eruptions, earthquakes, aircraft etc.), observation of the magnetic field variation in correlation with solar activity, observation of the variation of telluric currents.

Since July, 2002, a new seismic monitoring system, Bucovina Seismic Array (BURAR), has been established in the Northern part of the country (Fig. 9.6), in a joint effort of the Air Force Technical Applications Center (AFTAC), USA and NIEP. Data recorded by BURAR array are continuously transmitted in real time to the National Data Center of USA in Florida and to NDC, in Magurele. BURAR seismic array consists of 10 seismic stations located in boreholes and distributed over an area of 5 km^2. Nine stations are equipped with short-period vertical sensors (GS-21) and one station is equipped with broad-band three-component sensor (KS

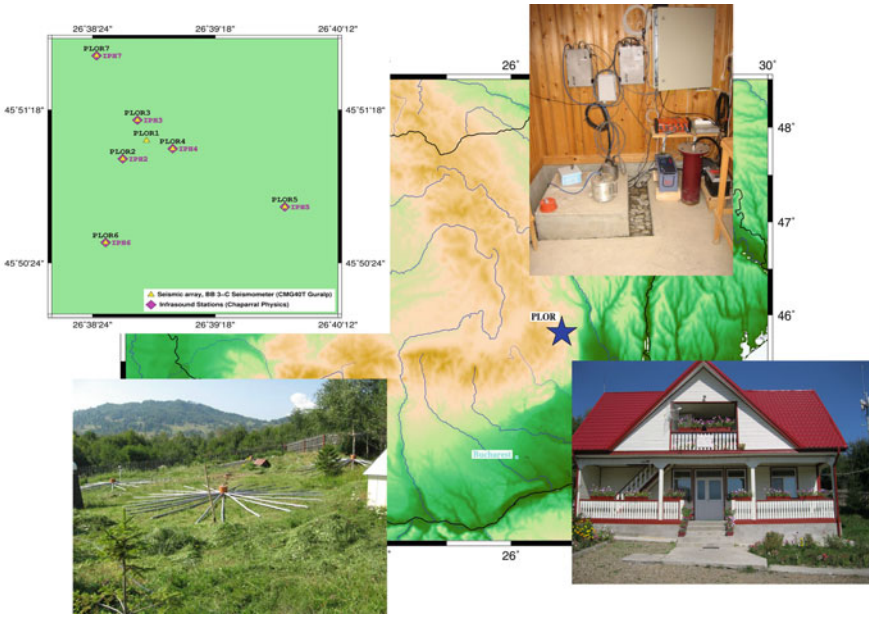

Fig. 9.5 Plostina observatory and elements of integrated system operating in the area (PLOR*—seismic array, IPH*—infrasonic array)

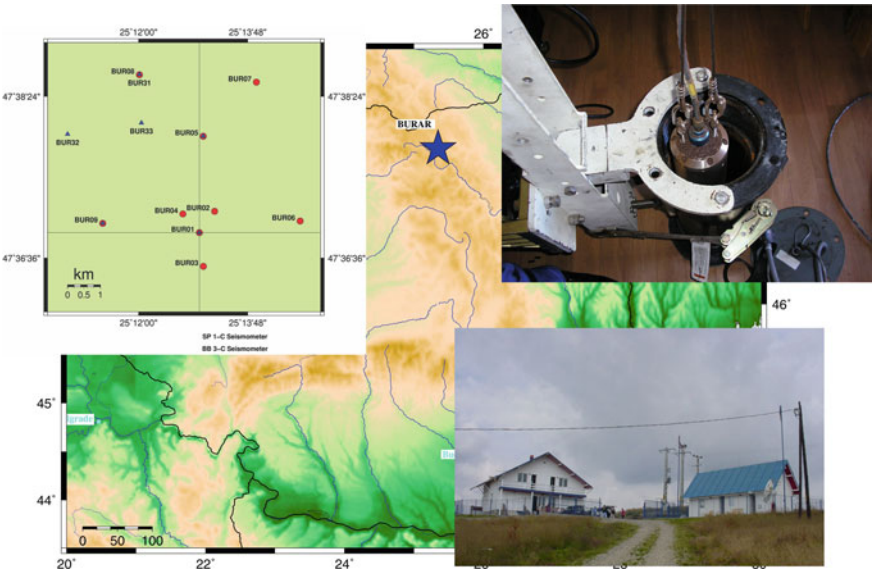

Fig. 9.6 Bucovina observatory (BURAR) and array elements distribution

54000) [2]. In 2007 two new elements equipped with 3-C broad-band sensors were installed aiming to obtain the most convenient array combination of 3-C elements for the recording and identification of the secondary seismic phases, to optimize the array response, achieving a superior sensitivity and resolution of BURAR in S-type seismic signals identification.

In 2008 a new modern Seismological Observatory EFOR was inaugurated at Eforie, in the Southern part of Dobrogea as back-up for the data acquisition and processing in Magurele and as monitoring center for Black Sea tsunamis. The observatory employers assure also the maintenance of other 10 seismic stations installed in the region. These stations are equipped with seismometers and accelerometers and the recorded data are transmitted in real time to NDC. Equipment to measure electromagnetic field and UV radiation is operating as well (Fig. 9.7).

A major strategic objective of NIEP is the integration and homogenization of seismic monitoring at the cross-border areas. To this aim, the cooperation with neighboring countries has been continuously renewed. Thus, in cooperation with the Institute of Geophysics and Seismology of Kishinev (Republic of Moldova), five seismic stations 9.8 have been installed at Leova (LEOM), Giurgiulesti (GIUM), Milestii Mici (MILM), Kisinev (KIS) and Soroca (SORM) between 2007 and 2010. Data recorded by these stations are currently received in real time at NIEP data Center

Fig. 9.7 Dobrogea (EFOR) observatory and the nearby stations under administration

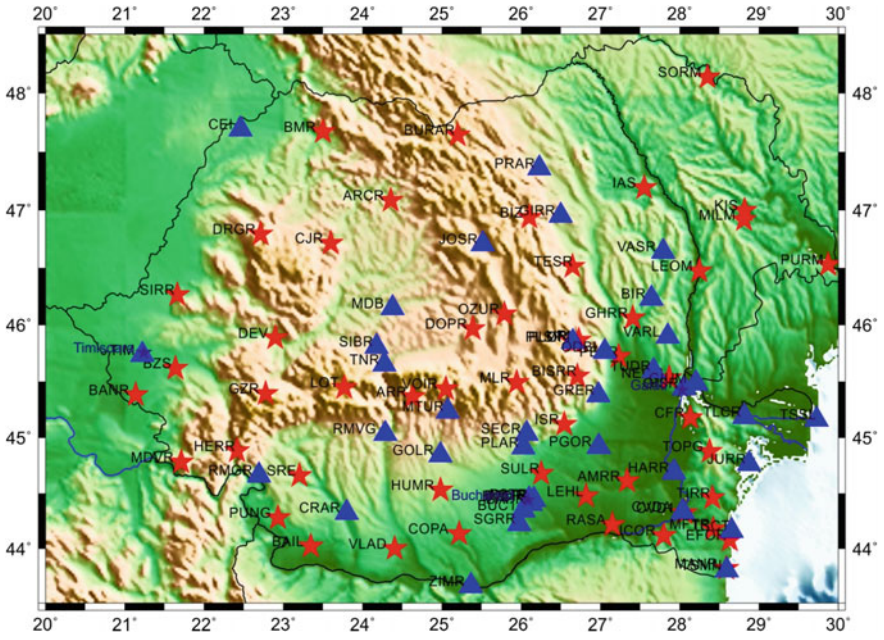

Fig. 9.8 National seismic network configuration (including stations installed in Republic of Moldova); (*triangles* short-period stations; *stars* broad-band stations)

using seedlink connections. In the framework of an ample cross-border project with Bulgaria (DACEA project, quakeinfo.eu) 32 new seismic stations were installed in the Danube area. 8 seismic stations on Romania territory and 8 in Bulgaria, equipped with Basalt digitizer, accelerometer EpiSensor and BB seismometer KS2000, were installed along the Danube River. Also, 7 accelerometers (EpiSensor) and warning and visual monitoring equipment were installed at the Emergency Situations Inspectorates in Romania and 9 in Bulgaria (Fig. 9.9). The general objective of Danube Cross-border system for Earthquakes Alert (DACEA) Project was to develop an Early Warning System in order to prevent the natural disasters caused by earthquakes in the cross-border area (Romania—Vrancea and Bulgaria—Shabla, Dulovo and Gorna Orjahovitza), taking into account the nuclear power plants (Kozloduy, Cernavoda) and the chemical plants located along the Danube.

The NIEP strong motion network (Fig. 9.10) consists of 120 strong motion stations using accelerometers (EpiSensor) with different digitizers (Q330, Q4120, K2 and DM24). Most of the accelerometers are co-located with the seismic sensors.

NIEP is operating also a GPS network (Fig. 9.11) for monitoring of crustal movements in Romania in correlation with tectonic processes in South-East Europe (Africa-Europe plate interaction), observation of surface-to-depth relationship in order to model the process of earthquake generation in the mantle in the area of the Eastern Carpathians bend zone (Vrancea region) and improving the accuracy of the

Fig. 9.9 DACEA project area (marked with *yellow*) and seismic station network (*blue points*)

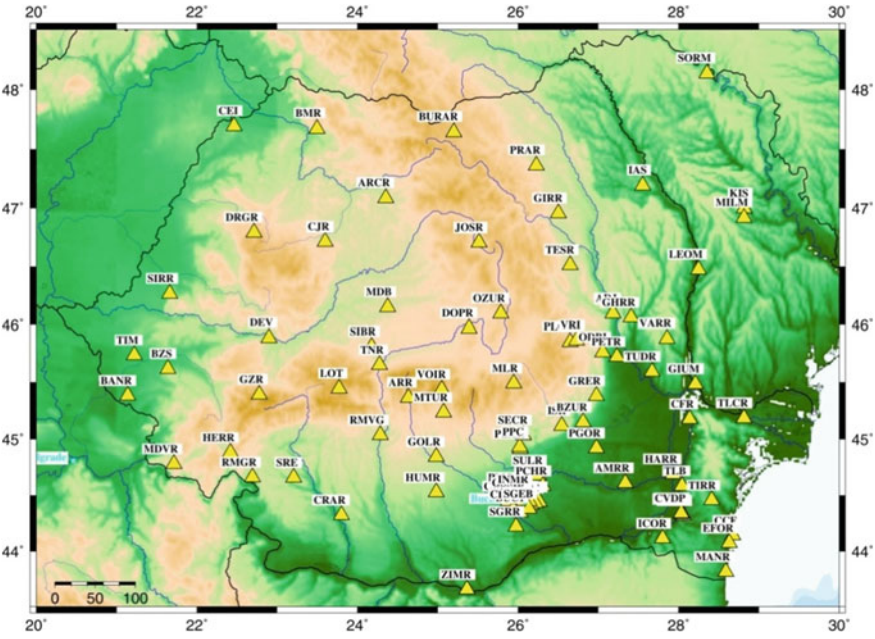

Fig. 9.10 Strong motion network in 2013

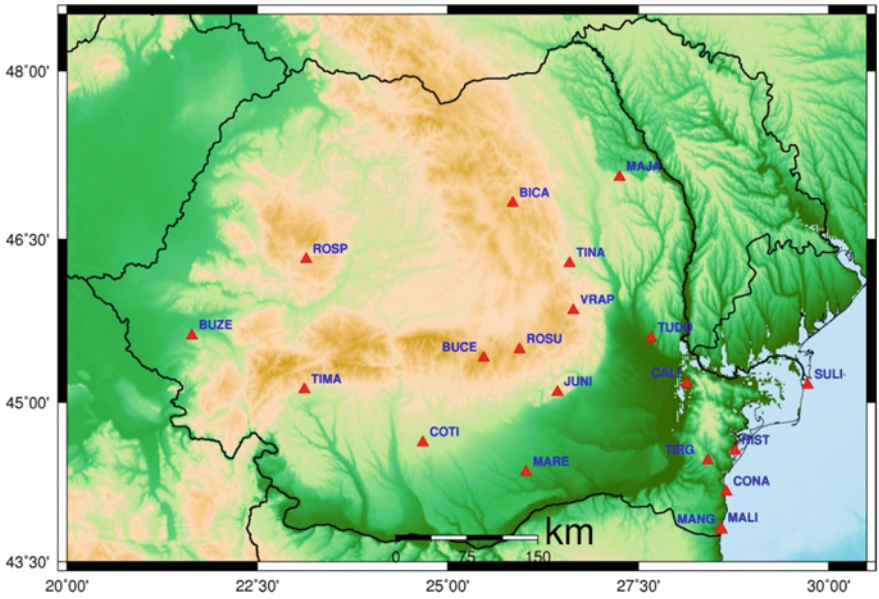

Fig. 9.11 GPS permanent network

coordinates of the national seismic network stations. The first station was installed in 2001 and now the network consists of 20 stations. The network was installed in cooperation with the Faculty of Geology and Geophysics—University of Bucharest (FGG), Delft University of Technology, the University of Utrecht and the Netherlands Research Center for Integrated Solid Earth Sciences (ISES). Data acquisition is made in real time, in RAW and RINEX DATA format using the Leica GNSS Spider and Septentrio Rx Software. All of the data recorded are transmitted in real time to the NIEP for automatic data processing, analysis and dissemination.

9.3 Data Management and Products

For the management of the real-time data, the Antelope data acquisition and processing software is used and adjusted to handle the increasing amount of recorded seismic data. Seedlink and Antelope program packages are used for the real-time data acquisition, accurate computation of the locations and magnitudes for local, regional and teleseismic events and data exchange. Preliminary and revised determinations of hypocenters are reported in automatic and reviewed seismological bulletins. For local events with magnitude greater than 3.5, moment tensor inversion is produced as well. The NIEP earthquake catalogue (ROMPLUS [4]) is monthly updated based on revised bulletins.

The Antelope data acquisition and processing software is running on two workstations for automatic, real-time processing and post processing. In case of earthquakes with magnitude greater than 3.0 occurred on Romania territory, a Shakemap is produced automatically by Antelope. For local events with magnitude greater than 4.0 the alerting system is sending e-mail and SMS messages to dedicated recipients. All the information produced by Antelope (near real-time earthquake information, Shakemaps, epicenter position, seismicity map in case of local event) is available on the NIEP website (www.infp.ro). Also, in case of felt earthquake people can fill out the "Did you feel it?" form from the website. The collected information is sent to the local authorities and used for intensity map (Fig. 9.12).

In parallel, SeisComP3 [6, 7] software is running for data acquisition, data quality control, real-time data exchange and processing, event alerts, waveform archiving, automatic data detection and location and network status monitoring.

The RSN ensures the global exchange of data and information with international seismological organizations and national data centers: ORFEUS, IRIS, National Earthquake Information Center, USA, European Mediterranean Seismological Centre, International Data Center of CTBTO, International Seismological Centre, UK; NDCs from: Hungary, Serbia, Bulgaria, Republic of Moldova, Ukraine, Poland (Fig. 9.13).

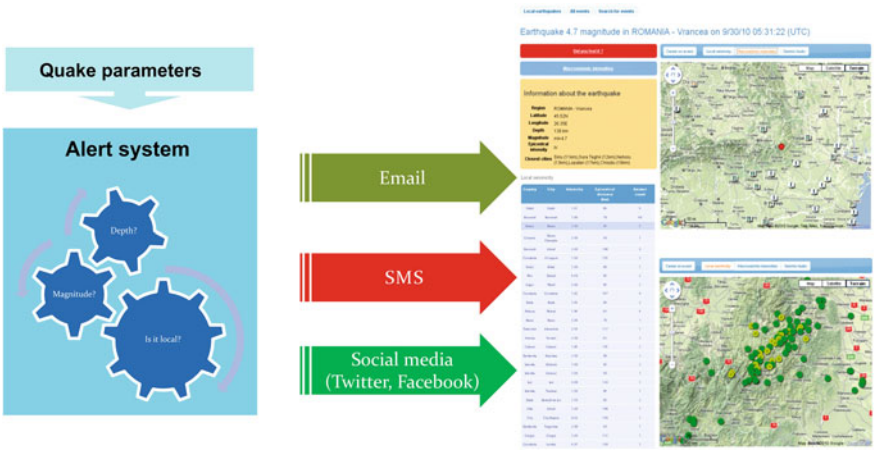

Fig. 9.12 Real-time data analysis and the products

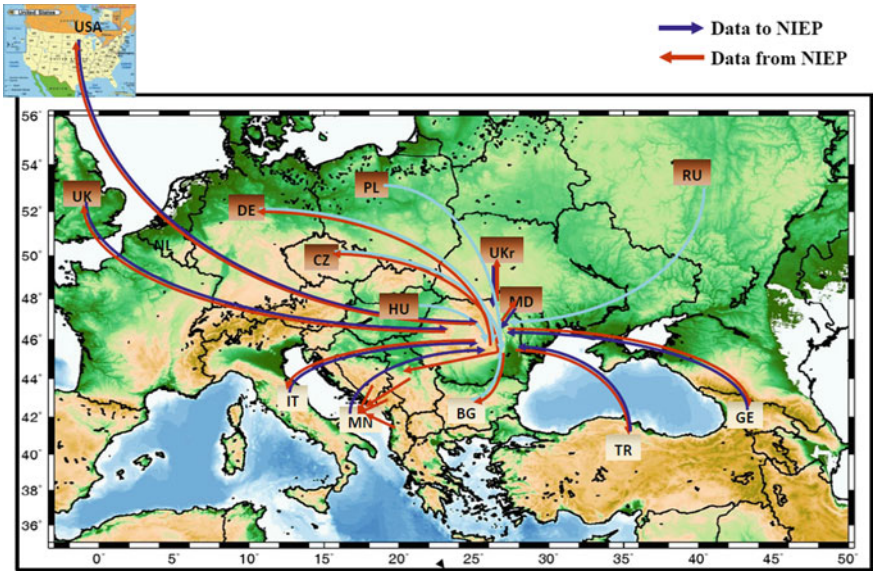

Fig. 9.13 Real-time data and products exchange

9.4 Statistics Regarding the Network Development and Increasing of Detection Capacity

Naturally, we expect an increase of the network capacity to detect and locate events in Romania as a consequence of the rather continuous improvement of the network on many aspects (number and quality of stations, operation system and coverage). The evolution of the earthquakes rate located yearly in Romania (Fig. 9.14) shows a significant increase starting with 2005. The main factor responsible for this variation was not this time related to an increase in station number and quality, but to the implementation of the Antelope system. On the contrary, the tendency of increasing rate after 2005 is explained essentially by the increase of the number of stations. The final jump of events number in 2013 is due to a massive earthquake swarm occurred in 2013 in the eastern part of the country (Galati region). The most spectacular increase rate is observed for smaller events and for shallow events (including quarry blasts) (Figs. 9.15 and 9.16). For the Vrancea deep events, the increase rate is significantly lower (roughly by a factor of 2 after 2005 versus before 2005) and is explained mainly by adopting Antelope data acquisition and processing software, which is presently used for the Romanian Seismic Network operated by NIEP. By using Antelope system, signals visualization, routine data analysis (bandpass filtering, phase association, location processing), or comparative inspection of the waveforms were significantly enhanced.

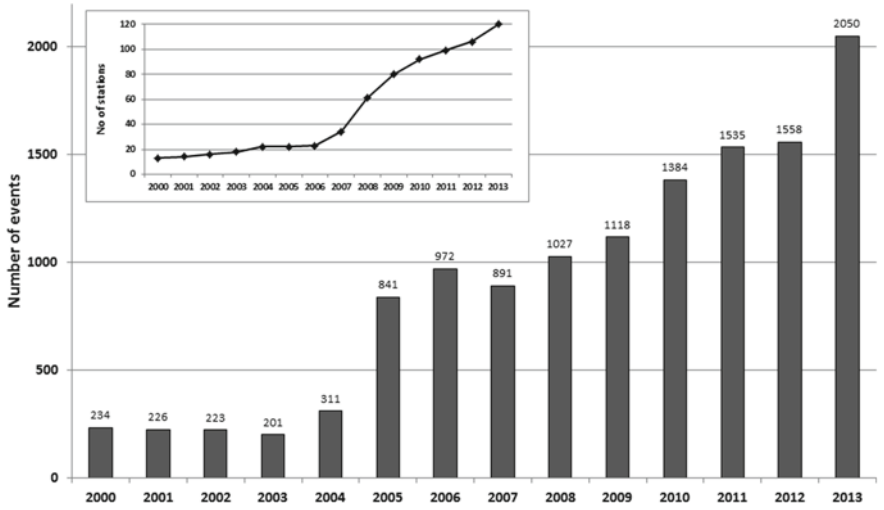

Fig. 9.14 Yearly number of events located by NIEP (up-dated Romplus catalogue). Insertion from left-up represent the number of real-time stations for each year

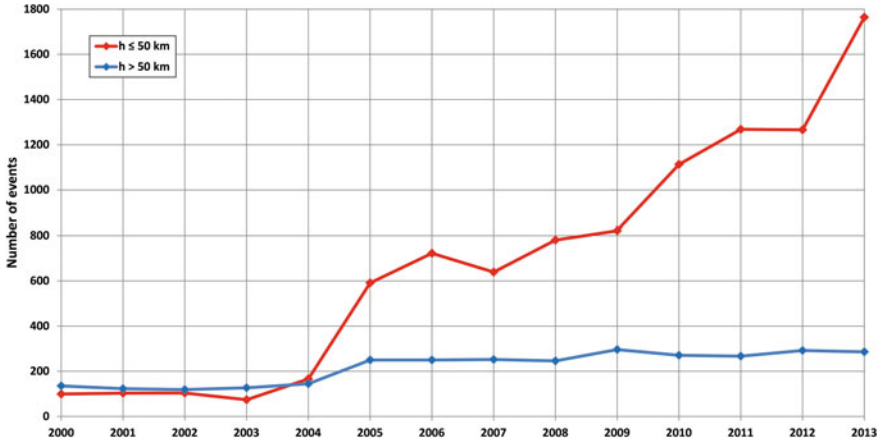

Fig. 9.15 Number of events versus depth intervals for each year between 2000 and 2013

The yearly distribution of the crustal and sub-crustal events is given in Fig. 9.15. Since for the most of the earthquakes located in the 2000–2013 time interval, the computed magnitude ranges between 2.1 and 2.5, we detailed in Fig. 9.16 the increase of events number in time.

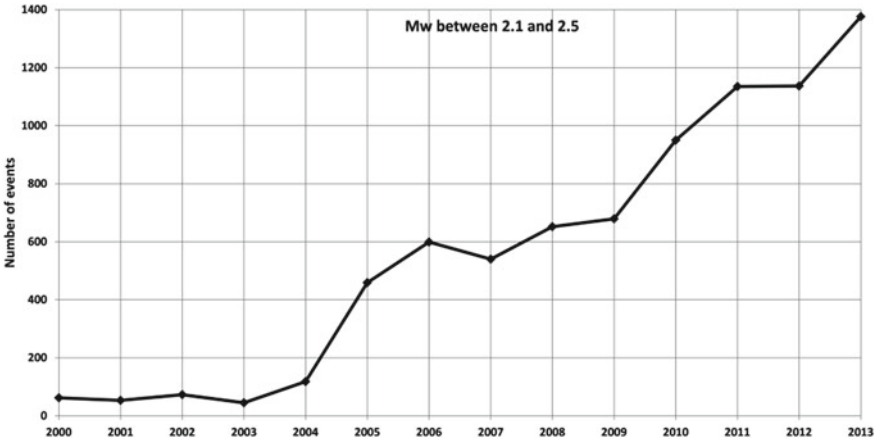

Fig. 9.16 Number of events with M_w magnitude between 2.1 and 2.5 for 2000–2013 time period

9.5 Conclusions

We present the significant development of Romanian Seismic Network during the last three decades and its impact on seismic monitoring of national territory and adjacent areas. Almost 100 seismic sites are presently in operation, contributing with real time data to fulfillment of NIEP mission: research tasks, earthquake survey, management of advanced seismic data collection, and Romania's participation in support of CTBT.

8 observatories, 88 stand-alone seismic sensors (short-period and broad-band) and 120 accelerometers, distributed all over the country, are components of the Romania's Seismic Network. In addition, three stations were installed in Republic of Moldova. Recently, a new Early Warning System for Danube cross-border region, consisting of 32 sites, was set-up in order to mitigate the destructive effects of large earthquakes occurred in Romania and Bulgaria.

Moreover, NIEP operates a modern integrated system deployed at Plostina, including advanced technologies such as: seismic and infrasound arrays, strong motion sensors, magnetic field and electric field monitoring, soil temperature measuring, and a weather station. As well, a GPS network consisting of 20 stations is in operation, mostly for monitoring of crustal movements in Romania and for modeling the process of earthquake generation in Vrancea region.

For data acquisition and exchange, signal processing and analysis, two program packages (Seedlink and Antelope) are used at NIEP to produce automatic and reviewed seismological bulletins, instrumental intensity maps (Shakemaps), rapid alerts, seismicity maps, email notifications. Supplementary products like updated earthquake catalogue, moment tensor inversion results, website information, and community internet intensity maps are generated as well.

During last decade, a significant enhancement could be observed in earthquake monitoring statistics. This is a consequence of the continuous improvement of the Romanian Seismic Network in terms of: number and quality of stations, better territory coverage, implementation of a new data acquisition and processing software. The number of detected and located events greatly increased, mainly after 2005, while magnitude threshold of detection decreased. The most remarkable increase rate is observed for smaller events (magnitude between 2.1 and 2.5) and for shallow events (including quarry blasts).

The continuous process of Romanian Seismic Network development represents a great opportunity for establishing of national and international cooperation in seismology and seismic engineering fields: seismic source and seismotectonics, site effects and microzonation, crustal structure and dynamics, assessment and mitigation of seismic risk.

References

1. K.-P. Bonjer, M.C. Oncescu, M. Rizescu, D. Enescu, L. Driad, M. Radulian, C. Ionescu, T. Moldoveanu, Source-and site-parameters of the April 28, 1999 intermediate depth Vrancea earthquakes; First results from the new K2 network in Romania, XXVII General Assembly of the European Seismological Commission, Lisbon, Portugal, Book of Abstracts and Papers, SSA-2-13-O, p. 53, 2000
2. D. Ghica, Detection capabilities of the BURAR seismic array-contributions to the monitoring of regional and distant seismicity. J. Seismol. 487–506 (2011). doi:10.1007/s10950-010-9204-9
3. B. Grecu, D. Ghica, M. Popa, M. Rizescu, C. Ionescu, Earthquake monitoring by the seismic network of the national institute for earth physics. Rev. Roum. Geophysique **46**, 47–57 (2002)
4. M.C. Oncescu, V.I. Marza, M. Rizescu, M. Popa, in *Vrancea Earthquakes: Tectonics, Hazard and Risk Mitigation*, ed. by F. Wenzel, D. Lungu, O. Novak (co-ed.) (Kluwer Academic Publishers, Dordrecht, 1999) The Romanian Earthquake Catalogue Between 1984–1997, pp. 43–47
5. M. Radulian, N. Mandrescu, G.F. Panza, E. Popescu, A. Utale, Characterization of seismogenic zones of Romania. Pure Appl. Geophys. **157**, 57–77 (2000)
6. SeisComP3.org. Introduction and scope (2011a). http://www.seiscomp3.org/wiki/doc/introduction-and-scope
7. SeisComP3.org, Software architecture (2011b). http://www.seiscomp3.org/wiki/doc/software-architecture/

Chapter 10
Seismic Monitoring and Data Processing in Seismological Observatory in Skopje—Republic of Macedonia—Basis for a Complex Geophysical Monitoring

D. Černih and V. Čejkovska

Abstract Seismological Observatory in Skopje with telemetric network of digital seismological stations systematically monitors the seismic activity in the territory of Republic of Macedonia and the bordering areas and also records the regional and teleseismic earthquakes The seismicity in Republic of Macedonia is studied on the base of instrumental seismological and macroseismic data available at the Seismological Observatory of the Faculty of Natural Sciences and Mathematics in Skopje. The data cover a period of about 1500 years. The earthquakes occurred before 1957, which is the year of foundation of the observatory, are included with locations obtained mainly from the maps of isoseismals, while the earthquakes occurred after 1957 are included with instrumental locations. Independent tectonic data are also used in the analysis. Seismic activity in the territory of the Republic of Macedonia is due to the permanent different intensities of movements of the higher order tectonic units within the seismic zones. It is concluded that the weak earthquakes are very frequent, that the light to moderate earthquakes are relatively rare, while the strong earthquakes are rare. The predominant hypocentral depth is within the Earth crust.

10.1 Introduction

The Seismological Observatory at the Faculty of Natural Sciences and Mathematics in Skopje is authorized and obliged to perform the Seismological service in Republic of Macedonia. The first independent seismological monitoring in Republic of Macedonia started on 1 July 1957, with foundation of the Seismological Station of the University in Skopje (SKO). This is the only institution in Republic of Macedonia authorized and obliged to perform seismological service. The Law for Participation of the Republic of Macedonia in Financing of Seismological and Engineering-Seismological Activities regulates the service.

D. Černih (✉) · V. Čejkovska
Seismological Observatory of the Faculty of Natural Sciences and Mathematics,
Ss. Cyril and Methodius University, Skopje, Macedonia
e-mail: dcernih@yahoo.com

B. Aneva and M. Kouteva-Guentcheva (eds.),
Nonlinear Mathematical Physics and Natural Hazards,
Springer Proceedings in Physics 163, DOI 10.1007/978-3-319-14328-6_10

It is organized into five sections: microseismics, macroseismics, seismological instrumentation and computer science laboratory. By using the network of analog and digital seismological stations, this Observatory performs permanent instrumental and macroseismic observations of the seismic activity in the territory of Republic of Macedonia and the bordering areas (40.7–42.4 N, 20.3–23.2 E) and also records the regional and teleseismic earthquakes.

The real-time data transmission from the field stations to the Observatory is accomplished via internet and real-time acquisition and data processing are performed.

The instrumental and macroseismic data are compiled, stored, analyzed and published in seismological bulletins and catalogues for international exchange of seismological data and for scientific, teaching and civil engineering purposes. In cases of earthquakes felt in the territory of Republic of Macedonia, the Observatory compiles and processes the data on the macroseismic effect of earthquakes.

The Observatory also performs scientific research, education and applications in the field of seismology and geophysics.

10.1.1 Stations and Equipment

Two mechanical seismographs MAINKA (EW and NS components, pendulum mass of 450 kg) (Fig. 10.2) and a contact timing device WIECHERT presented the first equipment. In February 1963, the mechanical seismograph CONRAD was mounted. After the devastating Skopje earthquake of 26 July 1963, electromagnetic seismometers VEGIK (short-period) and SKD (middle-period), with galvanometric registration, were installed.

Electromagnetic seismometers LEHNER-GRIFFITH, WILLMORE (short-period), PRESS-EWING (long-period) and STRONG-MOTION RECORDER AR-240, with galvanometric registration, were put into operation in March 1966 (Fig. 10.2).

In the 1960-ties, the Seismological Station in Skopje founded two new seismological stations, in Valandovo (VAY, 1966) and Ohrid (OHR, 1967). These stations were equipped with short-period electromagnetic seismometers LEHNER-GRIFFITH, with galvanometric registration. In 1966, Seismological Station in Skopje became Seismological Observatory within the University “Ss. Cyril and Methodius” in Skopje. In 1976, the Seismological Observatory in Skopje became Section of the Faculty of Physics in Skopje of the same university, while in 1984 it became Institute within the Faculty of Natural Sciences and Mathematics of the same university (Figs. 10.1 and 10.2). Following the new worldwide trends of development of instrumental seismology, the observatory started in 1990 to build a telemetric network of seismological stations with SS-1 (short-period) and WR-1 (wide-range period) seismometers (Kinemetrics, Inc.) with digital recorders SSR1, Wave 24 and Quantera Q330 (Fig. 10.3). The present telemetric seismological network maintained by the observatory is consisted of six permanent stations (Skopje/SKO, Valandovo/VAY,

Fig. 10.1 The present building of the seismological observatory in Skopje

Fig. 10.2 The seismological observatory in Skopje: (*left*) the NS component of the mechanical seismograph MAINKA; (*right*) the electromagnetic seismometers LEHNER-GRIFFITH, PRESS-EWING and SKD (*up*), which use galvanometric registration (*down*)

Ohrid/OHR, Bitola/BIA, Kruševo/KRUS and Štip/STIP) and five temporary stations that monitor the induced seismicity by the water accumulations at dams of new-build power stations. Nowadays, the observatory is the only institution that is authorized and obliged to perform the seismological service in the Republic of Macedonia.

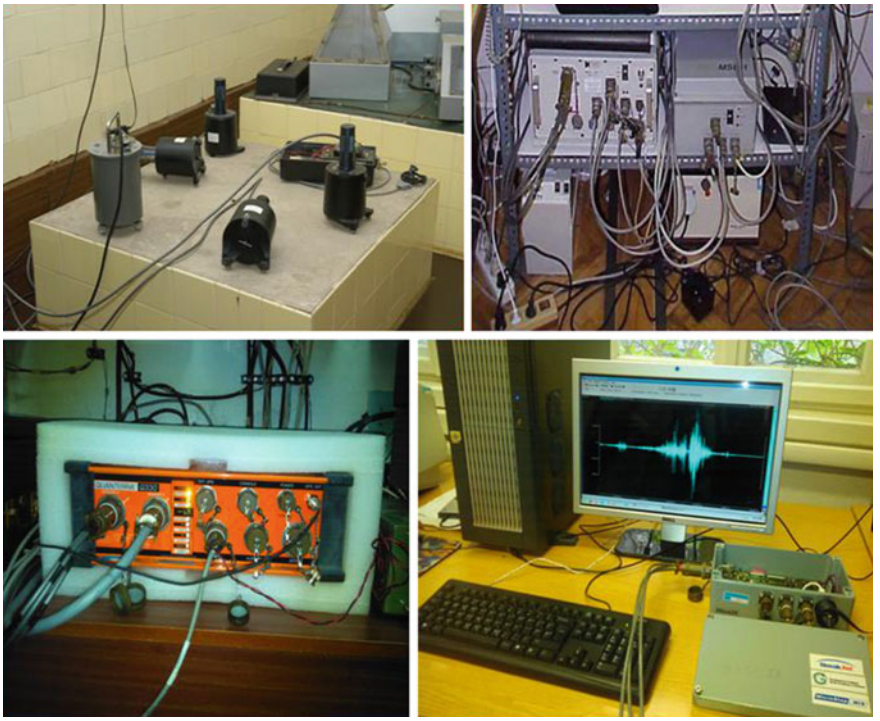

Fig. 10.3 Modern equipment in the seismological observatory in Skopje. (*Up* and *left*) electromagnetic seismometers SS-1 (short-period) and WR-1 (wide-range period); (*up* and *right*) digital recorder SSR-1; (*down* and *left*) digital recorder Quantera–Q330HRS; (*down* and *right*) digital recorder Wave-24

The observatory systematically instrumentally monitors the seismic activity in the territory of Republic of Macedonia and the bordering areas, and also records the regional and teleseismic earthquakes. In cases of felt earthquakes in the territory of Republic of Macedonia, the observatory compiles and processes the data on the macroseismic effect of earthquakes. The instrumental and macroseismic data are compiled, stored, analyzed and published in seismological bulletins and catalogues for scientific, teaching and civil engineering purposes. The exchange of the data with regional and international seismological institutions via Internet is regularly performed. The observatory is also engaged with scientific research, education and applications in the field of seismology and geophysics.

Present, seismic network is consisted of 11 stations (6 permanent seismic stations and five located at dams). Permanent stations are connected to the Observatory in Skopje and data are transferred to the observatory in real-time (Table 10.1, Fig. 10.4).

The instrumental seismological data at the Seismological Observatory in Skopje and at stations of its network have been always obtained by instrumentation which had followed the world trends. Actual scientific methods and, lately, the most sophisticated computer softwares have been used in analyses. With the latest

Table 10.1 SORM (Seismological Observatory Republic of Macedonia) seismic stations and instrumentation

Code	Latitude (°N)	Longitude (°E)	Elev. (m)	Station type (1)	Sensor type (2)	Rec. equipment (3)	Data transfer (4)
SKO	41.9721	21.4396	346	3C WB	WR-1	SSR-1	On site
				1C SP	SS-1	VR-1 pen r	On site
				3C SP	Leghn.-Grif.	Drum recorder	On site
				3C SP	VEGIK	Drum recorder	On site
				2C MP	MAINKA	SM recorder	On site
				3C SP	SKD	Drum recorder	On site
				3C LP	PressEwing	Drum recorder	On site
				1C SP	Conrad	SM recorder	On site
				3C WB	WR-1	Q330	Telemetric
OHR	41.1114	20.5989	739	3C WB	WR-1	WAVE-24	Telemetric
VAY	41.3211	22.5701	168	3C WB	WR-1	WAVE-24	Telemetric
BIA	41.0194	21.3239	720	3C SP	SS-1	WAVE-24	Telemetric
STIP	41.7754	22.4382	1,320	3C SP	SS-1	WAVE-24	Telemetric
KRUS	41.3689	21.2489	1,015	3C SP	SS-1	WAVE-24	Telemetric
KPJ	42.2092	22.3617	700	3C SP	SS-1	SSR-1	Dial up
KOZJ	41.8779	21.1951	533	3C SP	CMG-40T-1	IDS-24	Dial up
BELI	41.6827	21.2743	523	3C SP	CMG-40T-1	IDS-24	Dial up
SAMO	41.6928	21.1392	523	3C SP	CMG-40T-1	IDS-24	Dial up

(continued)

Table 10.1 (continued)

Code	Latitude (°N)	Longitude (°E)	Elev. (m)	Station type (1)	Sensor type (2)	Rec. equipment (3)	Data transfer (4)
LIS	41.6870	21.6007	638	3C SP	CMG-40T-1	Q330	Dial up
KNE	42.1091	22.3068	890	3C SP	SS-1	SSR-1	Dial up
SVPE	41.9217	21.2595	550	3C SP	CMG-40T-1	IDS-24	Dial up

(1) WB Wide band (0.05–20 Hz) 41.9217, 21.2595
MP Medium period (0.1–2 Hz)
SP Short period

(2) WR-1 Wide range seismometer (Kinemetrics Inc.)
SS-1 Short period seismometer (Kinemetrics Inc.)
CMG-40T-1 Short period (1 Hz) seismometer (Guralp Sys.)
SKD Medium-to-long period Kirnos seismometer
PRESS-EWING Long period seismometer
MAINKA 7 s
CONRAD 2.5 s

(3) Q330 26-bit Digital recorder (Kinemetrics Inc.)
IDS-24 24b Digital recorder (Terra Techn.)
SSR-1 16-bit Digital recorder (Kinemetrics Inc.)
VR-1 Pen recorder (Kinemetrics)
SM Smoked paper-recorder

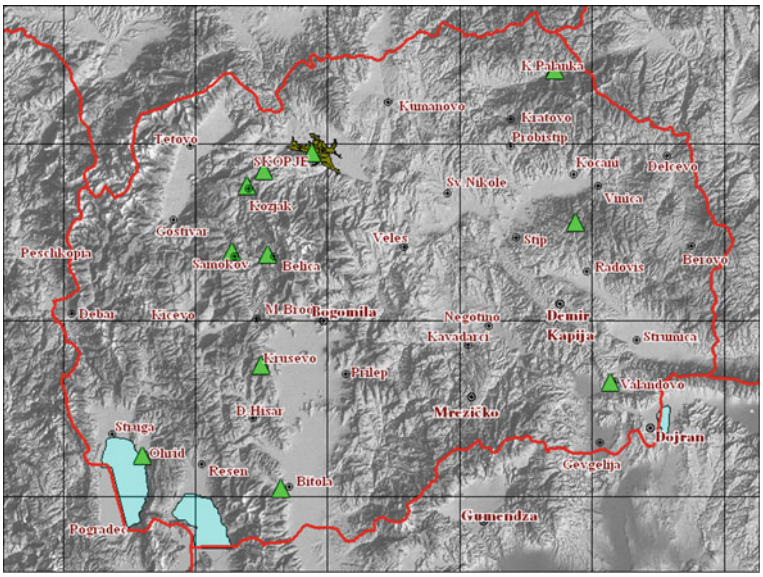

Fig. 10.4 Seismological stations on the territory of the Republic of Macedonia

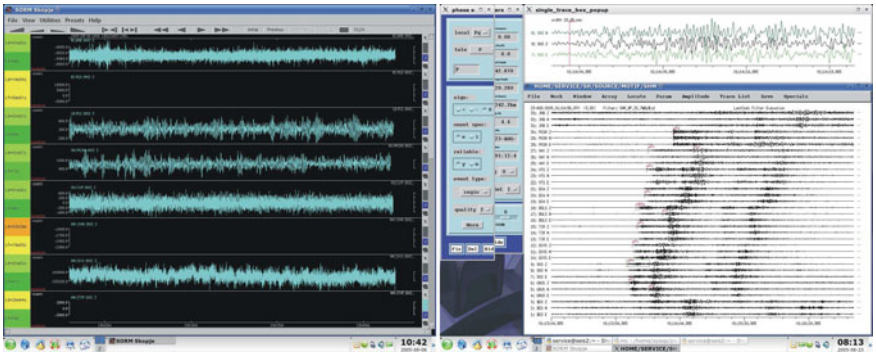

Fig. 10.5 Real-time data exchange (*left*) and earthquake analysis by the software Seismic Handler (*right*)

instrumentation, realtime telemetric network data exchange and used softwares, earthquakes with local magnitudes down to zero can be recorded and analyzed (Fig. 10.5). In the Catalogue files, all earthquakes are relocated and elaborated. The earthquake focal parameters and magnitude estimations, as well as the observational data are included into a disc storage system.

There are macroseismic data for all felt events collected in seismological catalogue. The epicentral intensity (I_0) is printed for the events for which maps of isosesmals are compiled. Intensity I_0 is expressed in degrees of European-macroseismic scale.

10.2 Seismicity in the Period 1901–2012

Distribution of epicentrers of the earthquakes in the territory of the Republic of Macedonia and neighboring regions for the period 1901–2012 is presented in Fig. 10.6, together with the neotectonic faults, the borders of the epicentral areas and the stations of the present seismological telemetric network [1–5].

Nearly all the parts of the territory of the Republic of Macedonia were seismically active in the period 1901–2012 (17,005 located earthquakes), as it can be seen from Fig. 10.6. Weak seismic activity was present in the Zletovo epicentral area (a part of the East Macedonia seismic zone), in the Kumanovo epicentral area (a part f the Vardar seismic zone), as well as in the area of the Pelagonia Anticlinorium (which is a part of the West Macedonia seismic zone) [6, 7]. As known [8], the reason for weak seismic activity of this anticlinorium is that it has been being a consolidated block with only oscillatory movement since the Precambrian times (starting 800 to 1,000 millions years ago), and still keeps the structure consisted of relicts of the Earth's Precambrian crust. This structure differs very much in comparison with the neighboring areas.

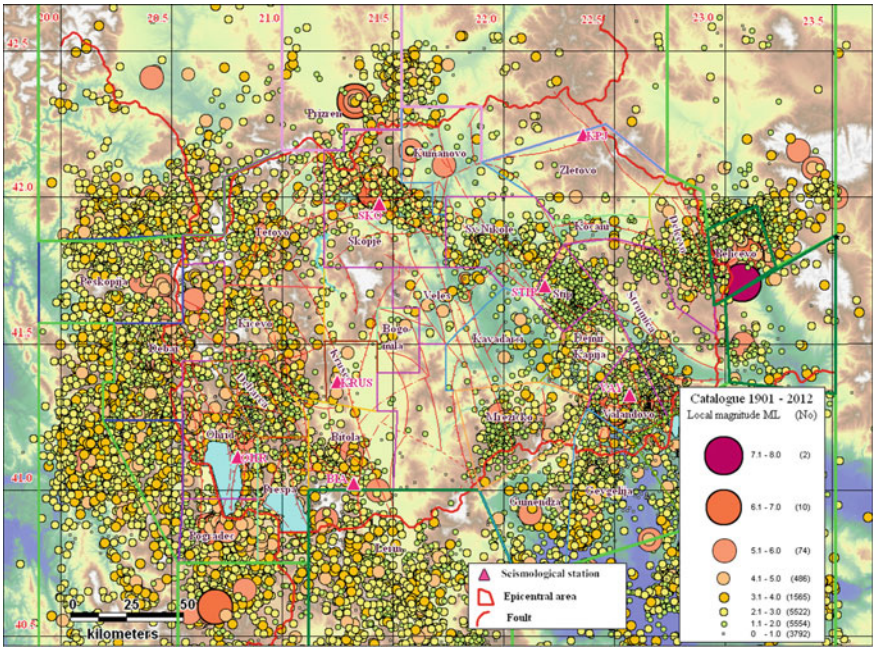

Fig. 10.6 Epicentral map of the earthquakes in te territory of the Republic of Macedonia and neighbouring regions for the period 1901–2012. Beside the neotectonic faults and the borders of the epicentral areas, the stations of the present seismological telemetric network are shown too, by *triangles*

From the bilateral cooperation between Seismological Observatory, Faculty of Natural Sciences and Mathematics, Sts. Cyril and Methodius University, Skopje, Macedonia and INRNE, Bulgarian Academy of Sciences and by EU FP7 IRSES the BlackSeaHazNet Project (Balkan, Black Sea, Caucasus, Caspian NETWORK for Complex Research of Earthquake's Forecasting Possibilities, Seismicity and Climate Change Correlationsis). The characteristics of the regional geomagnetic field were monitored. It was multilateral cooperation with 9 countries. More geomagnetic observatories like SKO, PAG, GCK, SUR, LVV, KIV, DSH are included in this monitoring.

References

1. L. Pekevski, V. Čejkovska, Catalogue of earthquakes in Republic of Macedoina from 1971 to 1980. Skopje: Seismological Observatory Faculty of Natural Sciences and Mathematics—Skopje (In print) (2013a) (in macedonian)
2. L. Pekevski, V. Čejkovska, Catalogue of earthquakes in Republic of Macedonia from 1971 to 1980. Skopje: Seismological Observatory Faculty of Natural Sciences and Mathematics—Skopje (In print) (2013b) (in macedonian)
3. E. Hadzievski, Catalogue of earthquakes in Macedonia. Part I, 1900–1930, Part II, 1931–1962, Part III, 1963–1974, Seismological Observatory of the University "St. Cyril and Methodius", Skopje (1976a) (in macedonian)
4. E. Hadzievski, Catalogue of earthquakes in Macedonia before 1900, Seismological Observatory of the University "St. Cyril and Methodius", Skopje (1976c) (in macedonian)
5. SORM—Seismological Observatory in Skopje, catalogues of earthquakes in Republic of Macedonia and border areas for the years 1991 to 2012, Fund of Seismological Observatory, Faculty of Natural Sciences and Mathematics—Skopje (1991–2012) (in macedonian)
6. E. Hadzievski, The seismicity of the territory of S. R. Macedonia, Seismological Observatory of the University, "St. Cyril and Methodius", Skopje (1976b) (in macedonian)
7. Lj. Jordanovski, L. Pekevski, V. Čejkovska, D. Černih, B. Hristovski, N. Vasilevski, Basic characteristics of seismicity of the territory of the Republic of Macedonia. University "Ss. Cyril and Methodius", Faculty of Natural Sciences and Mathematics, Seismological Observatory, Skopje (1998) (in macedonian)
8. M. Arsovski, *Tectonics of Macedonia* (Faculty of Mining and Geology, Stip, 1997) (in macedonian)